Rose-Hulman Institute of Technology
Rose-Hulman Scholar

Graduate Theses - Physics and Optical Engineering | Graduate Theses

5-2017

Study of Cu/SiO2/Cu Metamaterials: Design, Simulation, Fabrication, Testing, and Optical Applications

Minsu Oh
Rose-Hulman Institute of Technology, ohm@rose-hulman.edu

Follow this and additional works at: https://scholar.rose-hulman.edu/optics_grad_theses

Part of the Physics Commons

Recommended Citation
Oh, Minsu, "Study of Cu/SiO2/Cu Metamaterials: Design, Simulation, Fabrication, Testing, and Optical Applications" (2017). *Graduate Theses - Physics and Optical Engineering*. 19.
https://scholar.rose-hulman.edu/optics_grad_theses/19

This Thesis is brought to you for free and open access by the Graduate Theses at Rose-Hulman Scholar. It has been accepted for inclusion in Graduate Theses - Physics and Optical Engineering by an authorized administrator of Rose-Hulman Scholar. For more information, please contact weir1@rose-hulman.edu.

Study of Cu/SiO_2/Cu Metamaterials:

Design, Simulation, Fabrication, Testing, and Optical Applications

A Thesis

Submitted to the Faculty

of

Rose-Hulman Institute of Technology

by

Minsu Oh

In Partial Fulfillment of the Requirements for the Degree

of

Master of Science in Optical Engineering

May 2017

© 2017 Minsu Oh

ROSE-HULMAN INSTITUTE OF TECHNOLOGY

Final Examination Report

Minsu Oh
Name

Optical Engineering
Graduate Major

Thesis Title Study of Cu/SiO2/Cu Metamaterials: Design, Simulation, Fabrication, Testing, and Optical Applications

DATE OF EXAM: May 17, 2017

EXAMINATION COMMITTEE:

	Thesis Advisory Committee	Department
Thesis Advisor:	Richard Liptak	PHOE
	Sergio Granieri	PHOE
	Wonjong Joo	SNUST

PASSED X **FAILED** _____

ABSTRACT

Oh, Minsu

M.S.O.E

Rose-Hulman Institute of Technology

May 2017

Study of Cu/SiO_2/Cu Metamaterials: Design, Simulation, Fabrication, Testing, and Optical Applications

Thesis Advisors: Dr. Richard Liptak and Dr. Sergio Granieri (co-advisor)

In the past few years, “metamaterials” have grabbed attention of researchers in both science and engineering. They have revealed great potentials to realize unusual optical applications such as flat lenses or frequency-selective performances with their unusual electromagnetic properties. In this project, Cu/SiO_2/Cu metamaterials of diverse designs and parameters were studied towards discovering their unknown optical applications. From simulation work, it was found that some metamaterials exhibit a performance of a rectangle-shaped bandpass at optical frequencies. Their operational wavelength region can be adjusted by having a different scale of the structure or a different thickness of the constituent materials. This indicates that those metamaterials could be used instead of traditional optical filters. A few selected metamaterials were fabricated and tested for comparison with the simulation results.

Keywords: metamaterials, subwavelength structures, optical properties of materials, electromagnetism, nanofabrication

DEDICATION

I would like to dedicate this work to my family, friends, and all the others that I could talk to and have fun with. I could get a strength from them in my lonely life in a foreign country. This helped me perform better and creatively on this work.

ACKNOWLEDGEMENTS

I deeply appreciate the guidance and advice of my advisors Dr. Richard Liptak and Dr. Sergio Granieri (co-advisor). They guided me on the journey of this research with inspirations, encouragements, and methodologies. I also express my thanks to Dr. Sun Hong who helped me with CST simulation, Brian Fair who trained me on the electron-beam evaporator, Kevin Roberts at the University of Minnesota who assisted this project by preparing a substrate with a patterned electron-beam resist, and all the professors who allowed me to audit their class for a deeper and broader spectrum of knowledge. The courses audited, especially, were obviously helpful by inspiring me with creative ideas. Not to forget, I sincerely thank Dr. Wonjong Joo at the Seoul National University of Science and Technology in South Korea who first introduced me to the world of optics, where I found a new irresistible academic passion. I would not have achieved the results of this project without all their help.

TABLE OF CONTENTS

LIST OF FIGURES ..... **iv**

LIST OF TABLES ..... **viii**

LIST OF ABBREVIATIONS ..... **ix**

LIST OF SYMBOLS ..... **x**

1. INTRODUCTION **1**

1.1. Metamaterials 1

1.2. Diffraction in Sub-wavelength Structures 1

2. THEORY 3

2.1. Electromagnetic Waves 3

2.1.1. Maxwell's Equations in Materials 3

2.1.2. Maxwell's Equations in Vacuum 4

2.1.3. Propagation of Electromagnetic Waves 4

2.1.4. Electromagnetic Waves in Loss-free Dielectrics (J=0) 6

2.1.5. Electromagnetic Waves in Lossy Dielectrics or Conductors (J≠0) 8

2.2. Optical Properties of Materials 11

2.2.1. Overview 11

2.2.2. Dispersion in General Dielectrics (Lorentz model) 12

2.2.3. Dispersion in Conductors (Drude model) 17

2.2.4. Frequency-dependent Electrical Conductivity in Conductors (Drude model) 20

2.2.5. Values of Plasma and Damping Frequencies of Conductors 21

3. DESIGNS AND PARAMETERS 23

3.1. Design A 23

3.2. Design B 24

3.3. Design C 24

3.4. Design D 25

3.5. Design E 25

3.6. Design F 26

4. SIMULATION 27

4.1. Computational Electromagnetism: Finite Integration Technique.....27

4.2. Simulation Method 28

4.3. Parameter Study and Simulation Results 31

4.3.1. Design A.....31

4.3.2. Design B 43

4.3.3. Design C 46

4.3.4. Design D.....49

4.3.5. Design E 50

4.3.6. Design F 53

4.4 Extraction of Effective Properties of Metamaterials 56

4.4.1. Effective Thickness of Metamaterial 56

4.4.2. Extraction Method 56

4.4.3. Extracted Effective Parameters 58

5. FABRICATION 63

5.1. E-beam Evaporator and Profilometer 63

5.2. Design A-1-(5) 65

5.2.1. Calibration of E-beam evaporator 65

5.2.2. Metamaterial Fabrication 68

5.3. Design A-3-(5) 70

5.3.1. Calibration of E-beam evaporator 70

5.3.2. Metamaterial Fabrication 71

6. TEST AND MEASUREMENT 72

6.1 Design A-1-(5) 72

6.2 Design A-3-(5) 74

7. DISCUSSION 76

7.1 Results of Design A-1-(5) metamaterial 76

7.2 Results of Design A-3-(5) metamaterial 78

8. CONCLUSION 79

9. FUTURE WORK 80

LIST OF REFERENCES 81

APPENDIX A: Maple Coding for the Refractive Index and Reflectance of SiO_2 84

APPENDIX B: Maple Coding for the Refractive Index and Reflectance of Cu 85

LIST OF FIGURES

Figure Page

Figure 2.1 Illustration of electromagnetic wave propagation 5

Figure 2.2 Lorentz forced and damped oscillation model for dielectric media [9] 12

Figure 2.3 Optical properties of SiO_2 17

Figure 2.4 Optical properties of Cu 19

Figure 2.5 Plasma frequency vs. damping frequency of some metals. 22

Figure 3.1 Parameters of Design A metamaterials 23

Figure 3.2 Parameters of Design B metamaterials 24

Figure 3.3 Parameters of Design C metamaterials 24

Figure 3.4 Parameters of Design D metamaterials 25

Figure 3.5 Parameters of Design E metamaterials 25

Figure 3.6 Parameters of Design F metamaterials 26

Figure 4.1 Discretization for FIT with hexahedral meshes [23]. 27

Figure 4.2 Values of optical properties entered in CST Microwave Studio 28

Figure 4.3 Incident light and a top-view scheme of a metamaterial 30

Figure 4.4 Simulated reflectance for Table 4.1 32

Figure 4.5 Simulated transmittance for Table 4.1 33

Figure 4.6 Simulated reflectance for Table 4.2 35

Figure 4.7 Simulated transmittance for Table 4.2 36

Figure 4.8 Simulated reflectance for Table 4.3 38

Figure 4.9 Simulated transmittance for Table 4.3 39

Figure 4.10 Simulated reflectance for Table 4.4 41

Figure 4.11 Simulated transmittance for Table 4.4 42

Figure 4.12 Simulated reflectance for Table 4.5 44

Figure 4.13 Simulated transmittance for Table 4.5 45

Figure 4.14 Simulated reflectance for Table 4.6 47

Figure 4.15 Simulated transmittance for Table 4.6 48

Figure 4.16 Simulated reflectance for Table 4.7 49

Figure 4.17 Simulated transmittance for Table 4.7 49

Figure 4.18 Simulated reflectance for Table 4.8 51

Figure 4.19 Simulated transmittance for Table 4.8 52

Figure 4.20 Simulated reflectance for Table 4.9 54

Figure 4.21 Simulated transmittance for Table 4.9 55

Figure 4.22 Ports and ref. planes in CST Microwave Studio 57

Figure 4.23 Extracted effective parameters of Design A-1-(5) of Table 4.1 on page 31. (a) relative wave impedance, (b) refractive index, (c) relative permittivity, and (d) relative permeability. 59

Figure 4.24 Extracted effective parameters of Design A-2-(5) of Table 4.2 on page 34. (a) relative wave impedance, (b) refractive index, (c) relative permittivity, and (d) relative permeability. 60

Figure 4.25 Extracted effective parameters of Design A-3-(5) of Table 4.3 on page 37. (a) relative wave impedance, (b) refractive index, (c) relative permittivity, and (d) relative permeability. 61

Figure 4.26 Extracted effective parameters of Design A-4-(5) of Table 4.4 on page 40. (a) relative wave impedance, (b) refractive index, (c) relative permittivity, and (d) relative permeability. 62

Figure 5.1 Illustration of the e-beam evaporator's operation 63

Figure 5.2 Illustration of the profilometer's operation 64

Figure 5.3 A Cu layer deposited on a glass substrate 65

Figure 5.4 A SiO_2 layer deposited on a glass substrate 66

Figure 5.5 Cu/SiO_2/Cu layers deposited on a glass substrate 67

Figure 5.6 Schematic diagrams of the fabrication process 69

Figure 5.7 The fabricated Design A-1-(5) metamaterial on a glass substrate 69

Figure 6.1 Simulated and measured transmittances of the Design A-1-(5) metamaterial 72

Figure 6.2. SEM images of the fabricated Design A-1-(5) metamaterial 73

Figure 6.3. Simulated and measured transmittances of the Design A-3-(5) metamaterial 74

Figure 6.4. SEM images of the fabricated Design A-3-(5) metamaterial 75

Figure 7.1 Simulation for Cu re-attachment 77

Figure 7.2 Simulation of the Design A-3-(5) metamaterial based on the results of Figure 6.4 78

LIST OF TABLES

Table Page

Table 2.1 Plasma and damping frequencies of some metals [16] 22

Table 4.1 Thicknesses of dielectric and metallic layers 31

Table 4.2 Thicknesses of dielectric and metallic layers 34

Table 4.3 Thicknesses of dielectric and metallic layers 37

Table 4.4 Thicknesses of dielectric and metallic layers 40

Table 4.5 Thicknesses of dielectric and metallic layers 43

Table 4.6 Thicknesses of dielectric and metallic layers 46

Table 4.7 Thicknesses of dielectric and metallic layers 49

Table 4.8 Thicknesses of dielectric and metallic layers 50

Table 4.9 Thicknesses of dielectric and metallic layers 53

Table 5.1 Measured thicknesses of the Cu layer at the eight different locations shown in Figure 5.3 66

Table 5.2 Measured thicknesses of the SiO_2 layer at the eight different locations shown in Figure 5.4 67

Table 5.3 Measured thicknesses of the $Cu/SiO_2/Cu$ layers at the eight different locations shown in Figure 5.5 68

LIST OF ABBREVIATIONS

FIT	Finite Integration Technique
S-parameters	Scattering parameters
SEM	Scanning Electron Microscope
E-beam	Electron-beam

LIST OF SYMBOLS

English symbols

SiO_2	Silicon dioxide
MgF_2	Magnesium fluoride
Cu	Copper
$\vec{E}$	Electric field vector
E_0	Amplitude of electric field
$\vec{B}$	Magnetic field vector
B_0	Amplitude of magnetic field
$\vec{J}$	Electric current density vector
$\vec{P}$	Macroscopic electrical polarization vector
$\vec{k}$	Wavenumber vector
$\vec{r}$	Position vector
w	Angular frequency
w_p	Plasma frequency
w_0	Resonance frequency
t	Time
v	Light speed in matter
c	Light speed in vacuum
n	Refractive index
n_R	Real part of refractive index
n_I	Imaginary part of refractive index

m_e	Electron mass
z_r	Relative wave impedance
$Torr$	torr

Greek symbols

ρ	Electric charge density
ε	Absolute permittivity
ε_0	Vacuum permittivity
ε_r	Relative permittivity
ε_{eff}	Effective absolute permittivity
$\varepsilon_{eff,r}$	Effective relative permittivity
μ	Absolute permeability
μ_0	Vacuum permeability
μ_r	Relative permeability
γ	Damping frequency or collision frequency
σ_w	Frequency-dependent electrical conductivity
σ_{DC}	Static electrical conductivity
χ_e	Electric susceptibility
λ	Wavelength

Other symbols

Å	Ångström

1. INTRODUCTION

1.1 Metamaterials

When the wavelength of electromagnetic waves is much longer than the dimensions of a structured material that it propagates through, the material exhibits unusual electromagnetic properties compared to when the wavelength is much shorter than the dimensions [1]. With these unusual properties, the material behaves as if it were a uniform bulk material [1]. Metamaterials are artificial materials with those properties [2]. Although the name ends with 'material', it does not mean that a metamaterial is a homogeneous material such as SiO_2, MgF_2, or Cu. A metamaterial is a structured object made of a naturally existing material(s). The unusual electromagnetic properties of a metamaterial, therefore, originate from both its structure and the electromagnetic properties of its constituent natural materials.

With their unusual electromagnetic properties, metamaterials have exhibited extraordinary phenomena and applications such as negative-index refraction [3], unconventional flat lenses [4] at optical frequencies, power-dependent [5] and reconfigurable filters [6] at TV-microwave frequencies, and optical bandpass filters as studied in this thesis.

1.2 Diffraction in Sub-wavelength Structures

If the spacing and dimensions of a structured material's elements are much smaller than the incident wavelength of light, then high-order diffractions are evanescent and only the zeroth-

order diffraction survives [4], [7]. Consequently, metamaterials, which are based on sub-wavelength structures, do not produce high-order diffractions.

2. THEORY

2.1 Electromagnetic Waves

2.1.1 Maxwell's Equations in Materials

$$\left.\begin{array}{ll} (i)\ \nabla \cdot \vec{E}(\vec{r}) = \frac{\rho(\vec{r})}{\varepsilon} & (iii)\ \nabla \cdot \vec{B}(\vec{r}) = 0 \\ (ii)\ \nabla \times \vec{E}(\vec{r}) = -\frac{d\vec{B}(\vec{r})}{dt} & (iv)\ \nabla \times \vec{B}(\vec{r}) = \mu \vec{J}(\vec{r}) + \varepsilon\mu \frac{d\vec{E}(\vec{r})}{dt} \end{array}\right\} \quad (1)$$

where $\vec{E}(\vec{r})$: $electric\ field\ at\ space\ coordinate\ \vec{r}$

$\vec{B}(\vec{r})$: $magnetic\ field\ at\ space\ coordinate\ \vec{r}$

$\vec{J}(\vec{r})$: $electric\ current\ density\ at\ space\ coordinate\ \vec{r}$

$\rho(\vec{r})$: $electric\ charge\ density\ at\ space\ coordinate\ \vec{r}$

ε: permittivity of the material

μ: permeability of the material

The four equations provided above are Maxwell's equations (differential form) in SI units* [8]. According to (i) of Equation 1, the divergence of electric fields at a spatial point equals the electric charge density at that point divided by the permittivity of the material. (ii) of Equation 1 shows that the rotation of electric fields in space induces a time variation of magnetic fields nearby, and vice versa. (iii) of Equation 1 indicates there is no magnetic monopole; the N and S poles of

** This thesis is entirely based on SI units. However, some equations such as Maxwell's equations and plasma frequency equation (Equation 55) have a slightly different form in cgs units.*

magnetism always exist together*. (iv) of Equation 1 says that the rotation of magnetic fields in space induces an electric current and a time variation of electric fields nearby, and vice versa.

2.1.2 Maxwell's Equations in Vacuum

$$\left.\begin{array}{ll} (i)\ \nabla \cdot \vec{E}(\vec{r}) = 0 & (iii)\ \nabla \cdot \vec{B}(\vec{r}) = 0 \\ (ii)\ \nabla \times \vec{E}(\vec{r}) = -\frac{d\vec{B}(\vec{r})}{dt} & (iv)\ \nabla \times \vec{B}(\vec{r}) = \varepsilon_0 \mu_0 \frac{d\vec{E}(\vec{r})}{dt} \end{array}\right\} \quad (2)$$

Maxwell's equations listed in section 2.1.1 reduce to a simpler form in vacuum where the electric charge density and current density are zero ($\rho = \vec{J} = 0$) as shown in Equation 2.

2.1.3 Propagation of Electromagnetic Waves

Permittivity and permeability of materials are generally frequency-dependent, and they are treated as a tensor when the material is birefringent. Here vacuum is assumed to simply present how electromagnetic waves propagate in space.

Maxwell's equations indicate that the time variation of electric fields in space ($\frac{d\vec{E}(\vec{r})}{dt}$) induces magnetic fields nearby according to (iv) of Equation 2. If the time variation of the electric fields is not constant, in other words the electric field ($\vec{E}(\vec{r})$) is not linear with respect to time, then the induced magnetic fields also vary with time (where, therefore, $\frac{d\vec{B}(\vec{r})}{dt} \neq constant$). In this case, the time variation of the induced magnetic fields ($\frac{d\vec{B}}{dt}$) induces new electric fields nearby, and these induced electric fields also vary with time because of "$\nabla \times \vec{E} = -\frac{d\vec{B}}{dt} \neq$ constant" from (ii) of Equation

** If a magnetic monopole is found, then the humanity may have to change (iii) of Equation 1 [10].*

2. By (iv) of Equation 2 again, these induced time-dependent electric fields induce new magnetic fields nearby that are also time-dependent. These new induced time-dependent magnetic fields induce new time-dependent electric fields nearby by (ii) of Equation 2 again. These chain reactions occur over and over and the energy propagates in the form of electromagnetic waves. Part of this process is illustrated in Figure 2.1.

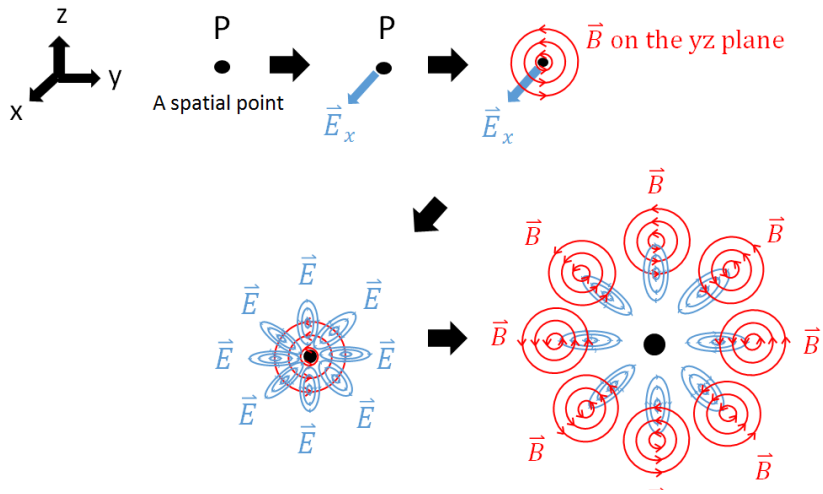

Figure 2.1 Illustration of electromagnetic wave propagation (reproduced from part of [11]). A time-varying electric field $\vec{E}_x$ applied at a spatial point P induces magnetic fields nearby that are rotating on the yz plane (here $\vec{E} \perp \vec{B}$). The induced magnetic fields induce new rotating electric fields nearby that are also perpendicular to the magnetic fields. These induced electric fields induce new rotating magnetic fields nearby and the same reaction happens over and over.

Figure 2.1 shows inter-induction of electric and magnetic fields only on two planes: the plane of the paper and the perpendicular plane to the paper. The same principles, however, apply to all other three-dimensional planes. One can see that the E and B fields propagate throughout space (all 360 solid angles, but not along the x and -x axes at P) when the same principles are applied to different planes. Therefore, Maxwell's equations mathematically explain the propagation of electromagnetic waves as well as the Huygens' principle, which states that every point on a wave front acts as a point source.

2.1.4 Electromagnetic Waves in Loss-free Dielectrics (J=0)

Here it is assumed that the dielectric medium has zero electrical conductivity and is not electrically charged so that $\vec{J} = \rho = 0$. Then Maxwell's equations of Equation 1 take a simpler form as shown in Equation 3 below.

$$\left.\begin{array}{ll} (i)\ \nabla \cdot \vec{E}(\vec{r}) = 0 & (iii)\ \nabla \cdot \vec{B}(\vec{r}) = 0 \\ (ii)\ \nabla \times \vec{E}(\vec{r}) = -\frac{d\vec{B}(\vec{r})}{dt} & (iv)\ \nabla \times \vec{B}(\vec{r}) = \varepsilon\mu \frac{d\vec{E}(\vec{r})}{dt} \end{array}\right\} \quad (3)$$

If we take the curl of (ii) *, then

$$\nabla \times \nabla \times \vec{E} = \nabla \times (-\frac{d\vec{B}}{dt}) \quad (4)$$

Suppose a harmonic plane wave and take the complex plane wave equations of $\vec{E}(\vec{r}, t) = \vec{E}_0 \cdot e^{i(\vec{k}\cdot\vec{r} - wt)}$ and $\vec{B}(\vec{r}, t) = \vec{B}_0 \cdot e^{i(\vec{k}\cdot\vec{r} - wt)}$** so that

$$\nabla \times \vec{E} = -\frac{d\vec{B}}{dt} = iw\vec{B} \quad (5)$$

and Equation 4 becomes

$$\nabla \times \nabla \times \vec{E} = \nabla \times \left(-\frac{d\vec{B}}{dt}\right) = iw \cdot \left(\nabla \times \vec{B}\right) \quad (6)$$

** This is an intuitive mathematical method that results in Equation 9.*

*** The complex wave notation with the Euler's formula gives an intuition to mathematically express loss and propagation of electromagnetic waves in media, which are physical (discussed in Chapter 2.2). Moreover, this mathematical notation provides convenience in dealing with waves (i.e. easy visualization of the superposition of waves with different amplitudes and phases on the complex plane).*

*** If one rather chooses to use $\vec{E}(\vec{r}, t) = \overrightarrow{E_0} \cdot e^{-i(\vec{k}\cdot\vec{r} - wt)}$ and $\vec{B}(\vec{r}, t) = \vec{B}_0 \cdot e^{-i(\vec{k}\cdot\vec{r} - wt)}$, some signs of other derived equations based on them might be flipped, but physical meanings are the same as long as one is consistent in using the same form.*

By (iv) of Equation 3, Equation 6 becomes

$$\nabla\times\nabla\times\vec{E} = iw\cdot\left(\varepsilon\mu\frac{d\vec{E}}{dt}\right) = w^2\varepsilon\mu\vec{E} \tag{7}$$

The Vector Laplacian (∇^2) is defined as

$$\nabla^2\vec{E} \equiv \left(\nabla^2\vec{E}_x, \nabla^2\vec{E}_{y,}\nabla^2\vec{E}_z\right) \equiv \nabla\left(\nabla\cdot\vec{E}\right) - \nabla\times(\nabla\times\vec{E}) \tag{8}$$

By inserting (i) of Equation 3 into Equation 8, Equation 7 can be represented by

$$\nabla^2\vec{E} = -w^2\varepsilon\mu\vec{E} \tag{9}$$

Through the same process, it is obtained

$$\nabla^2\vec{B} = -w^2\varepsilon\mu\vec{B} \tag{10}$$

Knowing that the vector operator "$\nabla\cdot$" can be replaced by "$i\vec{k}\cdot$" for the complex plane wave form $\vec{E}(\vec{r},t) = \vec{E}_0\cdot e^{i(\vec{k}\cdot\vec{r}\,-\,wt)}*$, the Vector Laplacian operator becomes

$$\nabla^2 = \nabla\cdot\nabla = i\vec{k}\cdot i\vec{k} = -\vec{k}\cdot\vec{k} \tag{11}$$

(note that the vector operator "$\nabla\cdot$" can be replaced by "$-i\vec{k}\cdot$" for the complex plane wave form of $\vec{E}(\vec{r},t) = \vec{E}_0\cdot e^{-i(\vec{k}\cdot\vec{r}\,-\,wt)}$)

By inserting Equation 11 into Equation 9, it is obtained

$$\nabla^2\vec{E} = -w^2\varepsilon\mu\vec{E} = -\vec{k}\cdot\vec{k}\vec{E} \tag{12}$$

$$\begin{aligned} * \nabla\cdot\vec{E} &= \left(\frac{d}{dx}[E_{0x}\cdot e^{i(k_x\cdot x\,-\,wt)}], \frac{d}{dy}[E_{0y}\cdot e^{i(k_y\cdot y\,-\,wt)}, \ \frac{d}{dz}[E_{0z}\cdot e^{i(k_z\cdot z\,-\,wt)}\right) \\ &= \left(ik_x[E_{0x}\cdot e^{i(k_x\cdot x\,-\,wt)}], \ ik_y[E_{0y}\cdot e^{i(k_y\cdot y\,-\,wt)}, \ ik_z\left[E_{0z}\cdot e^{i(k_z\cdot z\,-\,wt)}\right)\right. \\ &= i\vec{k}\cdot\vec{E} \end{aligned}$$

From Equation 12, it is obtained

$$k^2 = w^2 \varepsilon \mu \tag{13}$$

and therefore

$$k = w\sqrt{\varepsilon \mu} \tag{14}$$

Also, by applying

$$\varepsilon \mu = \frac{1}{v^2} = \left(\frac{n}{c}\right)^2 \tag{15}$$

to Equation 13 and 14, it is obtained

$$k^2 = \frac{w^2 n^2}{c^2} \tag{16}$$

and

$$k = \frac{wn}{c} \tag{17}$$

(where c is the speed of light in vacuum)

2.1.5 Electromagnetic Waves in Lossy Dielectrics or Conductors (J≠0)

Maxwell's equations in materials are as shown in Equation 18 below.

$$\left.\begin{array}{ll} (i)\ \nabla \cdot \vec{E}(\vec{r}) = \frac{\rho(\vec{r})}{\varepsilon} & (iii)\ \nabla \cdot \vec{B}(\vec{r}) = 0 \\ (ii)\ \nabla \times \vec{E}(\vec{r}) = -\frac{d\vec{B}(\vec{r})}{dt} & (iv)\ \nabla \times \vec{B}(\vec{r}) = \mu \vec{J}(\vec{r}) + \varepsilon \mu \frac{d\vec{E}(\vec{r})}{dt} \end{array}\right\} \tag{18}$$

Conductors have free electrons that may produce a non-zero value of the electric charge density ρ at a spatial point in an oscillating electromagnetic wave. This makes the left-hand of (i) of Equation 18 non-zero, which results in more complicated math compared to that of Chapter 2.1.4. It is assumed that, in the incidence of electromagnetic waves, free electrons in conductors immediately dissipate to the edges so that the electric charge density (ρ) is always zero everywhere inside the conductor [12]. For lossy dielectrics, $\rho = 0$ is assumed, which is reasonable because no significant current flows in dielectrics [13]. Thus, for both conductors and dielectrics, Maxwell's equations of Equation 18 can be represented as follows.

$$\left.\begin{array}{ll} (i)\ \nabla \cdot \vec{E}(\vec{r}) = 0 & (iii)\ \nabla \cdot \vec{B}(\vec{r}) = 0 \\ (ii)\ \nabla \times \vec{E}(\vec{r}) = -\frac{d\vec{B}(\vec{r})}{dt} & (iv)\ \nabla \times \vec{B}(\vec{r}) = \mu\vec{J}(\vec{r}) + \varepsilon\mu\frac{d\vec{E}(\vec{r})}{dt} \end{array}\right\} \quad (19)$$

Using the same plane wave notations of $\vec{E}(\vec{r},t) = \vec{E}_0 \cdot e^{i(\vec{k}\cdot\vec{r} - wt)}$ and $\vec{B}(\vec{r},t) = \vec{B}_0 \cdot e^{i(\vec{k}\cdot\vec{r} - wt)}$ as in Chapter 2.1.4 and the frequency-dependent electrical conductivity σ_w*,

$$\nabla\times\nabla\times\vec{E} = \nabla\times\left(-\frac{dB}{dt}\right) \quad (20\text{-}1)$$

$$= iw(\nabla\times\vec{B}) \quad (20\text{-}2)$$

$$= iw(\mu\vec{J} + \varepsilon\mu\frac{d\vec{E}}{dt}) \quad (20\text{-}3)$$

$$= iw(\mu\sigma_w\vec{E} + \varepsilon\mu(-iw\vec{E})) \quad (20\text{-}4)$$

$$= iw\mu(\sigma_w - iw\varepsilon)\vec{E} \quad (20\text{-}5)$$

** Generally, electrical conductivity of materials depends on the frequency of the incident light. The subscript 'w' represents this property. The frequency-dependent property of electrical conductivity is further discussed in Chapter 2.2.4.*

Define the complex effective permittivity* of lossy/conducting media as

$$\varepsilon_{eff} = \varepsilon + i\frac{\sigma_w}{w} \quad [13]\ [15] \text{ (terms on the right hand were defined previously)} \tag{21}$$

By inserting Equation 21 into Equation 20-5, Equation 20-5 becomes

$$\nabla\times\nabla\times\vec{E} = w^2\varepsilon_{eff}\mu\vec{E} \tag{22}$$

which has the same form as Equation 7.

By the definition of Vector Laplacian, Equation 22 is given by

$$\nabla^2\vec{E} = -w^2\varepsilon_{eff}\mu\vec{E} \tag{23}$$

which has the same form as Equation 9.

By applying Equation 11 to Equation 23, it is obtained

$$k^2 = w^2\varepsilon_{eff}\mu \tag{24}$$

and

$$k = w\sqrt{\varepsilon_{eff}\mu} \tag{25}$$

Assuming $\mu \approx \mu_0$, the refractive index of the lossy/conducting medium is represented by

$$n = \sqrt{(\varepsilon_{eff,r})(\mu_r)} \approx \sqrt{\varepsilon_{eff,r}} = \sqrt{\frac{\varepsilon_{eff}}{\varepsilon_0}} \quad [14] \tag{26}$$

** Permittivity values of loss-free and lossy media differ; the permittivity of loss-free media is a purely real number while the permittivity of lossy media is a complex number (also called the effective permittivity [14]). Here the notation "ε_{eff}" is used to avoid confusion with 'ε' in Chapter 2.1.4 which does not contain an imaginary part. It is inferred that the electric current causes loss of electromagnetic waves in matter. Note that the notation 'effective' or subscript 'eff' is omitted or replaced by other words in some literature such as [16] and [17].*

By applying Equation 26 to Equation 24, it is obtained

$$k^2 = \frac{w^2 n^2}{c^2} \tag{27-1}$$

$$= \frac{w^2 \varepsilon_{eff,r}}{c^2} \tag{27-2}$$

and by the Equation 21, it is obtained

$$k^2 = \frac{w^2}{c^2} \left(\frac{\varepsilon}{\varepsilon_0} + i\frac{\sigma_w}{\varepsilon_0 w}\right) \tag{27-3}$$

Therefore,

$$k = \frac{wn}{c} \tag{28-1}$$

$$= \frac{w}{c}\sqrt{\left(\frac{\varepsilon}{\varepsilon_0} + i\frac{\sigma_w}{\varepsilon_0 w}\right)} \tag{28-2}$$

From Equations 28-1 and 28-2, the complex refractive index of the lossy dielectric/conducting media becomes

$$n = (n_R + in_I) = \sqrt{\left(\frac{\varepsilon}{\varepsilon_0} + i\frac{\sigma_w}{\varepsilon_0 w}\right)} \tag{29}$$

2.2 Optical Properties of Materials

2.2.1 Overview

Generally, permittivity, permeability, and electrical conductivity of a material vary with the frequency of the incident electromagnetic wave, which is called the frequency-dependent

property. Hence, by Equation 26, the refractive index also becomes frequency-dependent. This leads to different interactions between the material and wave depending on the frequency of the wave (such as different loss, speed of light, or reflectance). This frequency-dependent property of refractive index is also called "dispersion". In this section, how the wave frequency and material constants relate to dispersion is described.

2.2.2 Dispersion in General Dielectrics (Lorentz model)

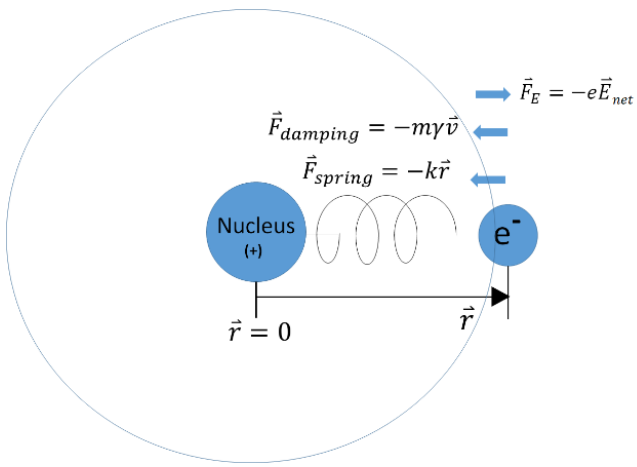

Figure 2.2 Lorentz forced and damped oscillation model for dielectric media [9].

In this work, the term "general dielectrics" is used to refer to both loss-free and lossy dielectrics. In Figure 2.2, $\vec{E}_{net}$ represents the vector sum of the incident electric field from an external source and the electric fields due to surrounding dipoles near the electron [9]. That is,

$$\vec{E}_{net} = \vec{E}_{incident\ wave} + \vec{E}_{surrounding\ dipoles} \tag{30}$$

If an electric field is incident on an area of matter, it generates electric dipoles out of neighboring atoms. These dipoles produce additional electric fields that affect the area in return. This phenomenon is also implied in the polarization equation below

$$\vec{P} = \varepsilon_0 \chi_e \vec{E}_{net} \tag{31}$$

(where χ_e is the electric susceptibility of the material)

From the Lorentz oscillation model, it is given

$$\vec{F}_{net} = m_e \frac{d^2\vec{r}}{dt^2} = \vec{F}_E + \vec{F}_{damping} + \vec{F}_{spring} \tag{32}$$

which leads to

$$m_e \frac{d^2\vec{r}}{dt^2} = -e\vec{E}_{net} - m_e\gamma \frac{d\vec{r}}{dt} - k_{spring}\vec{r} \tag{33}$$

(where γ is the damping frequency ([1/s] or [rad/s]) of the oscillation system and m_e is the mass of an electron). The force $F_m = q\vec{v}\times\vec{B}$ exerting on the electron due to the magnetic fields of the wave is ignored in that $B = \frac{E}{c}$, which leads to $|F_E| = \left|q\vec{E}\right| \gg |F_m| = \left|q\vec{v}\times\frac{\vec{E}}{c}\right|$ [18]. Assuming harmonic fields and oscillation,

$$\vec{E}_{net} = \vec{E}_0 \cdot e^{-i\omega t} \tag{34}$$

$$\vec{r} = \vec{r}_0 \cdot e^{-i\omega t} \tag{35}$$

By inserting Equation 34 and 35 into Equation 33, it is obtained

$$-e\vec{E}_{net} + m_e\gamma iw\vec{r} - k_{spring}\vec{r} = -w^2 m_e\vec{r} \tag{36}$$

Solving Equation 36 for $\vec{r}$,

$$\vec{r} = \frac{\frac{e}{m_e}\vec{E}_{net}}{w^2 - \frac{k_{spring}}{m_e} + iw\gamma} \tag{37}$$

Applying the definition of (electric) resonance frequency of the system

$$w_0 = \sqrt{\frac{k_{spring}}{m_e}} \tag{38}$$

to Equation 37,

$$\vec{r} = \frac{\frac{e}{m_e}\vec{E}_{net}}{(w^2 - w_0^2) + iw\gamma} \tag{39}$$

Polarization per unit volume is written as

$$\vec{P} = -Ne\vec{r} \tag{40}$$

(where *N* is the number of dipoles per unit volume)

From the combination of Equation 39 and 40, it is obtained

$$\vec{P} = \frac{\frac{Ne^2}{m_e}\vec{E}_{net}}{(w_0^2 - w^2) - iw\gamma} \tag{41}$$

By equating Equation 31 and 41 and defining the plasma frequency $w_p = \sqrt{\frac{Ne^2}{m_e\varepsilon_0}}$,

$$\chi_e = \frac{\frac{Ne^2}{m_e\varepsilon_0}}{(w_0^2 - w^2) - iw\gamma} \tag{42-1}$$

$$= \frac{w_p^2}{(w_0^2 - w^2) - iw\gamma} \tag{42-2}$$

Assuming $\varepsilon_r\mu_r \approx \varepsilon_r$ and by the relation $\varepsilon_r = 1 + \chi_e$, the refractive index of the dielectric medium becomes

$$n^2 \approx \varepsilon_r = 1 + \chi_e \tag{43}$$

From Equations 42-2 and 43, it is obtained

$$* \, n^2 = (n_R + in_I)^2 = 1 + \frac{w_p^2}{(w_0^2 - w^2) - iw\gamma} \tag{44}$$

$$n = \sqrt{1 + \frac{w_p^2}{(w_0^2 - w^2) - iw\gamma}} \tag{45}$$

By inserting Equation 44 into Equation 27-1, it is obtained

$$* \, k^2 = (k_R + ik_I)^2 = \frac{w^2}{c^2}\left(1 + \frac{w_p^2}{(w_0^2 - w^2) - iw\gamma}\right) \tag{46}$$

$$k = \frac{w}{c}\sqrt{\left(1 + \frac{w_p^2}{(w_0^2 - w^2) - iw\gamma}\right)} \tag{47}$$

Using the complex effective permittivity in Chapter 2.1.5, it is obtained

$$n^2 = \varepsilon_{eff,r} \tag{48}$$

Therefore,

$$k^2 = \frac{w^2}{c^2}\left(\frac{\varepsilon}{\varepsilon_0} + i\frac{\sigma_w}{w\varepsilon_0}\right) \tag{49}$$

By inserting $\frac{1}{c^2} = \varepsilon_0\mu_0$ into Equation 49,

$$k^2 = \frac{w^2\varepsilon_r}{c^2} + iw\mu_0\sigma_w \tag{50}$$

** Here the complex notations of $n = n_R + in_I$ and $k = k_R + ik_I$ are used. If $n = n_R - in_I$ and $k = k_R - ik_I$ are used, some signs of derived equations based on them might be flipped, but physical meanings remain the same as long as one is consistent in using the same notations.*

By inserting $\varepsilon_r = 1 + \chi_e$ into Equation 50, it is obtained

$$k^2 = \frac{w^2(1+\chi_e)}{c^2} + iw\mu_0\sigma_w \tag{51}$$

So far, it has been assumed that each atom in dielectric media has only one electron or all electrons behave the same way. This resulted in a single value of the resonance frequency and damping frequency [9] [18]. Considering that the electrons may have different values of resonance and damping frequencies, Equation 39 can be re-written with the fraction term f_j, which ranges from 0 to 1, as follows.

$$\vec{r} = \frac{e}{m_e}\vec{E}_{net}\sum_j \frac{f_j}{(w^2 - w_j^2) + iw\gamma_j} \quad [9]\ [18] \tag{52}$$

Thus, Equation 44 changes to

$$n^2 = 1 + \frac{Ne^2}{m_e\varepsilon_0}\sum_j \frac{f_j}{\left(w_j^2 - w^2\right) - iw\gamma_j} \tag{53}$$

Figures 2.3 shows some optical properties of silicon dioxide as a function of the wavelength -plots were generated by Maple as shown in Appendix A.

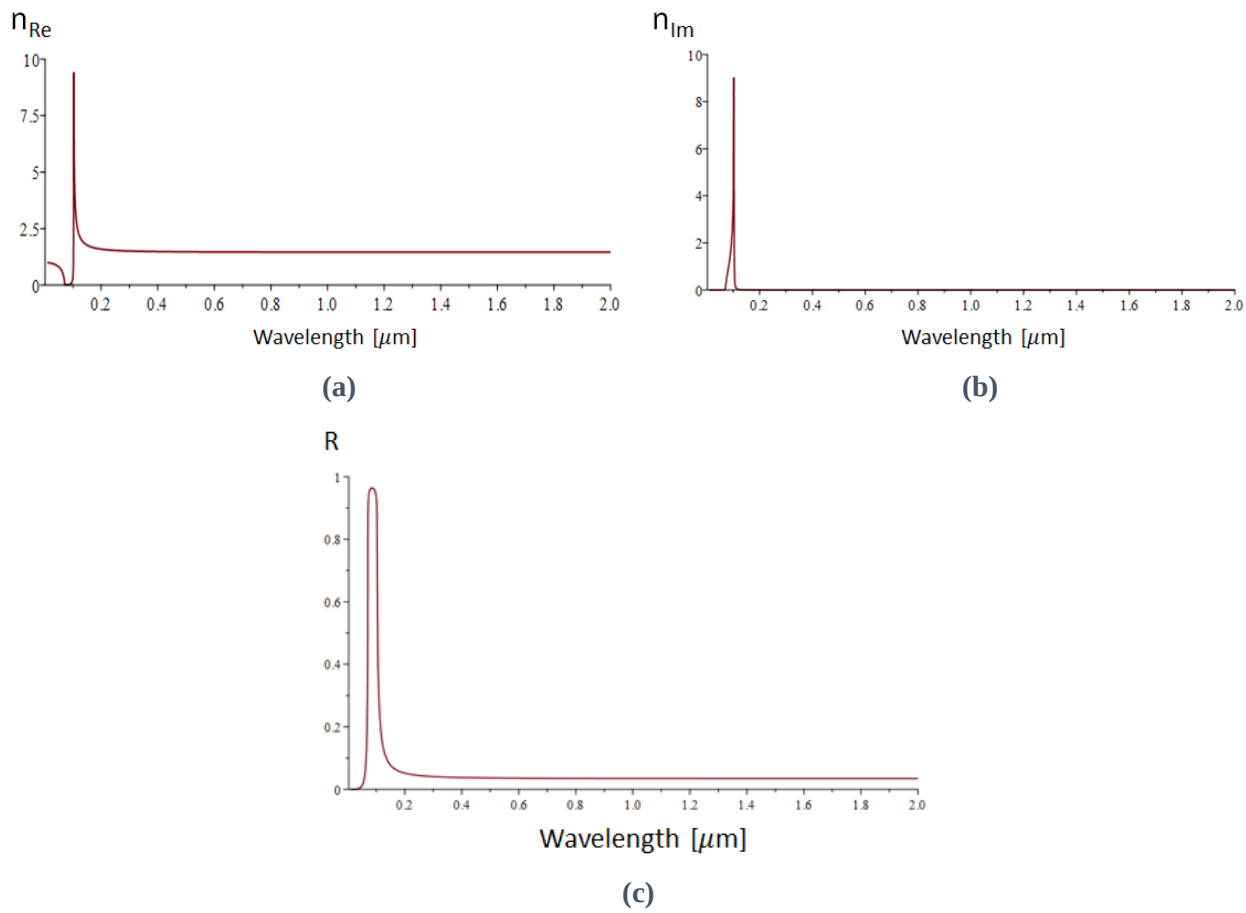

Figure 2.3 Optical properties of SiO_2: (a) real part and (b) imaginary part of the refractive index, and (c) reflectance. Of the refractive index, the real part meets the inflection point and imaginary part peaks at the resonance wavelength 0.103 μm (here a single resonance frequency was employed as shown in Appendix A).

2.2.3 Dispersion in Conductors (Drude model)

For conductors, the effects of atomic electrons (those bound to a nucleus) are ignored because free electrons dominate their electromagnetic properties [18]. Thus, compared to the Lorentz model previously, the spring force of the conductor's oscillation system is assumed to be zero ($\vec{F}_{spring} = 0$). Due to this fact, for the Drude model, Equation 44 becomes

(54)

$$n^2 = 1 - \frac{\frac{Ne^2}{m_e \varepsilon_0}}{w^2 + iw\gamma}$$

where N is the number of free electrons per unit volume. Define the plasma frequency of the medium as

$$w_p = \sqrt{\frac{Ne^2}{m_e \varepsilon_0}} \tag{55}$$

Then we obtain

$$n^2 = 1 - \frac{w_p^2}{w^2 + iw\gamma} \tag{56}$$

$$k^2 = \frac{w^2}{c^2}\left(1 - \frac{w_p^2}{w^2 + iw\gamma}\right) \tag{57}$$

Using the complex effective permittivity in Chapter 2.1.5, Equation 57 is also given by

$$k^2 = \frac{w^2}{c^2}\left(\frac{\varepsilon}{\varepsilon_0} + i\frac{\sigma_w}{w\varepsilon_0}\right) \tag{58}$$

By inserting $\frac{1}{c^2} = \varepsilon_0 \mu_0$ into Equation 58, it is obtained

$$k^2 = \frac{w^2 \varepsilon_r}{c^2} + iw\mu_0 \sigma_w \tag{59}$$

By inserting $\varepsilon_r = 1 + \chi_e$ into Equation 59, it is obtained

$$k^2 = \frac{w^2(1 + \chi_e)}{c^2} + iw\mu_0 \sigma_w \tag{60}$$

which is the same form as Equation 51 of dielectric media. If the electric susceptibility of the conductor is ignored ($\chi_e \approx 0$), Equation 60 becomes

$$k^2 = \frac{w^2}{c^2} + iw\mu_0\sigma_w \tag{61}$$

Figures 2.4 shows some optical properties of copper as a function of the wavelength -plots were generated by Maple as shown in Appendix B.

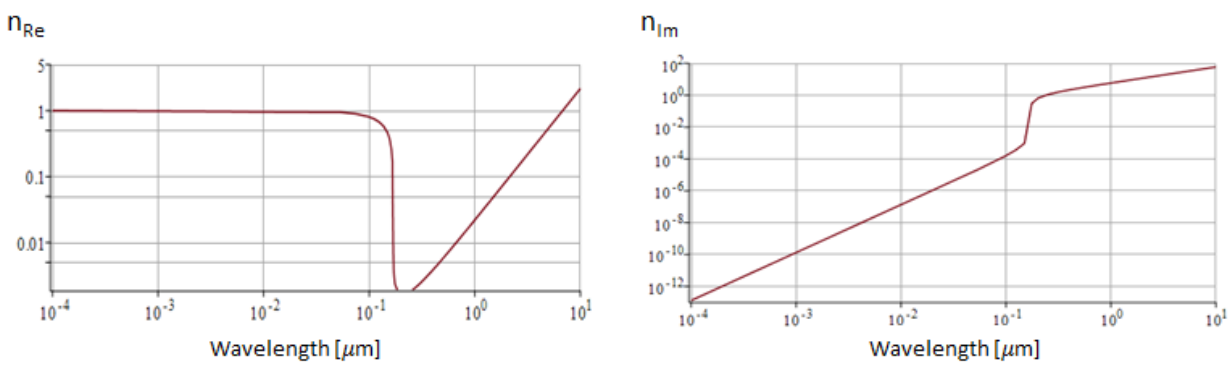

(a)

(b)

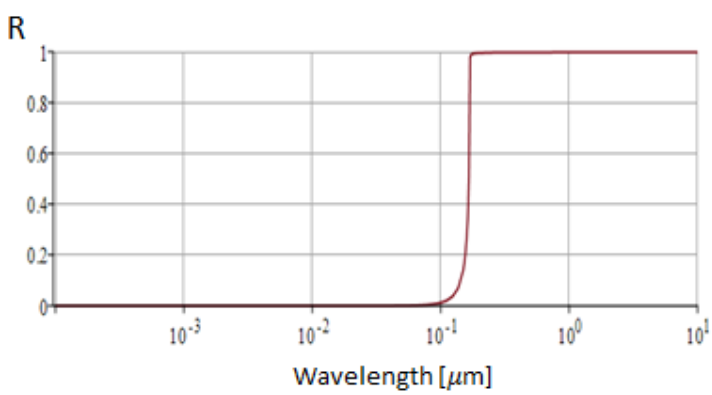

(c)

Figure 2.4 Optical properties of Cu: (a) real part and (b) imaginary part of the refractive index, and (c) reflectance. At near the plasma wavelength (0.168 μm), the real part of refractive index drops down close to 0 and the reflectance dramatically changes between approximately 0 and 1.

2.2.4 Frequency-dependent Electrical Conductivity in Conductors (Drude model) [19]

The spring force ($\vec{F}_{spring}$) in the Drude model is ignored as discussed in Chapter 2.2.3. Thus, for conductors, Equation 33 becomes

$$m_e \frac{d^2\vec{r}}{dt^2} = -e\vec{E} - m_e\gamma\frac{d\vec{r}}{dt} \tag{62}$$

Re-write Equation 62 as

$$m_e \frac{d\vec{v}}{dt} + m_e\gamma\vec{v} = -e\vec{E} \tag{63}$$

(where $\vec{v}$ is the drift velocity of free electrons in the conductor)

By inserting

$$\vec{v} = \frac{-\vec{J}}{Ne} \tag{64}$$

(where N *and* $\vec{J}$ are the number density of free electrons and electric current density respectively) into Equation 63, it is obtained

$$\frac{d\vec{J}}{dt} + \gamma\vec{J} = (\frac{Ne^2}{m_e})\vec{E} \tag{65}$$

Assuming $\vec{E} = \vec{E}_0 e^{-i\omega t}$ and $\vec{J} = \vec{J}_0 e^{-i\omega t}$, Equation 65 becomes

$$(-iw + \gamma)\vec{J} = (\frac{Ne^2}{m_e})\vec{E} \tag{66}$$

If $w = 0$, the current density is given by

$$\vec{J} = \left(\frac{Ne^2}{m_e\gamma}\right)\vec{E} = \sigma_{DC}\vec{E} \tag{67}$$

Accordingly, the static electrical conductivity (when $w = 0$) is

$$\sigma_{DC} = \left(\frac{Ne^2}{m_e\gamma}\right) \tag{68}$$

and the frequency-dependent current density is represented by

$$\vec{J} = \left[\frac{\sigma_{DC}}{1 - \left(\frac{iw}{\gamma}\right)}\right]\vec{E} = \sigma_w\vec{E} \tag{69}$$

Therefore, the frequency-dependent electrical conductivity is given by

$$\sigma_w = \frac{\sigma_{DC}}{1 - \left(\frac{iw}{\gamma}\right)} \tag{70}$$

Also, by inserting Equation 68 into Equation 55, another expression of a conductor's plasma frequency w_p is obtained as

$$w_p{}^2 = \frac{\gamma\sigma_{DC}}{\varepsilon_0} = \gamma\sigma_{DC}c^2\mu_0 \tag{71}$$

2.2.5 Values of Plasma and Damping Frequencies of Conductors

Plasma frequency and damping frequency (or collision frequency) values of some metals are shown in Table 2.1. Strictly speaking, the unit of damping frequency is defined as [1/s] [20]. In some literature, however, the unit [1/s] of damping frequency is replaced by [rad/s] without conversion of the value by multiplying 2π [20]. Therefore, both [1/s] and [rad/s] are written in Table 2.1 to avoid confusion. However, 2π must be multiplied when converting a plasma frequency value in [1/s] to the value in [rad/s] because $w = 2\pi f$.

Table 2.1 Plasma and damping frequencies of some metals [16] (note that the reference is based on cgs units).

	w_p [rad/s]	γ [1/s] or [rad/s]
Al	2.2431E+16	1.24407E+14
Co	6.03187E+15	5.56063E+13
Cu	1.12344E+16	1.37979E+13
Au	1.37225E+16	4.05266E+13
Fe	6.22037E+15	2.77089E+13
Pb	1.11967E+16	3.07248E+14
Mo	1.13475E+16	7.76604E+13
Ni	7.42674E+15	6.63506E+13
Pd	8.29382E+15	2.33735E+13
Pt	7.82258E+15	1.05181E+14
Ag	1.37037E+16	2.73319E+13
Ti	3.82647E+15	7.20055E+13
V	7.84143E+15	9.21745E+13
W	9.74524E+15	9.17976E+13

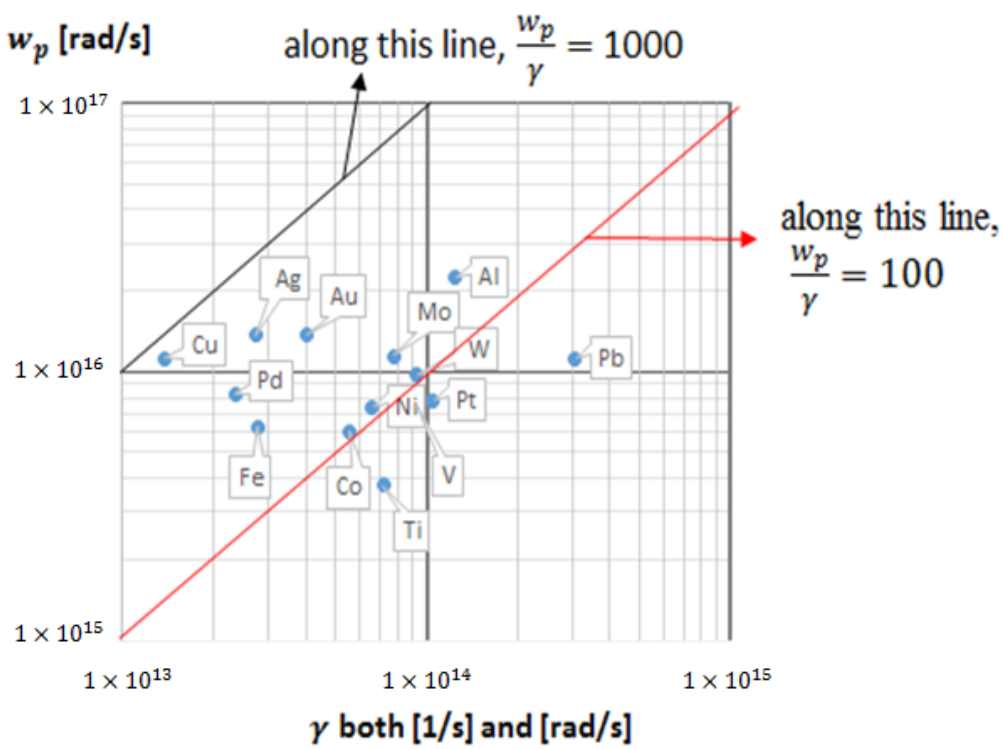

Figure 2.5 Plasma frequency vs. damping frequency of some metals (the plot is produced based on Table 2.1).

3. DESIGNS AND PARAMETERS

3.1 Design A

The fishnet structure [21] [22] was selected as the first design. Figure 3.1 shows parameters of the fishnet-structured metamaterials defined throughout this work.

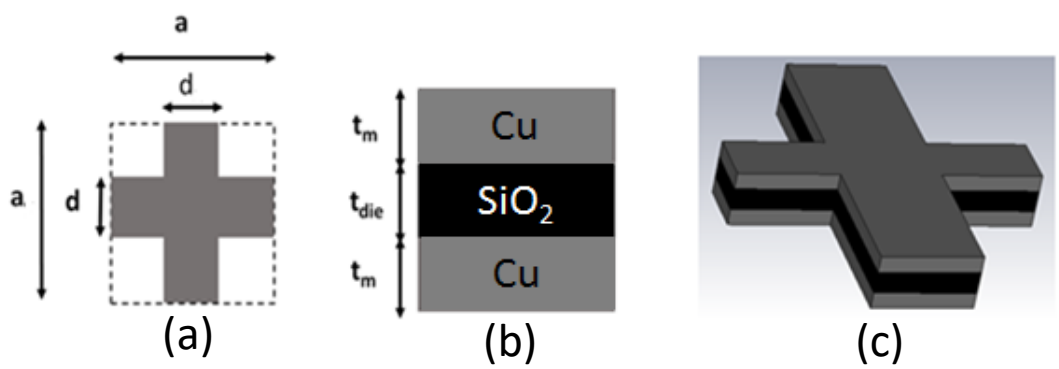

Figure 3.1 Parameters of Design A metamaterials. (a): Top-view of the unit cell of the metamaterial (empty part is air). Coordinate centers of the horizontal and vertical elements are the same. (b): Stacking sequence and thicknesses of the constituent materials. (c): Oblique-view of the unit cell.

3.2 Design B

Figure 3.2 shows parameters of the Design B defined throughout this work.

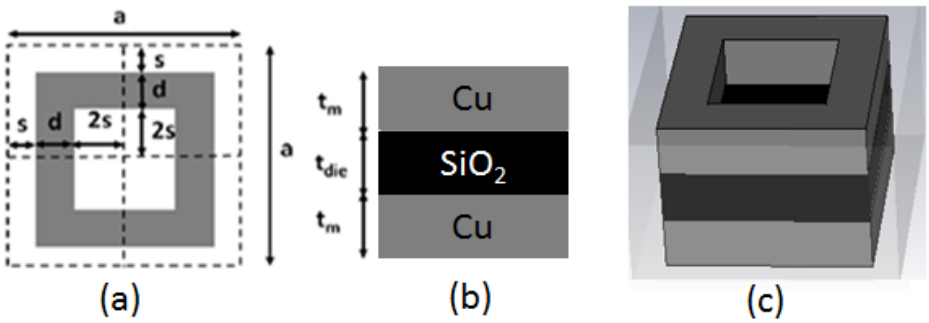

Figure 3.2 Parameters of Design B metamaterials. (a): Top-view of the unit cell of the metamaterial (empty part is air and $s + d + 2s = \frac{a}{2}$.). (b): Stacking sequence and thicknesses of the constituent materials. (c): Oblique-view of the unit cell.

3.3 Design C

Figure 3.3 shows parameters of the Design C defined throughout this work.

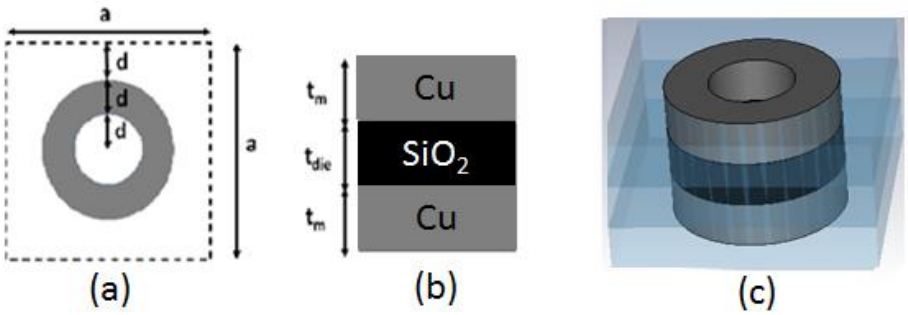

Figure 3.3 Parameters of Design C metamaterials. (a): Top-view of the unit cell (empty part is air). (b): Stacking sequence and thicknesses of the constituent materials. (c): Oblique-view of the unit cell.

3.4 Design D

Figure 3.4 shows parameters of the Design D defined throughout this work.

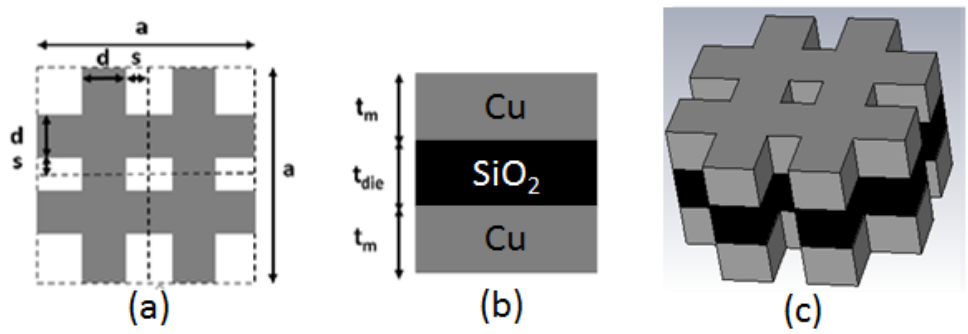

Figure 3.4 Parameters of Design D metamaterials. (a): Top-view of the unit cell (empty part is air). (b): Stacking sequence and thicknesses of the constituent materials. (c): Oblique-view of the unit cell.

3.5 Design E

Figure 3.5 shows parameters of the Design E defined throughout this work.

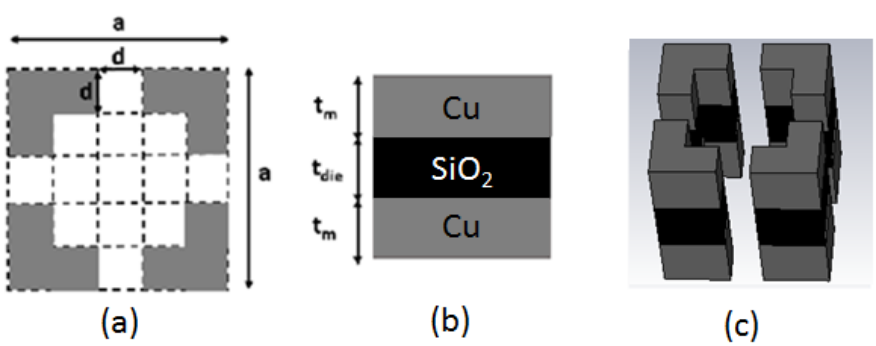

Figure 3.5 Parameters of Design E metamaterials. (a): Top-view of the unit cell (empty part is air). (b): Stacking sequence and thicknesses of the constituent materials. (c): Oblique-view of the unit cell.

3.6 Design F

Figure 3.6 shows parameters of the Design F defined throughout this work. The structure of Design F is opposite to that of Design E.

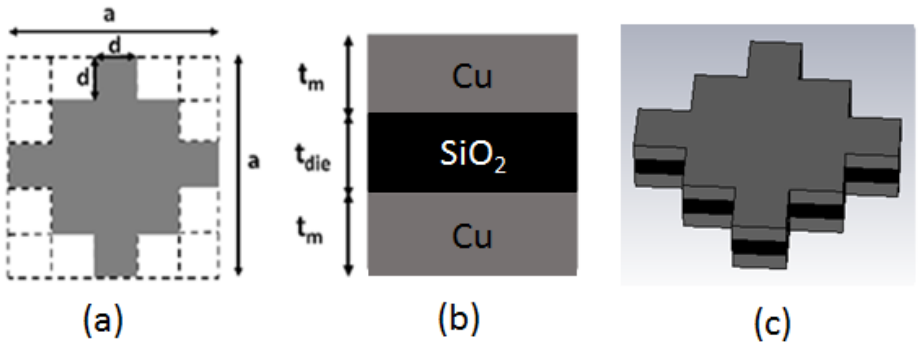

Figure 3.6 Parameters of Design F metamaterials. (a): Top-view of the unit cell (empty part is air). (b): Stacking sequence and thicknesses of the constituent materials. (c): Oblique-view of the unit cell.

The unit cells of the six designs above are all symmetric with respect to x and y axes that are originating from the center of the unit cell (note that the z axis is perpendicular to the paper). These symmetric designs were chosen not to produce a difference between the TE and TM mode of the incident wave. The both top and bottom metallic layers of a unit cell were chosen to be the same metal, expecting the same results regardless of which face of the metamaterial the light is incident on. Then, copper and silicon dioxide were selected for the constituent materials, considering their cheaper price and slower oxidation rate.

4. SIMULATION

4.1 Computational Electromagnetism: Finite Integration Technique

Finite Integration Technique (FIT) is a numerical method for computational electromagnetic simulation. The FIT solves electromagnetic problems by discretizing space under electromagnetic effects and applying Maxwell's equations to all those discretized sections [23] as described in Figure 4.1. The time domain solver in CST Microwave Studio uses the FIT [23].

$$\left.\begin{aligned} &\oint_{\partial A} \vec{E}\cdot d\vec{s} = -\int_{A} \frac{\partial \vec{B}}{\partial t}\cdot d\vec{A}\ , && \oint_{\partial A} \vec{H}\cdot d\vec{s} = \int_{A}\left(\frac{\partial \vec{D}}{\partial t}+\vec{J}\right)\cdot d\vec{A} \\ &\oint_{\partial V} \vec{D}\cdot d\vec{A} = \int_{V} \rho\, dV\ , && \oint_{\partial V} \vec{B}\cdot d\vec{A} = 0\ . \end{aligned}\right\} \quad (72) \qquad [23]$$

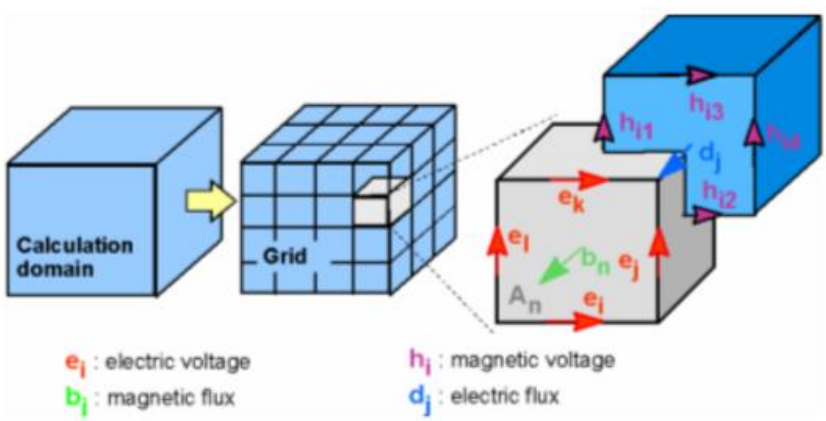

Figure 4.1 Discretization for FIT with hexahedral meshes [23].

4.2 Simulation Method

1) Defining Optical Property Values of Materials

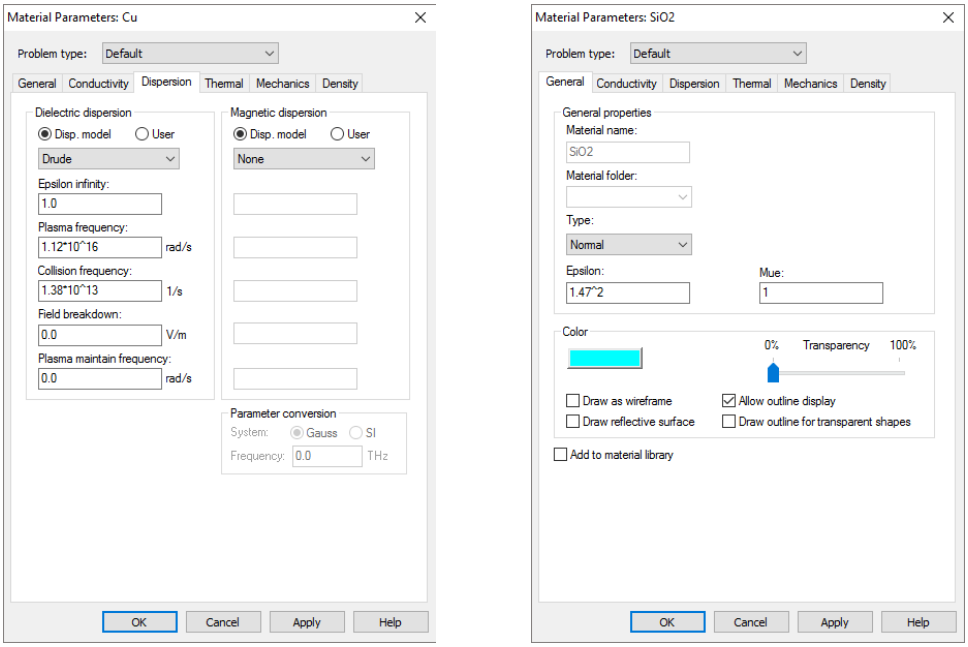

Figure 4.2 Values of optical properties entered in CST Microwave Studio. (Left: Cu, right: SiO_2)

Reflectance and transmittance of Cu/SiO_2/Cu metamaterials of the designs in Chapter 3 were studied with their varying parameters to explore their performance variation as a function of the parameter. Optical property values of Cu are employed from Table 2.1 to represent its dispersion. A single mean value 1.47 is employed for the SiO_2's refractive index over the wavelengths of 400 nm ~ 1500 nm [24] for ease of defining values in the software since SiO_2 exhibits little variation of its refractive index over those wavelengths.

For dielectric media, from Chapter 2.2.2, the complex-valued relative permittivity is

$$\varepsilon_r = 1 + \frac{w_p^2}{(w_0^2 - w^2) - iw\gamma} \tag{73}$$

Define the relative epsilon static $(\varepsilon_{s,r})$* with the relative epsilon infinity $(\varepsilon_{\infty,r})$* as

$$\varepsilon_{s,r} = \varepsilon_{\infty,r} + \frac{{w_p}^2}{{w_0}^2} \quad [25] \tag{74}$$

(where $\varepsilon_{s,r} = \varepsilon_r(w \to 0) = \frac{\varepsilon_r}{\varepsilon_0}$, $\varepsilon_{\infty,r} = \varepsilon_r(w \to \infty) = \frac{\varepsilon_\infty}{\varepsilon_0}$).

If $\varepsilon_{\infty,r} = 1$, Equation 74 becomes

$$\varepsilon_{s,r} = 1 + \frac{{w_p}^2}{{w_0}^2} \tag{75}$$

Then Equation 73 can be represented by

$$\varepsilon_r = \varepsilon_{\infty,r} + \frac{(\varepsilon_{s,r} - \varepsilon_{\infty,r})w_0^2}{(w_0^2 - w^2) - iw\gamma} \quad [25] \tag{76}$$

For conducting media, from Chapter 2.2.3, the complex-valued relative (effective) permittivity is

$$\varepsilon_{eff,r} = 1 - \frac{w_p^2}{w^2 + iw\gamma} \tag{77}$$

If $\varepsilon_{\infty,r} = 1$, Equation 77 becomes

$$\varepsilon_{eff,r} = \varepsilon_{\infty,r} - \frac{w_p^2}{w^2 + iw\gamma} \quad [20] \tag{78}$$

where often $\varepsilon_{\infty,r} = 1$ is assumed [26] and is used for the simulation work.

** In literature such as [20], [25], and [26], $\varepsilon_{s,r}$ and $\varepsilon_{\infty,r}$ are notated without the subscript 'r' even though they are relative values. However, here the subscript 'r' is written to avoid confusion.*

2) Excitation of the metamaterial with electromagnetic waves

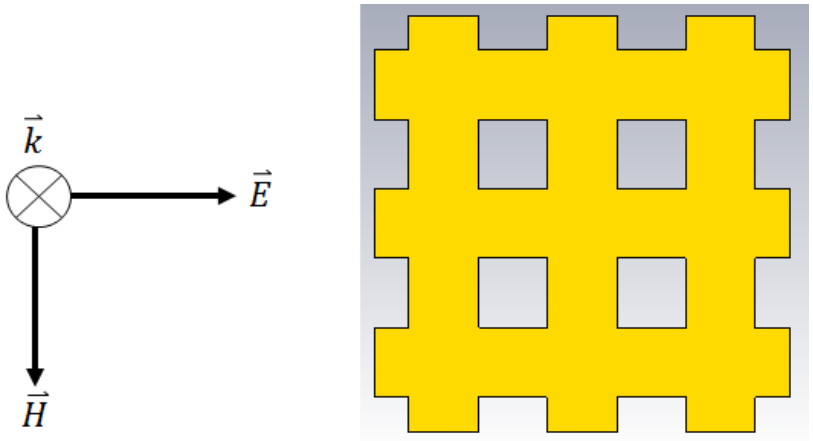

Figure 4.3 Incident light and a top-view scheme of a metamaterial.

Boundary conditions were used for a unit cell to represent the plane wave of Figure 4.3 as the excitation signal. The polarization and propagation direction of the incident light are shown in Figure 4.3. Although the object in Figure 4.3 is a fishnet-structured metamaterial, all designs in Chapter 3 were simulated with the same conditions as in Figure 4.3. Plus, all metamaterials in this study are symmetric and at normal incidence, hence the TE or TM mode of the incident wave does not affect their simulation results. Also, excitation ports (the planes where the input and output waves are evaluated for their magnitude and phase) were defined with a distance from the surface of the metamaterial so that the ports exist in the region where the input and output waves act as a plane wave.

4.3 Parameter Study and Simulation Results

4.3.1 Design A

1) When a = 300 nm and d = 150 nm

Table 4.1 Thicknesses of dielectric and metallic layers.

t_{die} [nm] / t_m [nm]	70	75	80
20	(1)	(4)	(7)
25	(2)	(5)	(8)
30	(3)	(6)	(9)

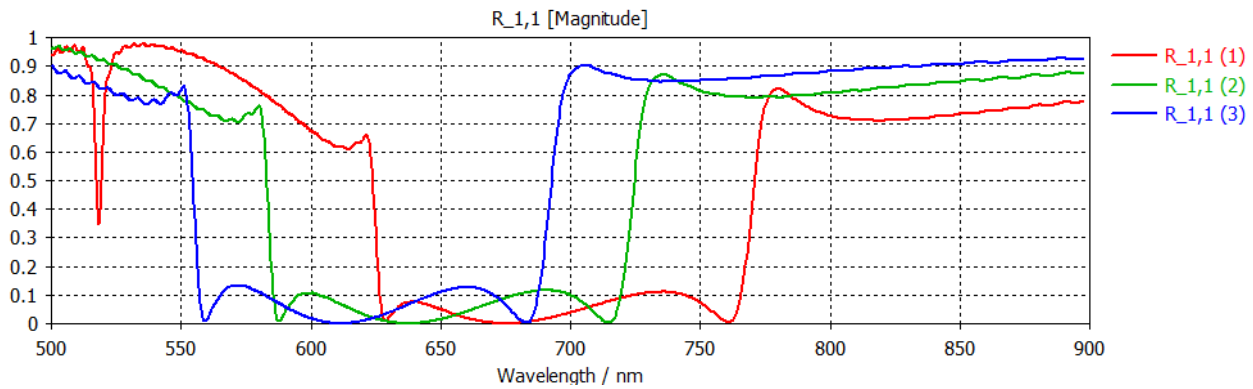

(a)

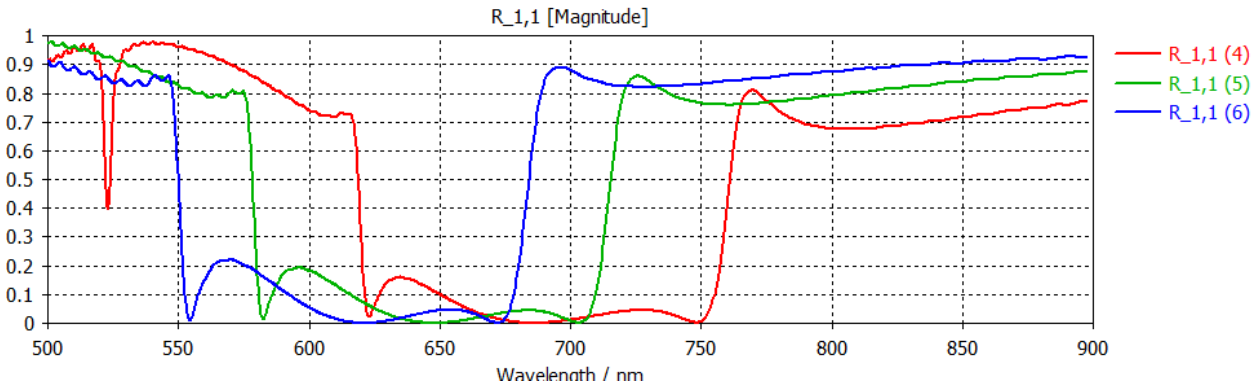

(b)

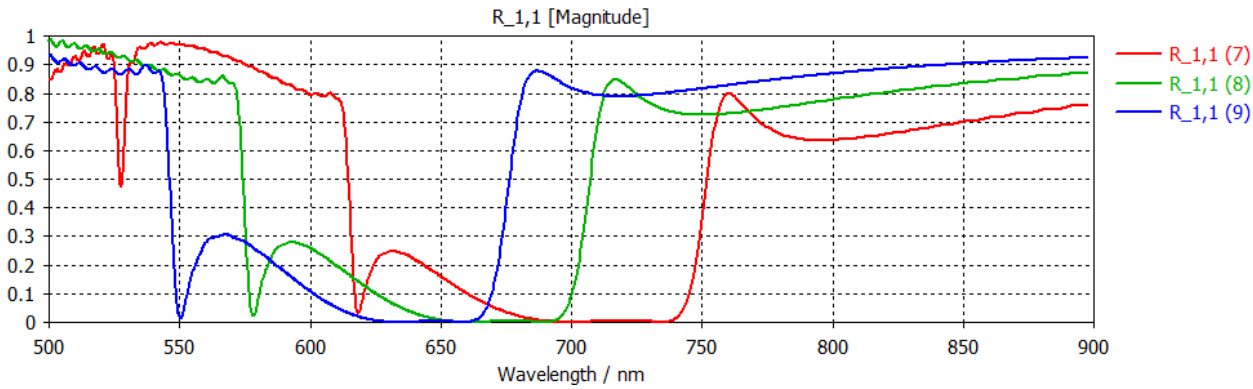

(c)

Figure 4.4 Simulated reflectance for Table 4.1.

The plots of Figure 4.4 show a bandpass performance in the red-light region. The reflectance shifts to the left as the copper's or silicon dioxide's thickness increases.

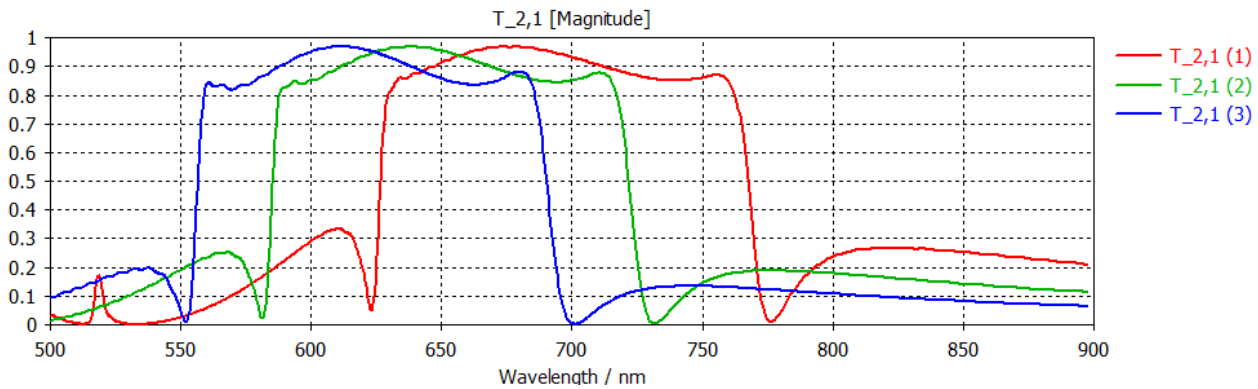

(a)

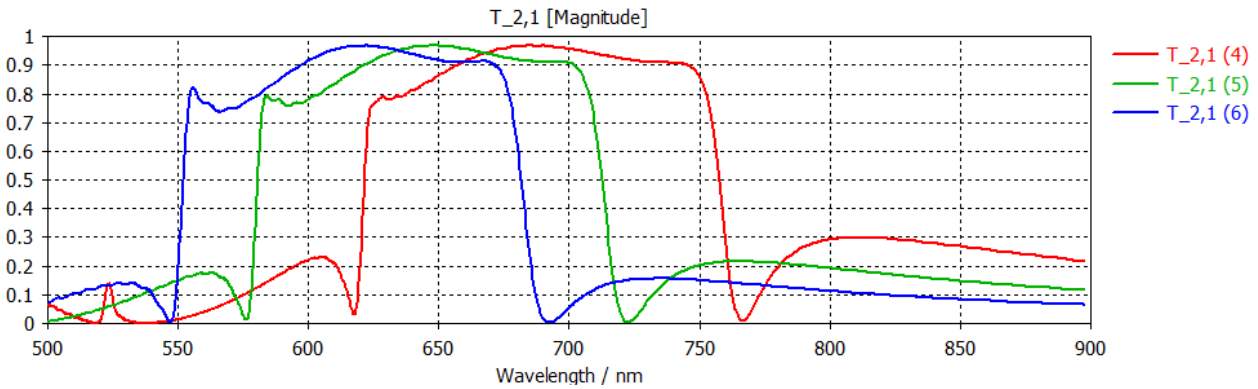

(b)

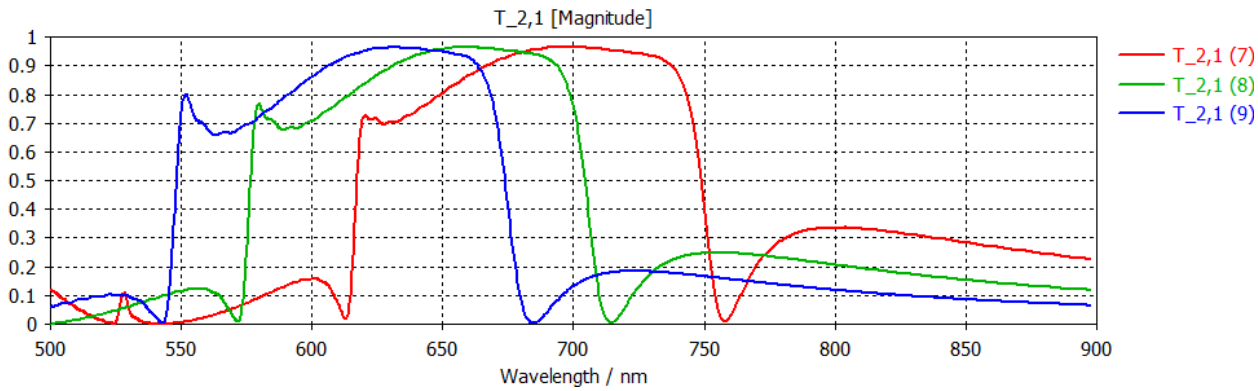

(c)

Figure 4.5 Simulated transmittance for Table 4.1.

The plots of Figure 4.5 show a bandpass performance in the red-light region. The transmittance shifts to the left as the copper's or silicon dioxide's thickness increases.

2) When a = 400 nm and d = 200 nm

Table 4.2 Thicknesses of dielectric and metallic layers.

t_{die} [nm] / t_m [nm]	90	100	110
30	(1)	(4)	(7)
40	(2)	(5)	(8)
50	(3)	(6)	(9)

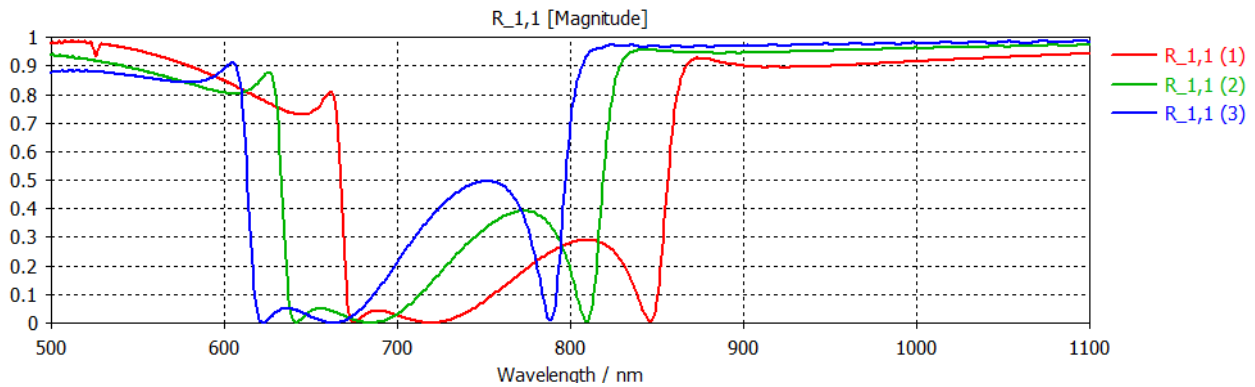

(a)

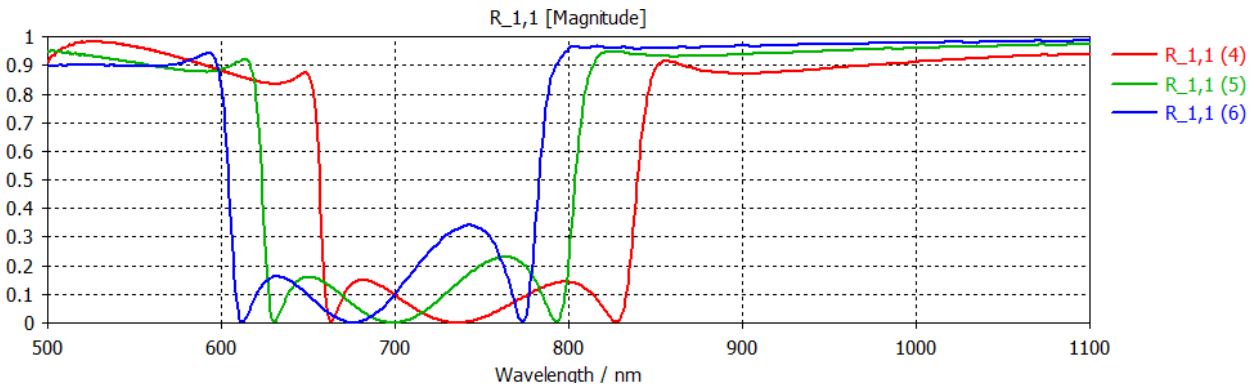

(b)

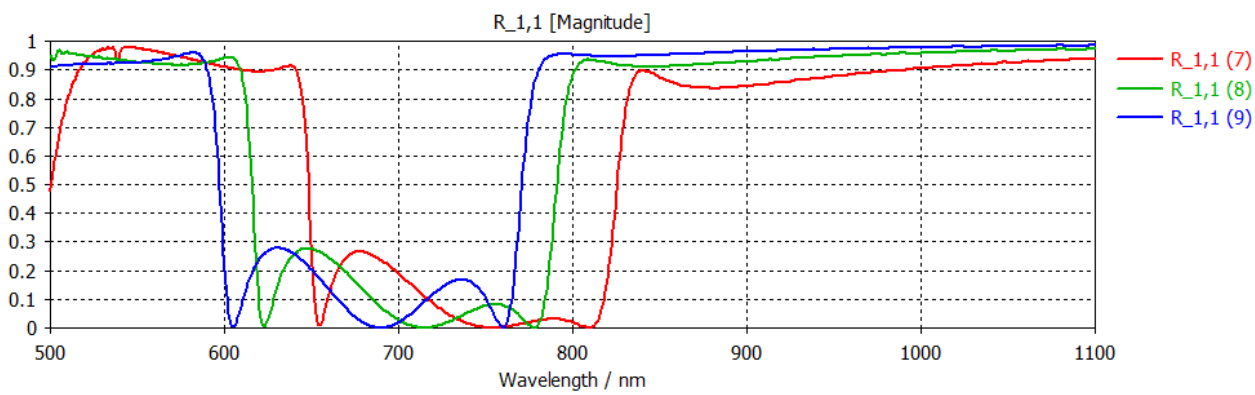

(c)

Figure 4.6 Simulated reflectance for Table 4.2.

The plots of Figure 4.6 show a bandpass performance. The reflectance shifts to the left as the copper's or silicon dioxide's thickness increases.

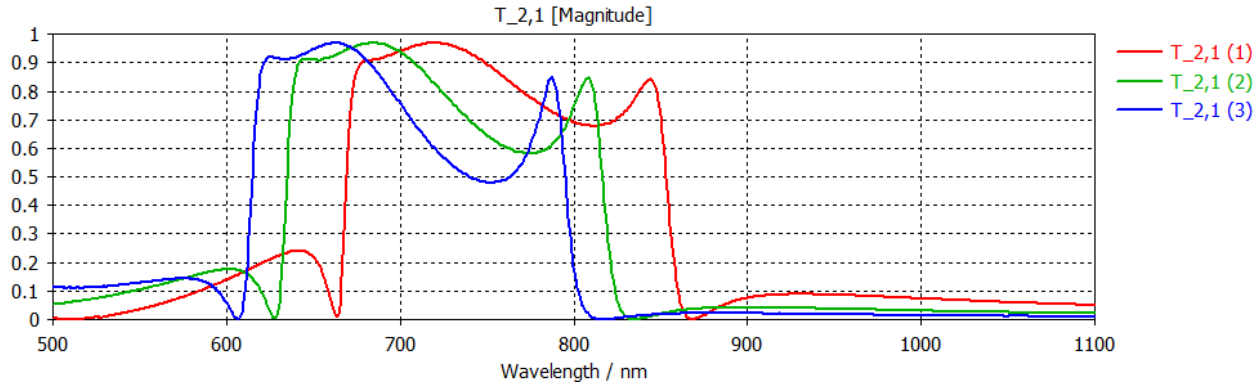

(a)

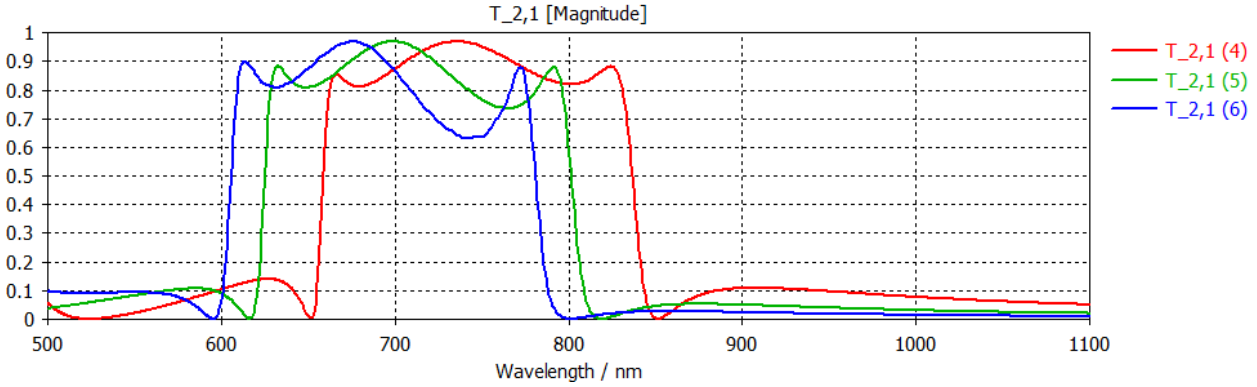

(b)

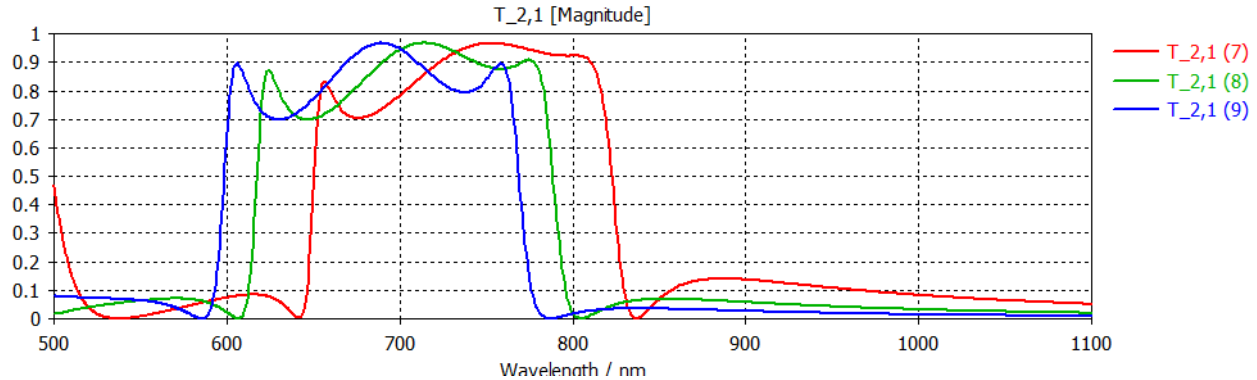

(c)

Figure 4.7 Simulated transmittance for Table 4.2.

The plots of Figure 4.7 show a bandpass performance. The transmittance shifts to the left as the copper's or silicon dioxide's thickness increases.

3) When a = 500 nm and d = 250 nm

Table 4.3 Thicknesses of dielectric and metallic layers.

t_{die} [nm] / t_m [nm]	120	130	140
30	(1)	(4)	(7)
40	(2)	(5)	(8)
50	(3)	(6)	(9)

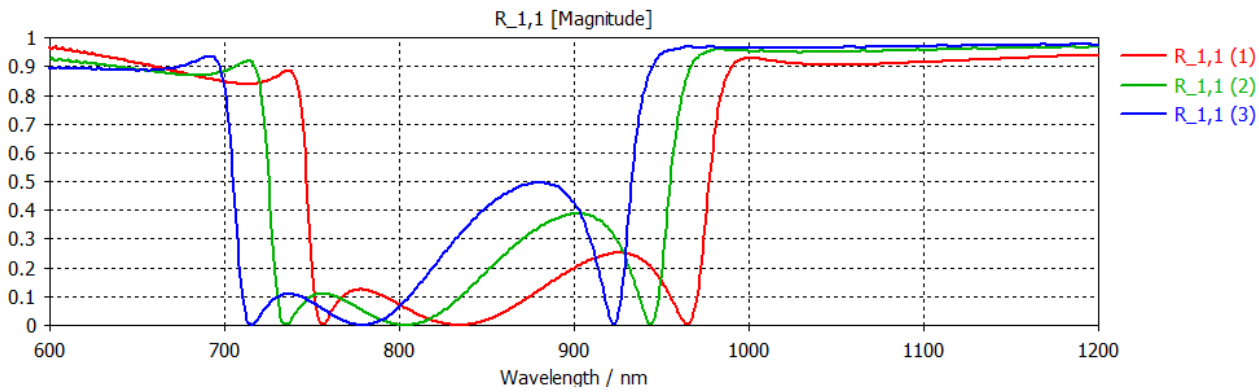

(a)

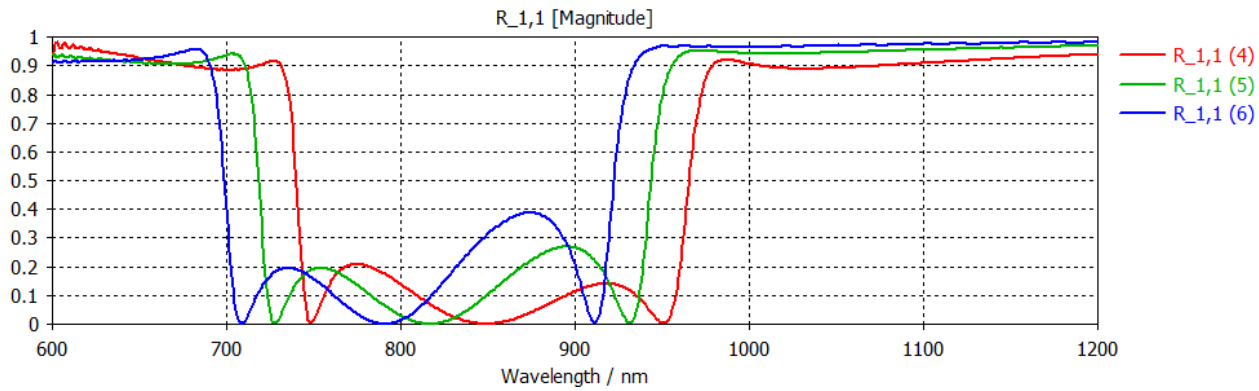

(b)

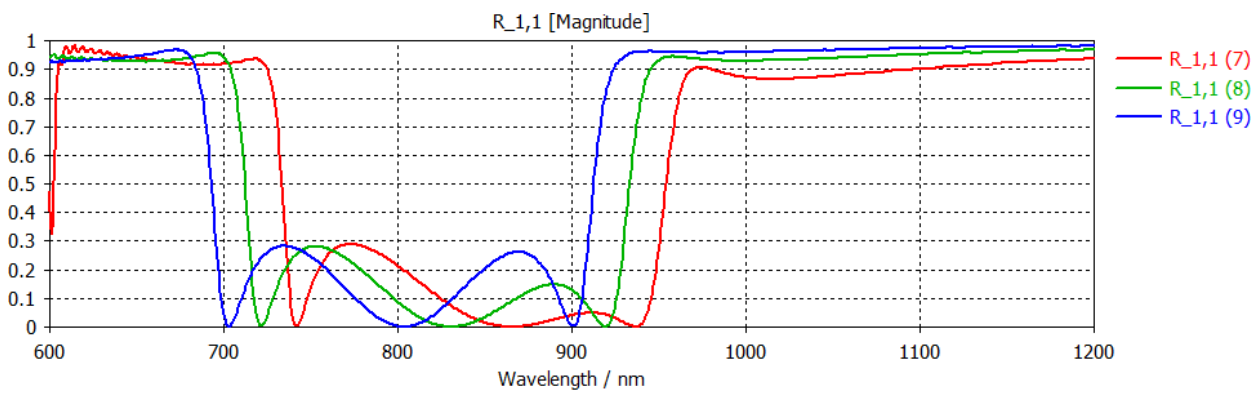

(c)

Figure 4.8 Simulated reflectance for Table 4.3.

The plots of Figure 4.8 show a bandpass performance. The reflectance shifts to the left as the copper's or silicon dioxide's thickness increases.

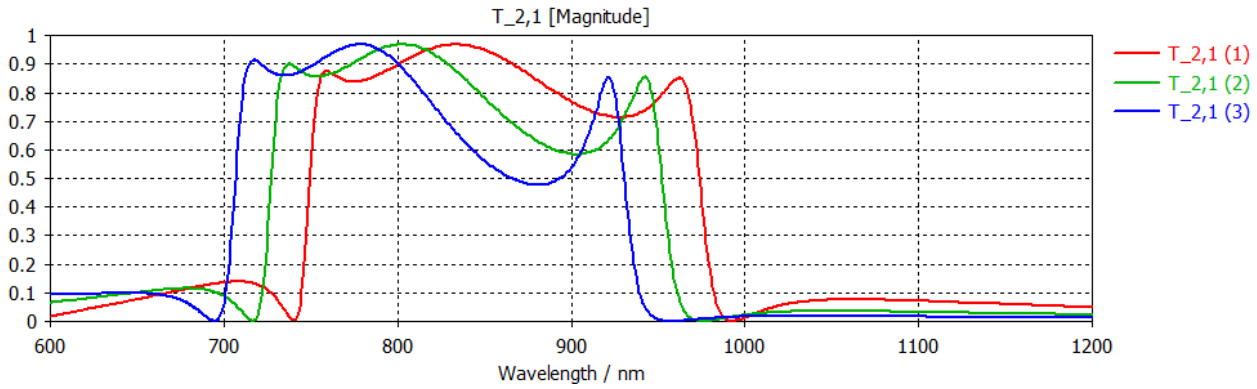

(a)

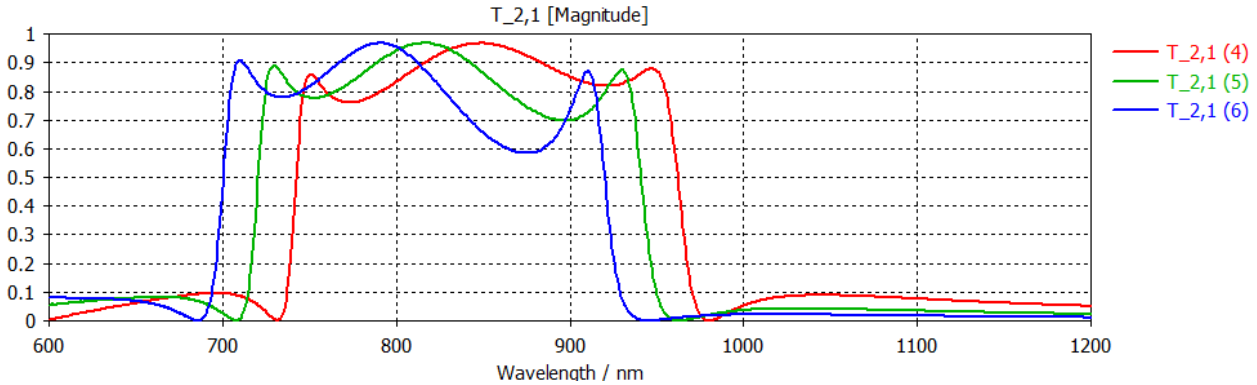

(b)

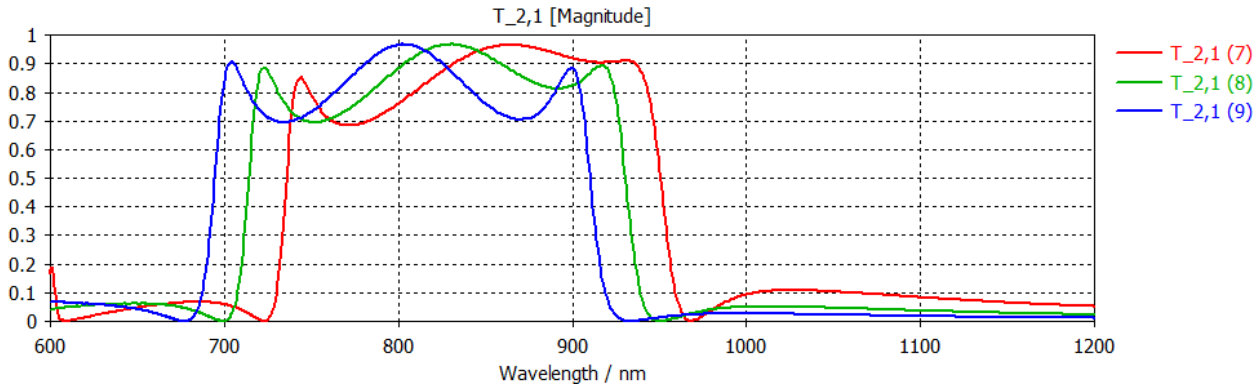

(c)

Figure 4.9 Simulated transmittance for Table 4.3.

The plots of Figure 4.9 show a bandpass performance. The transmittance shifts to the left as the copper's or silicon dioxide's thickness increases.

4) When a = 600 nm and d = 300 nm

Table 4.4 Thicknesses of dielectric and metallic layers.

t_{die} [nm] / t_m [nm]	150	160	170
30	(1)	(4)	(7)
40	(2)	(5)	(8)
50	(3)	(6)	(9)

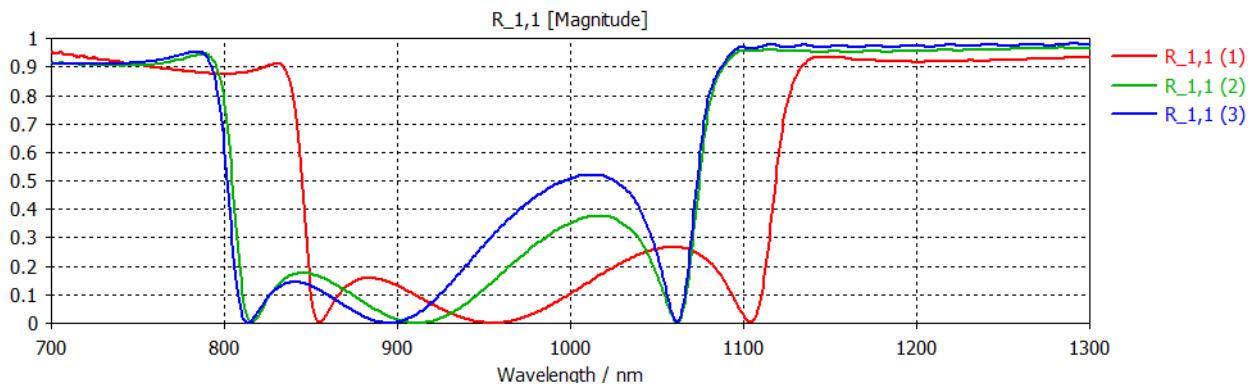

(a)

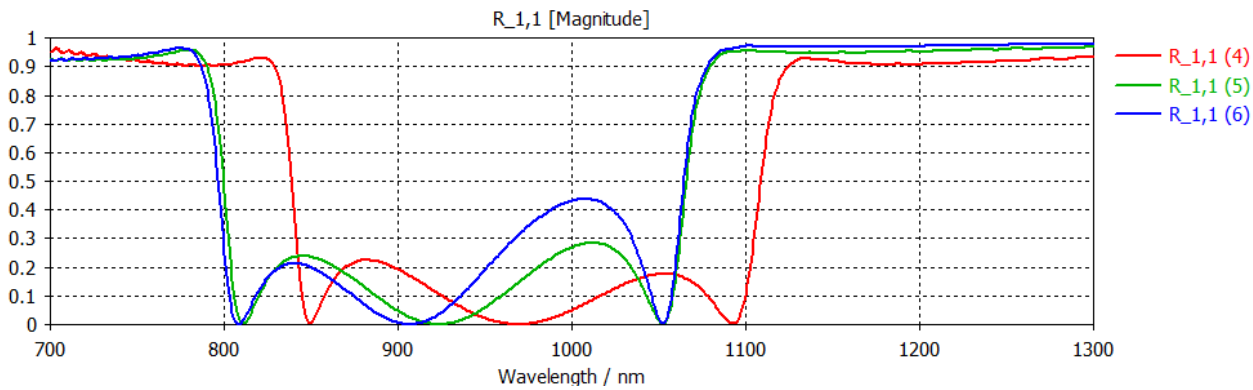

(b)

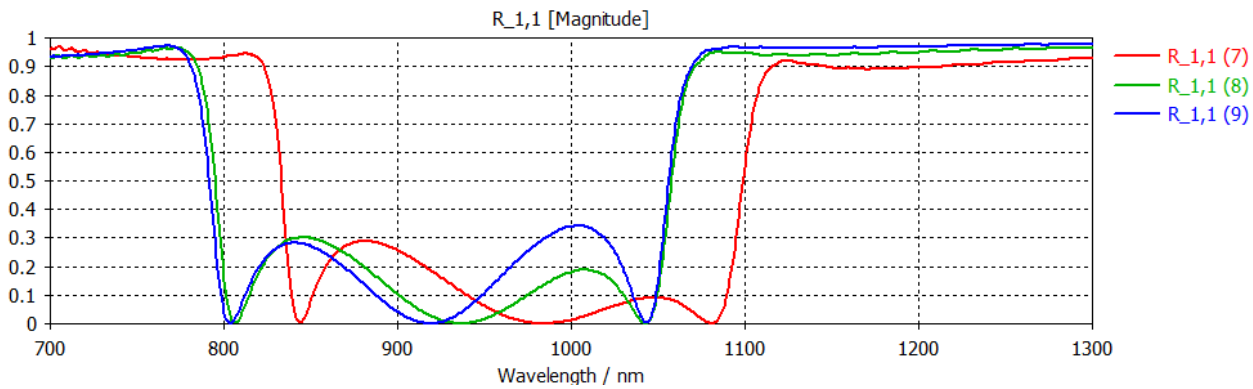

(c)

Figure 4.10 Simulated reflectance for Table 4.4.

The plots of Figure 4.10 show a bandpass performance. The reflectance shifts to the left as the copper's or silicon dioxide's thickness increases.

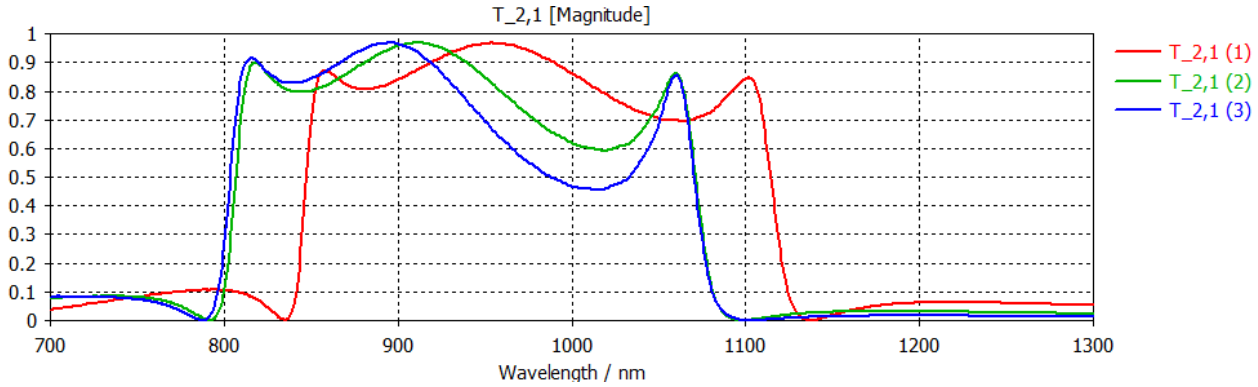

(a)

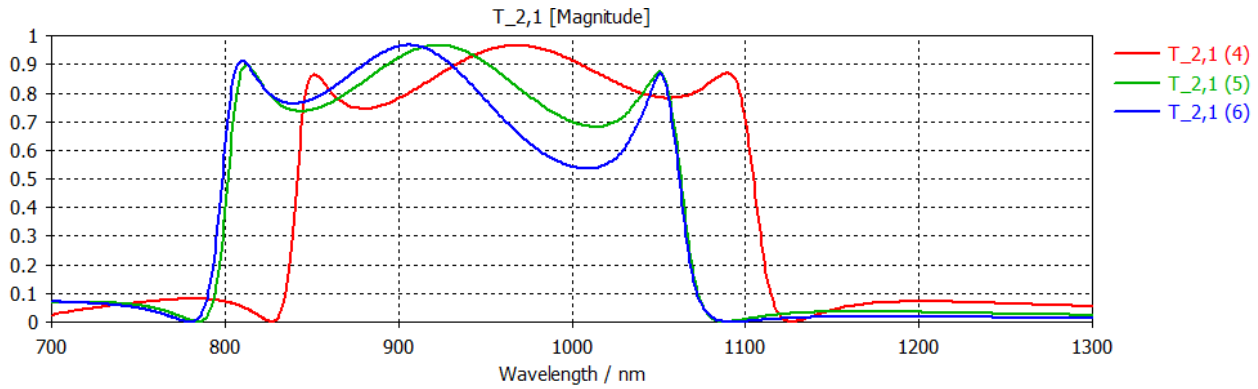

(b)

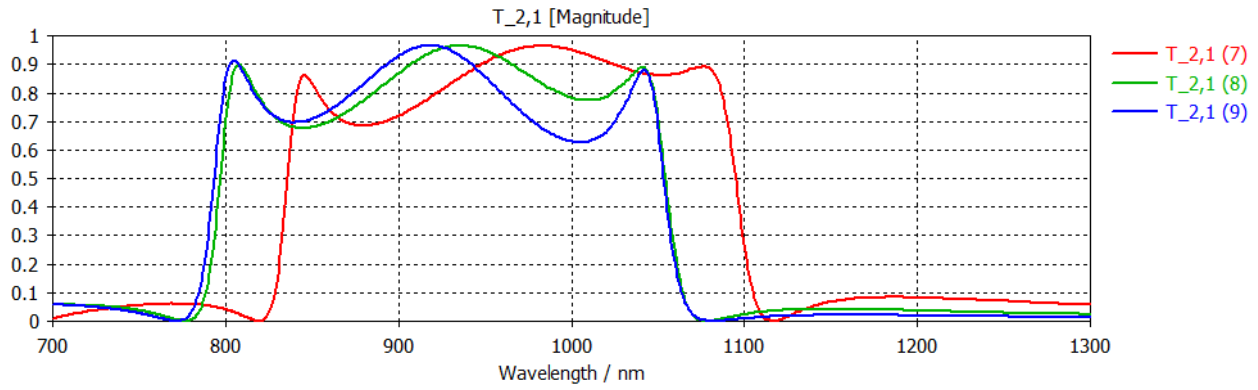

(c)

Figure 4.11 Simulated transmittance for Table 4.4.

The plots of Figure 4.11 show a bandpass performance. The transmittance shifts to the left as the copper's or silicon dioxide's thickness increases.

4.3.2 Design B

When a = 600 nm and d = 100 nm

Table 4.5 Thicknesses of dielectric and metallic layers.

t_{die} [nm] / t_m [nm]	60	80	100
60	(1)	(4)	(7)
80	(2)	(5)	(8)
100	(3)	(6)	(9)

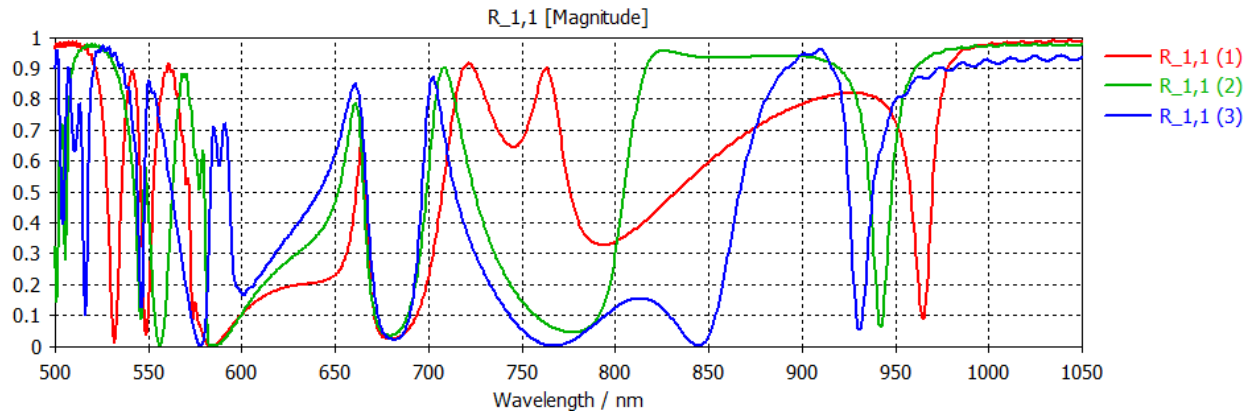

(a)

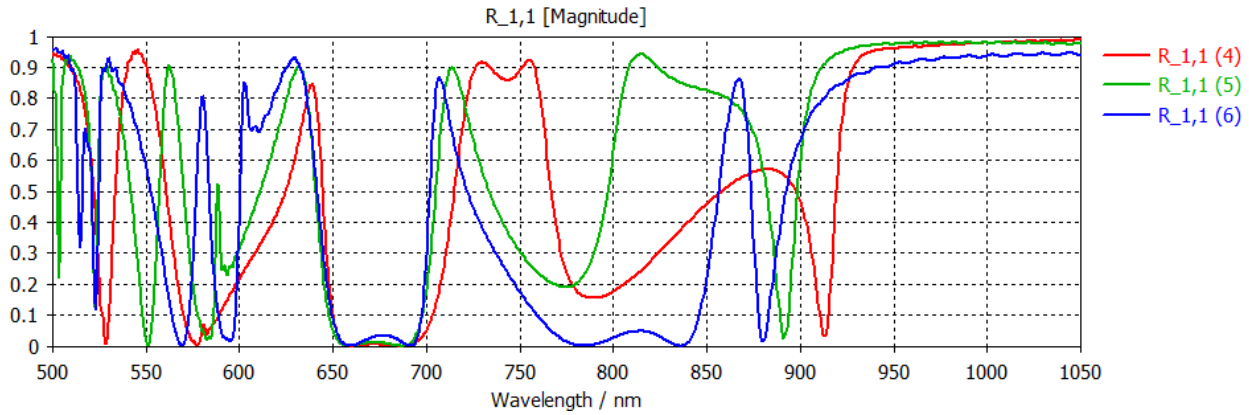

(b)

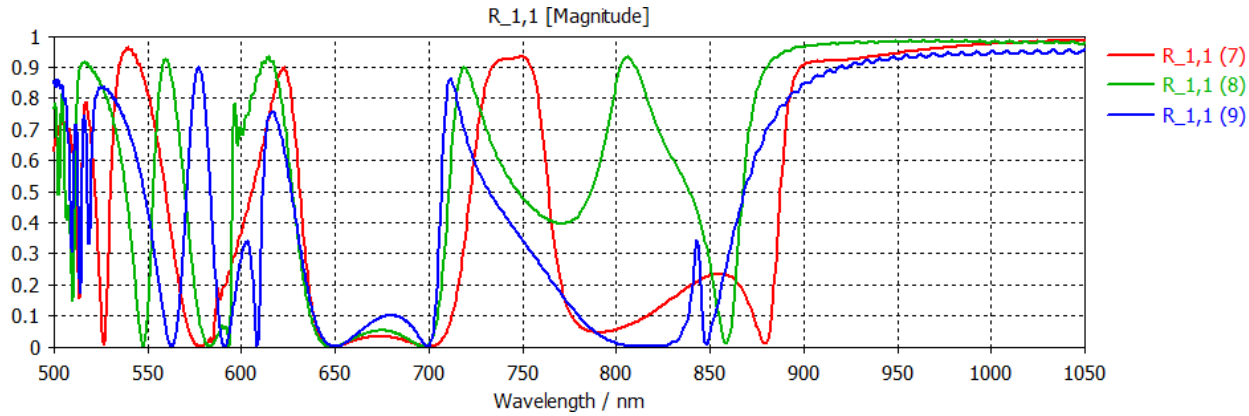

(c)

Figure 4.12 Simulated reflectance for Table 4.5.

For the plots of Figure 4.12, a thicker silicon dioxide layer broadens the well between 650 nm and 700 nm of wavelength.

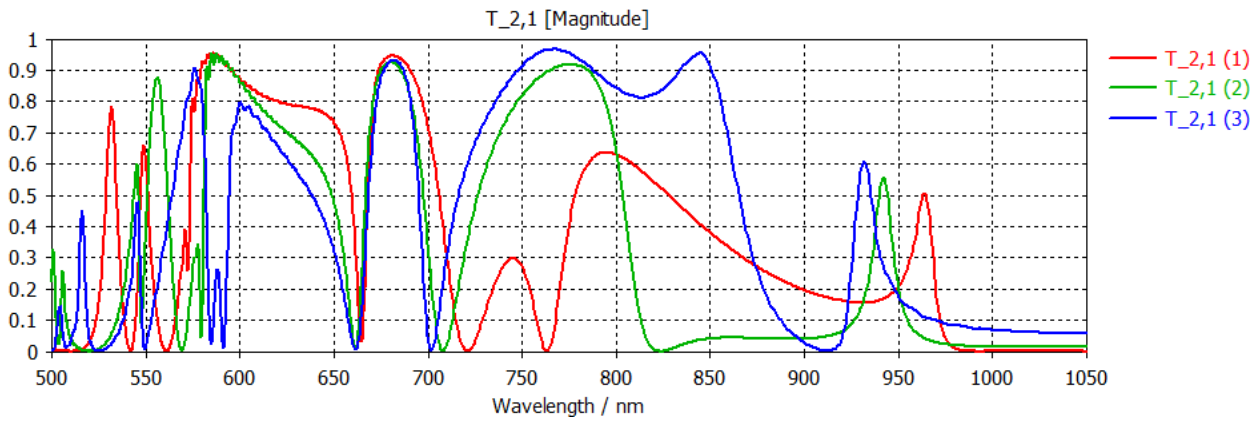

(a)

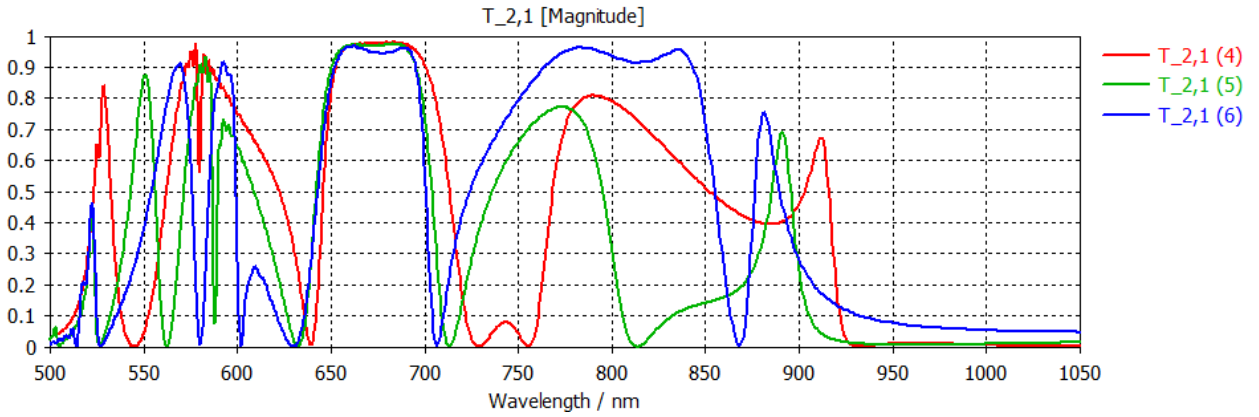

(b)

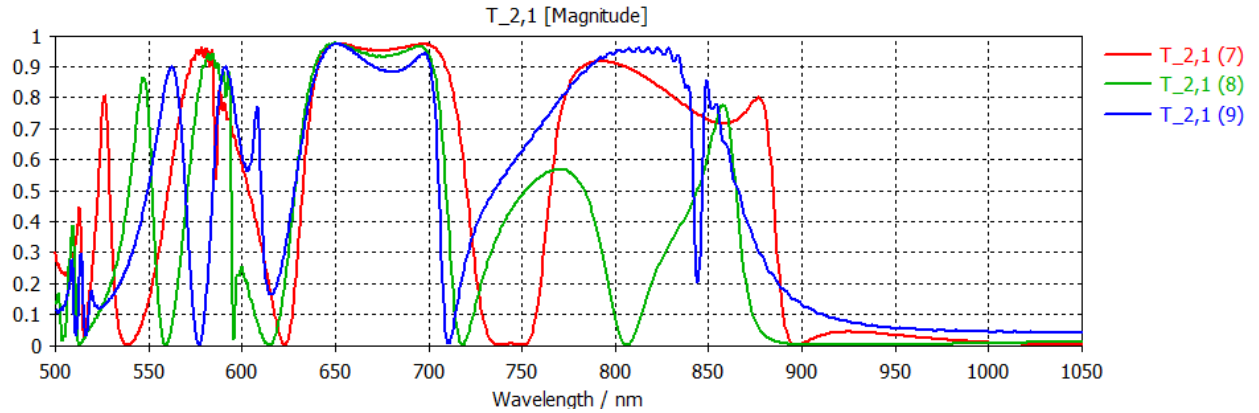

(c)

Figure 4.13 Simulated transmittance for Table 4.5.

For the plots of Figure 4.13, a thicker silicon dioxide layer broadens the plateau between 650 nm and 700 nm of wavelength.

4.3.3 Design C

When a = 600 nm and d = 100 nm

Table 4.6 Thicknesses of dielectric and metallic layers.

t_{die} [nm] / t_m [nm]	60	80	100
60	(1)	(4)	(7)
80	(2)	(5)	(8)
100	(3)	(6)	(9)

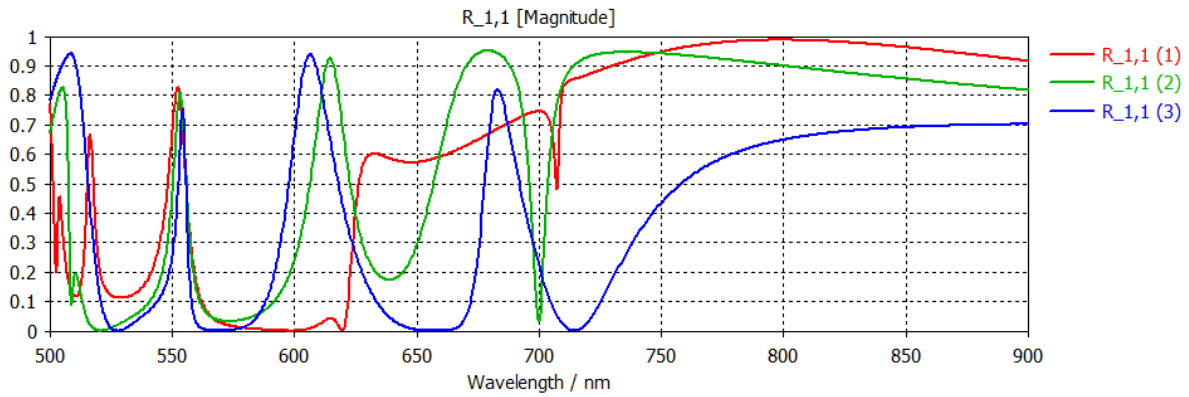

(a)

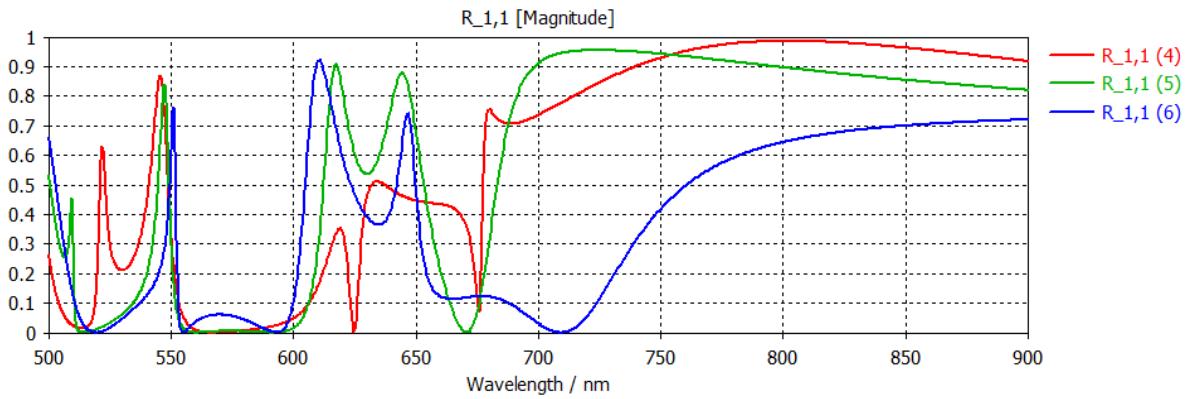

(b)

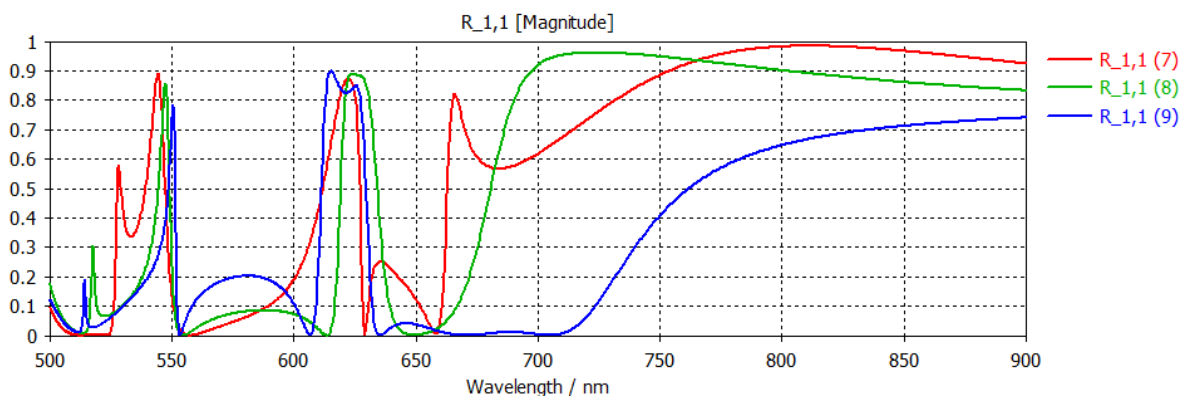

(c)

Figure 4.14 Simulated reflectance for Table 4.6.

The two green and blue upward peaks between 575 nm and 725 nm in Figure 4.14 (a) get closer to and mix with each other as the silicon dioxide's thickness increases.

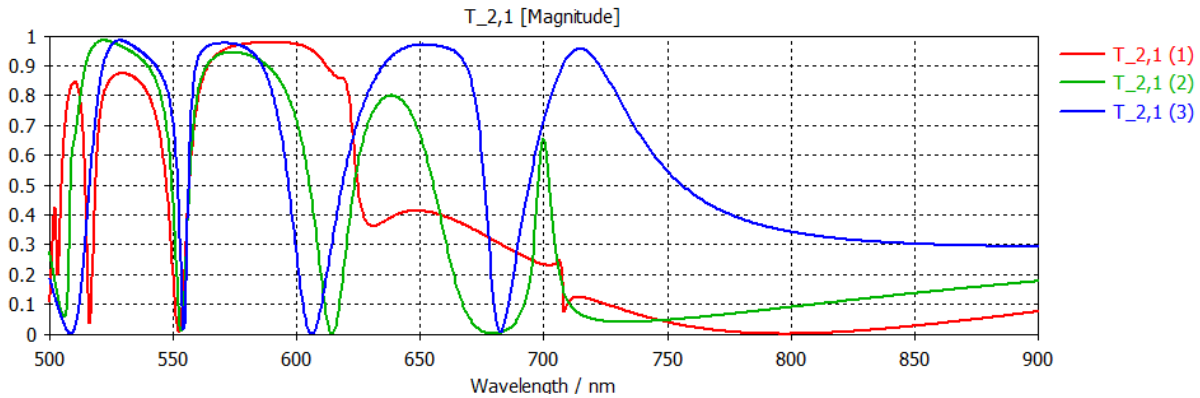

(a)

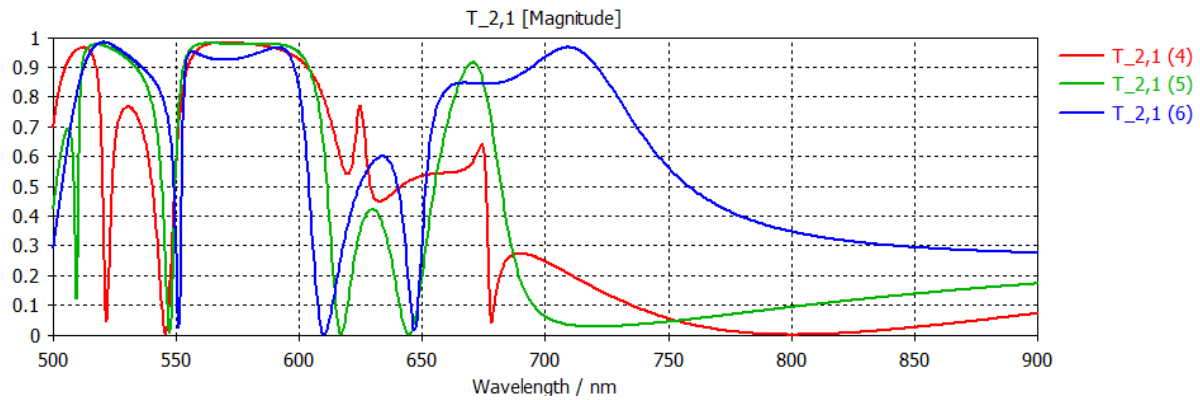

(b)

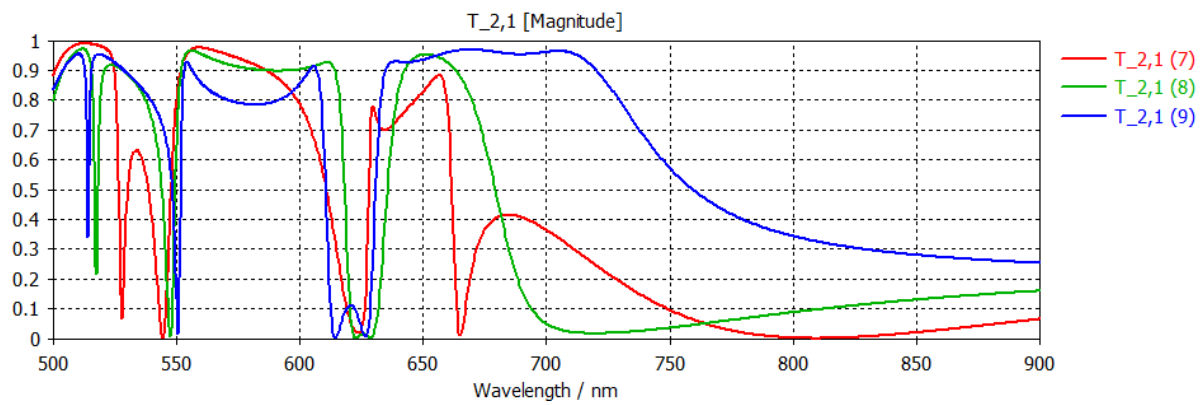

(c)

Figure 4.15 Simulated transmittance for Table 4.6.

The two green and blue downward peaks between 575 nm and 725 nm in Figure 4.15 (a) get closer to and mix with each other as the silicon dioxide's thickness increases.

4.3.4 Design D

When a = 840 nm, d = 180 nm, and s = 90 nm

Table 4.7 Thicknesses of dielectric and metallic layers.

t_{die} [nm] / t_m [nm]	60
60	(1)
80	(2)
100	(3)

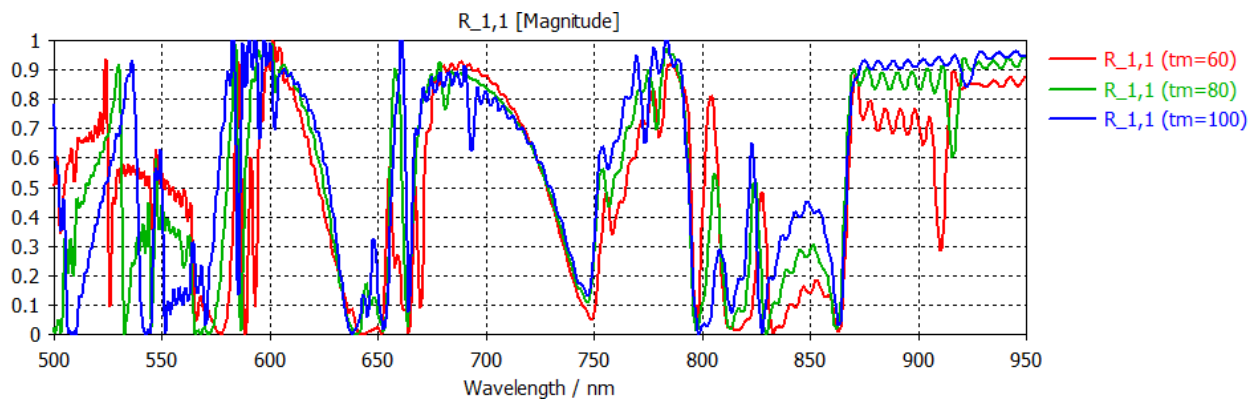

Figure 4.16 Simulated reflectance for Table 4.7.

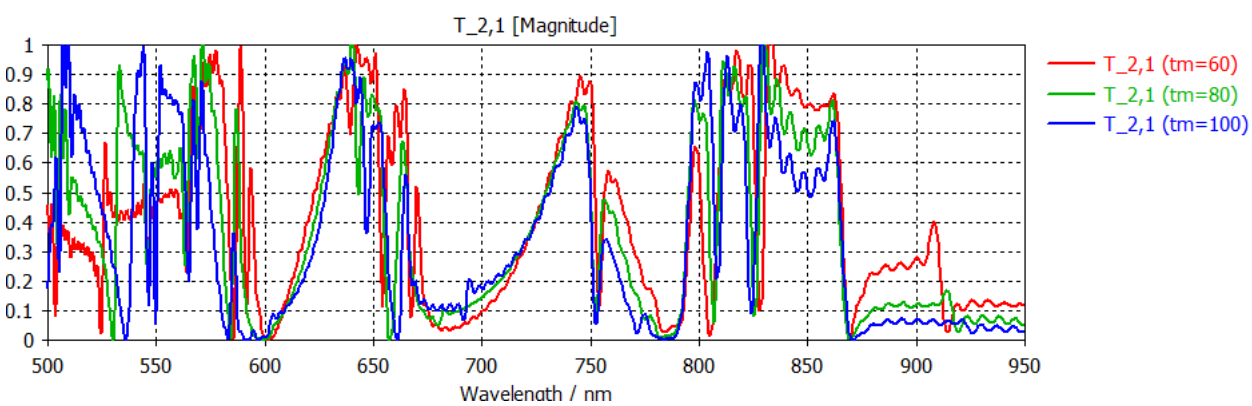

Figure 4.17 Simulated transmittance for Table 4.7.

No significant effect of a different thickness of the copper layers is found for Figures 4.16 and 4.17.

4.3.5 Design E

When a = 1000 nm, d = 200 nm, and s = 100 nm

Table 4.8 Thicknesses of dielectric and metallic layers.

t_{die} [nm] / t_m [nm]	60	80	100
60	(1)	(4)	(7)
80	(2)	(5)	(8)
100	(3)	(6)	(9)

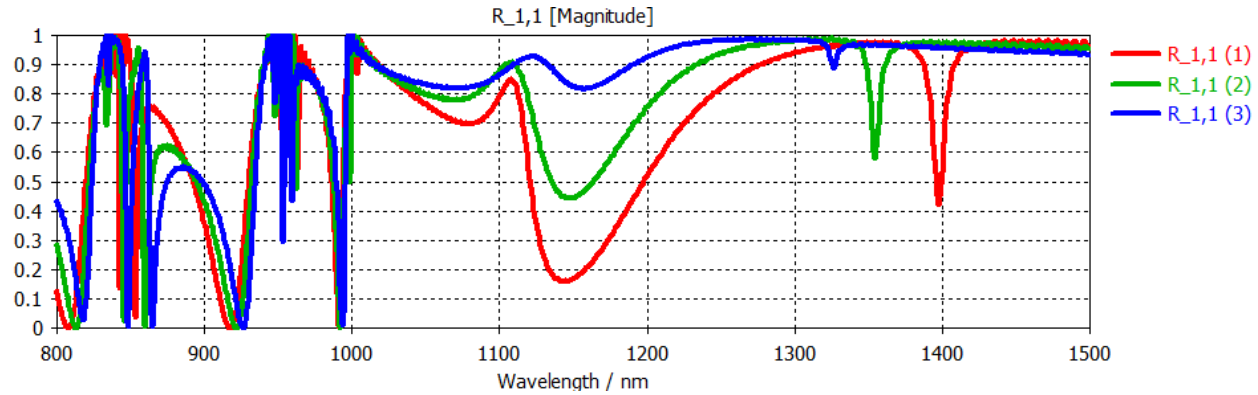

(a)

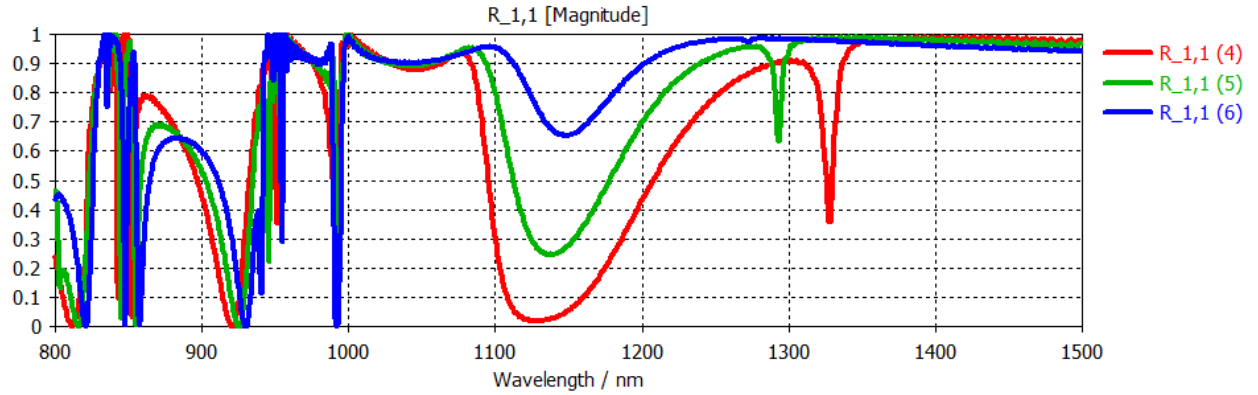

(b)

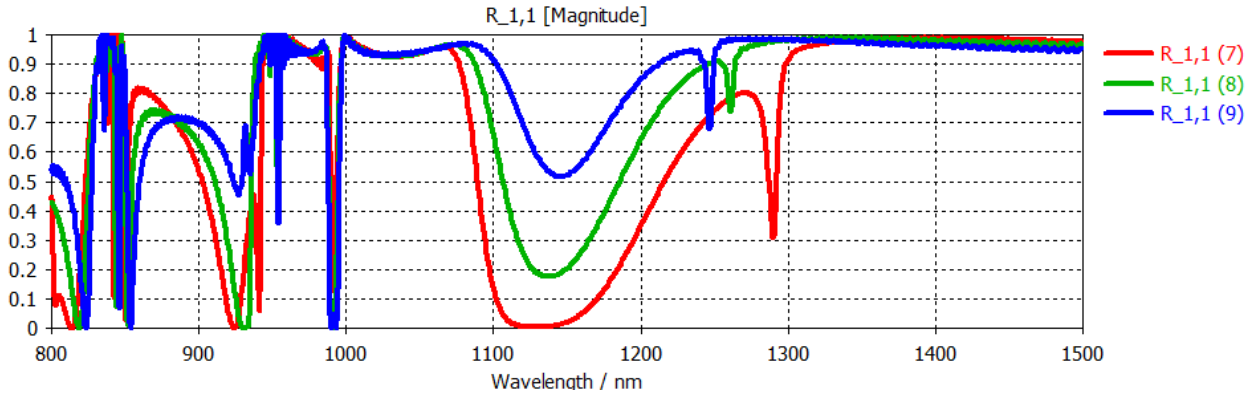

(c)

Figure 4.18 Simulated reflectance for Table 4.8.

For Figure 4.18, a thicker copper/silicon dioxide layer heightens/broadens the well between 1100 and 1200 nm of wavelength respectively.

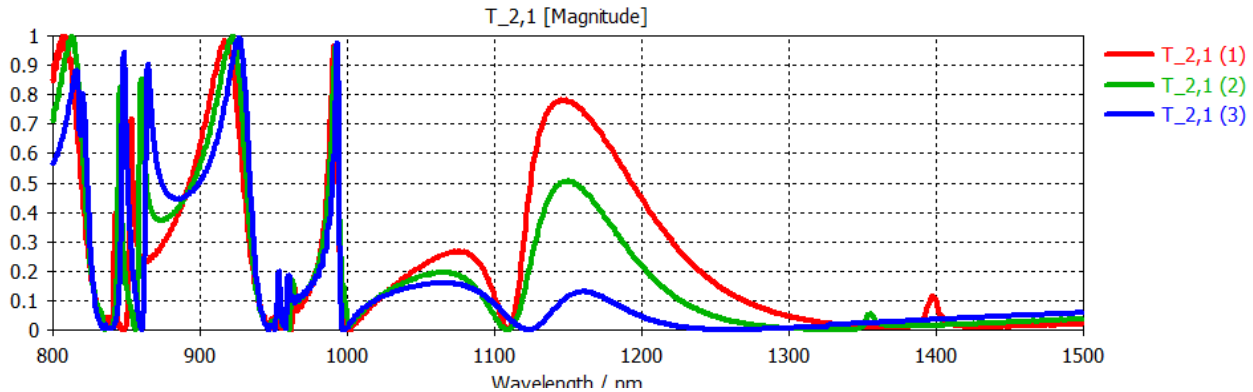

(a)

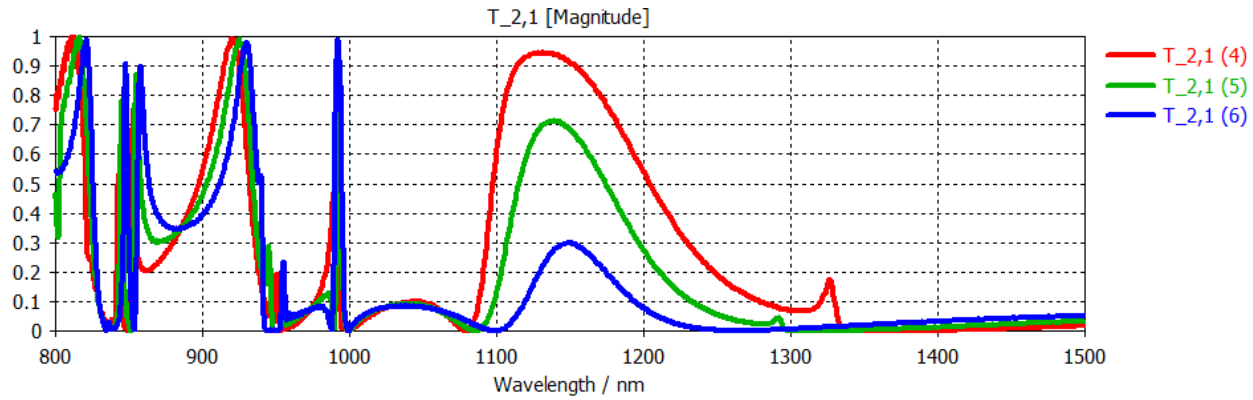

(b)

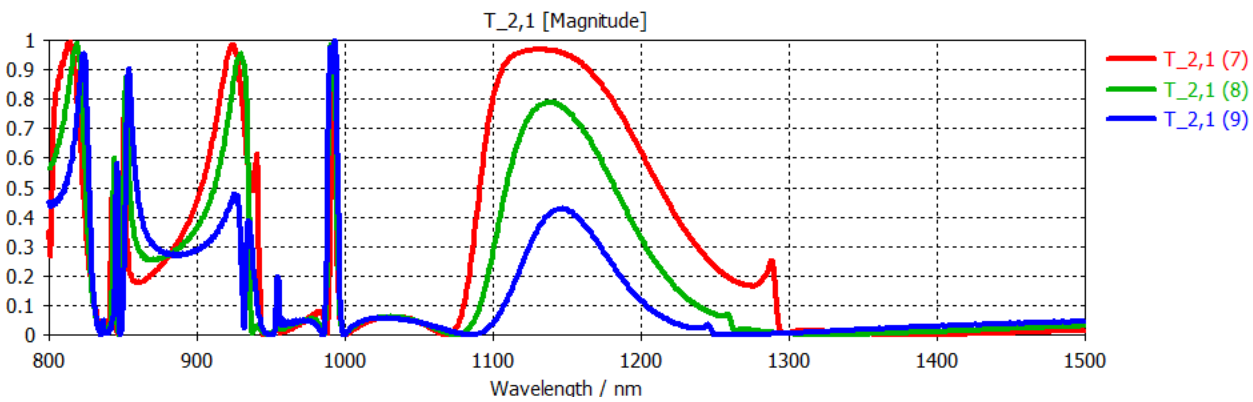

(c)

Figure 4.19 Simulated transmittance for Table 4.8.

For Figure 4.19, a thicker copper/silicon dioxide layer lowers/broadens the parabolic area between 1100 and 1200 nm of wavelength respectively.

4.3.6 Design F

When a = 1000 nm, d = 200 nm, and s = 100 nm

Table 4.9 Thicknesses of dielectric and metallic layers

t_{die} [nm] / t_m [nm]	60	80	100
60	(1)	(4)	(7)
80	(2)	(5)	(8)
100	(3)	(6)	(9)

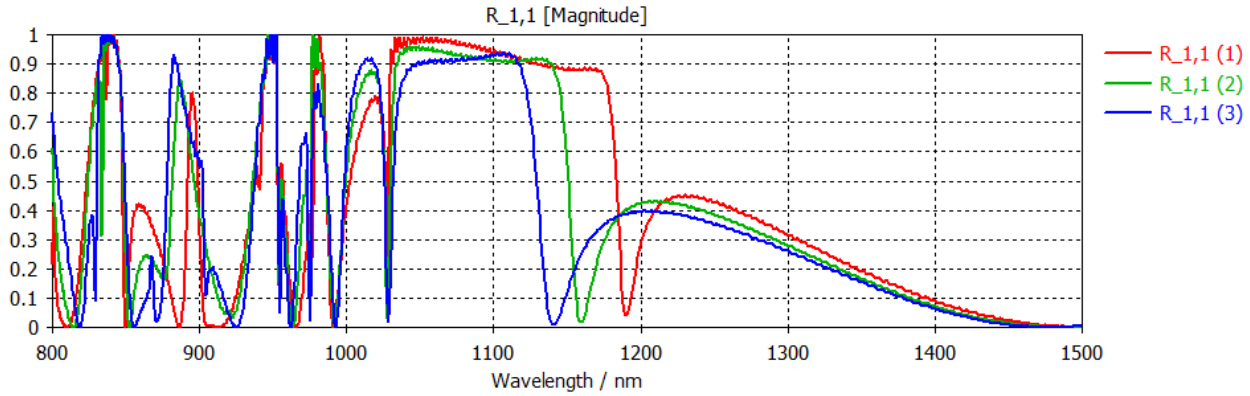

(a)

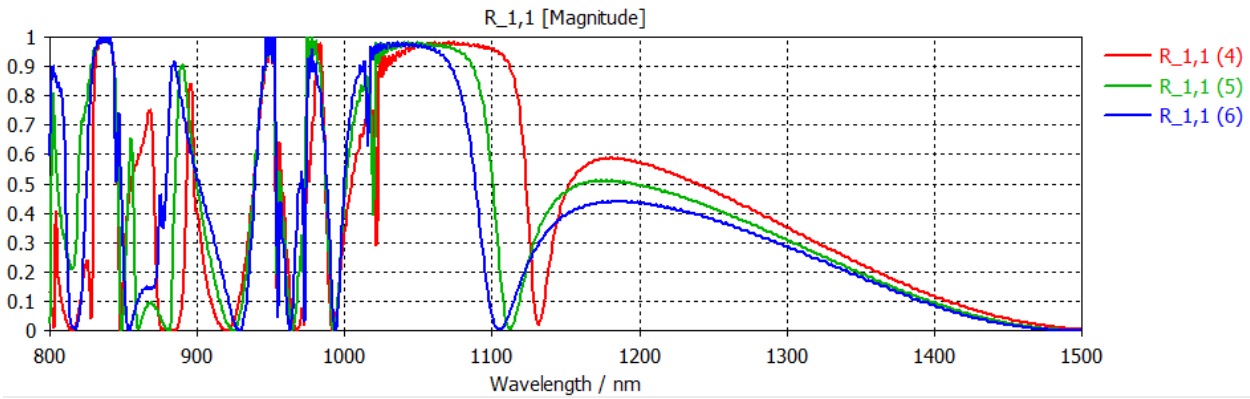

(b)

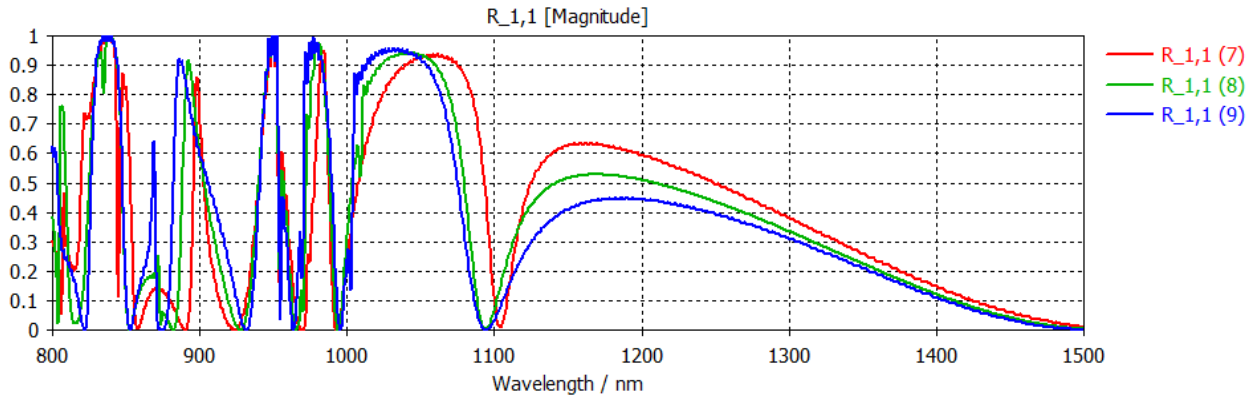

(c)

Figure 4.20 Simulated reflectance for Table 4.9.

For Figure 4.20, both thicker copper and silicon dioxide layers slightly shift the plots at wavelengths greater than 1000 nm to the left.

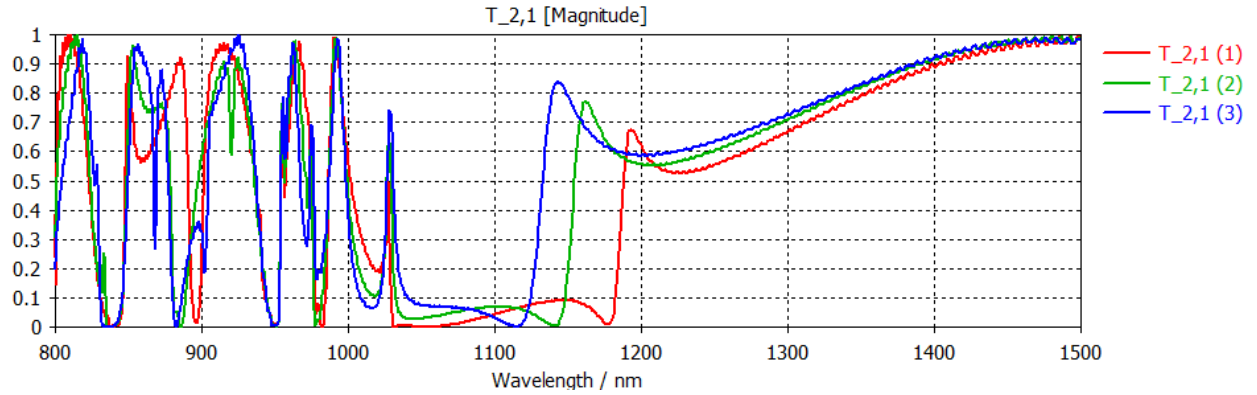

(a)

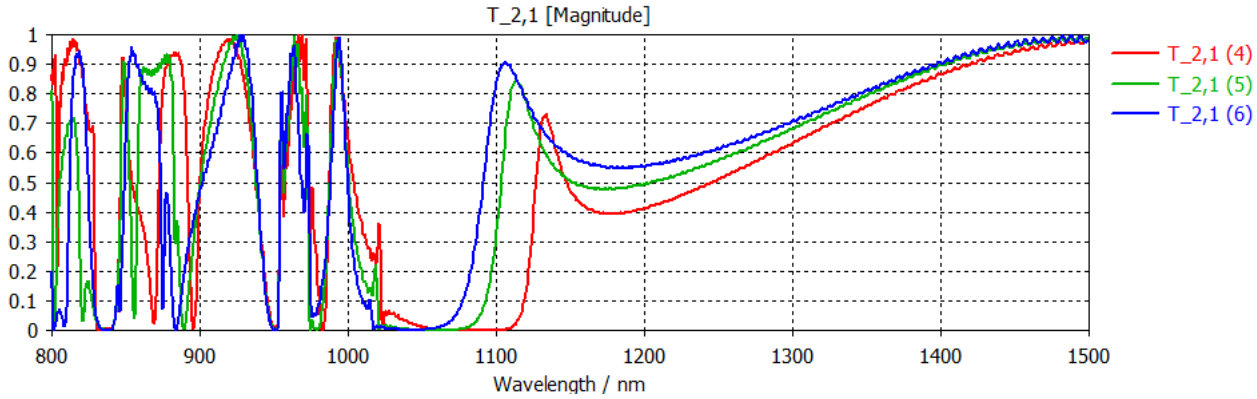

(b)

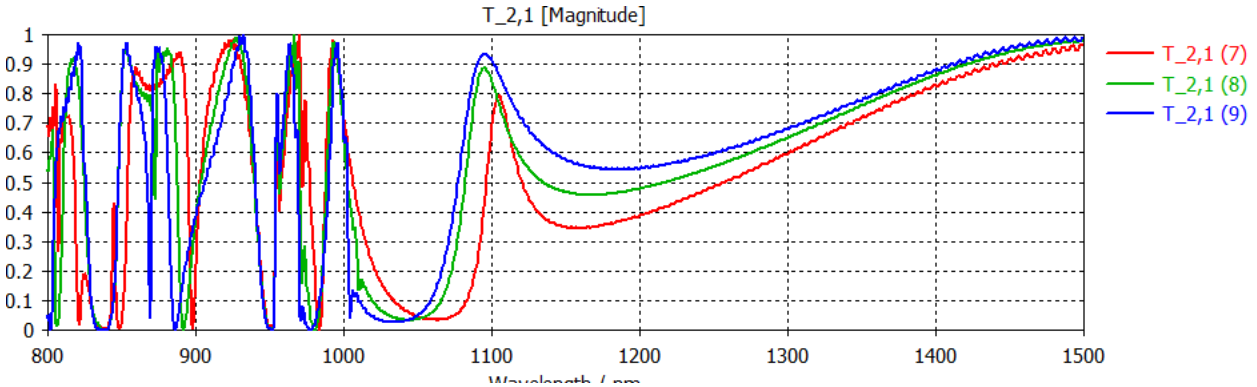

(c)

Figure 4.21 Simulated transmittance for Table 4.9.

For Figure 4.21, both thicker copper and silicon dioxide layers slightly shift the plots at wavelengths greater than 1000 nm to the left.

4.4 Extraction of Effective Properties of Metamaterials

4.4.1 Effective Thickness of Metamaterial

As discussed in Chapter 1, a metamaterial is not a single homogeneous material such as SiO_2 or Cu, and its unusual electromagnetic properties are from its structure and the properties of its constituent materials. Hence, optical properties of a metamaterial such as permittivity, permeability, or refractive index should be different from those of its constituent materials. However, a metamaterial slab can be treated as if it were a single homogeneous material that produces the same S-parameters (scattering parameters) [27]. The thickness of that virtual homogenous material slab is understood to be the distance between two planes where the wave behaves like a plane wave (when the incident wave was a plane wave). This thickness is called the "effective thickness" of a metamaterial [27] (note that the effective thickness of a metamaterial is generally not the same as the actual thickness of the metamaterial).

4.4.2 Extraction Method

Based on the effective thickness and simulated S-parameters of the metamaterial, its optical property values can be extracted. However, the dependency of effective thickness on the incident wave's frequency makes it challenging to efficiently retrieve the effective values. If this dependency is too large, then one may have to retrieve the effective parameters for each different frequency with the corresponding effective thickness. However, based on simulated electric fields, the effective thicknesses of Design A metamaterials in Chapter 4 were found to be barely dependent on the frequency over their simulated frequency range. Also, their effective thickness was quite similar to their actual thickness. Thus, in this thesis, effective optical values were

extracted for Design A metamaterials (their effective thickness was defined same as their actual thickness in the simulation).

As there have been efforts of researchers to retrieve effective parameters of metamaterials such as [27] and [28], CST Microwave Studio extracts the effective parameters based on the method suggested in "[27]" [29]. They, in [27], assume a plane wave and S-parameters are derived based on the wave's fields that are at the interfaces of the virtual homogeneous slab (the distance between the interfaces of the homogeneous slab is the effective thickness). However, it was observed that excitation ports defined at those interfaces (same as the air/material interfaces for Design A metamaterials) could produce inaccuracy as compared to literature. For this reason, excitation ports were defined with a distance from the air/material interfaces. The phase mismatch of S-parameters, compared to [27], due to the introduced distance was compensated by introducing phase de-embedding as shown in Figure 4.22. After introducing phase de-embedding, the metamaterial was simulated for S-parameters. These S-parameters were employed to extract effective parameters of the metamaterial.

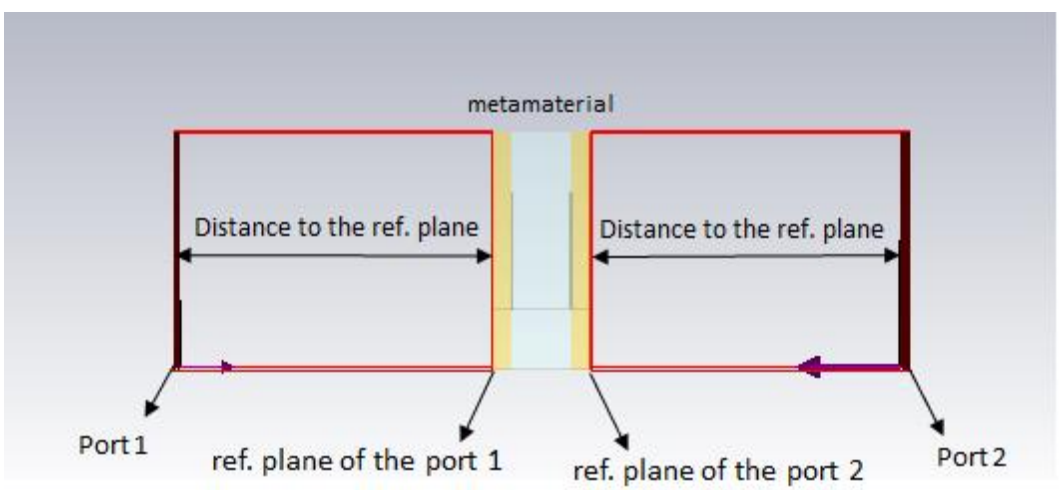

Figure 4.22 Ports and ref. planes in CST Microwave Studio. The magnitude and phase of waves are evaluated at the locations of 'ports' and 'ref. planes of the port' respectively for the S-parameter calculation.

4.4.3 Extracted Effective Parameters

The relative wave impedance and refractive index of a material is given by $z_r = \sqrt{\frac{\mu_r}{\varepsilon_r}}$ [30] and $n = \frac{\mu_r}{z_r} = \varepsilon_r z_r$ [27] respectively. The same equations can be applied to a metamaterial for its effective parameters* (where the notations $z_r, n, \varepsilon_r, and\ \mu_r$ represent the effective values of the metamaterial). Figures 4.23 ~ 4.26 show extracted effective values of some metamaterials of Design A.

** In case of metamaterials, compared to natural materials, the equation $n = \sqrt{\varepsilon_r \mu_r}$ can cause a sign disagreement in some cases while the equation $n^2 = \varepsilon_r \mu_r$ holds true.; when both the permittivity and permeability are negative real numbers for example. Details are found in [27] and [31].*

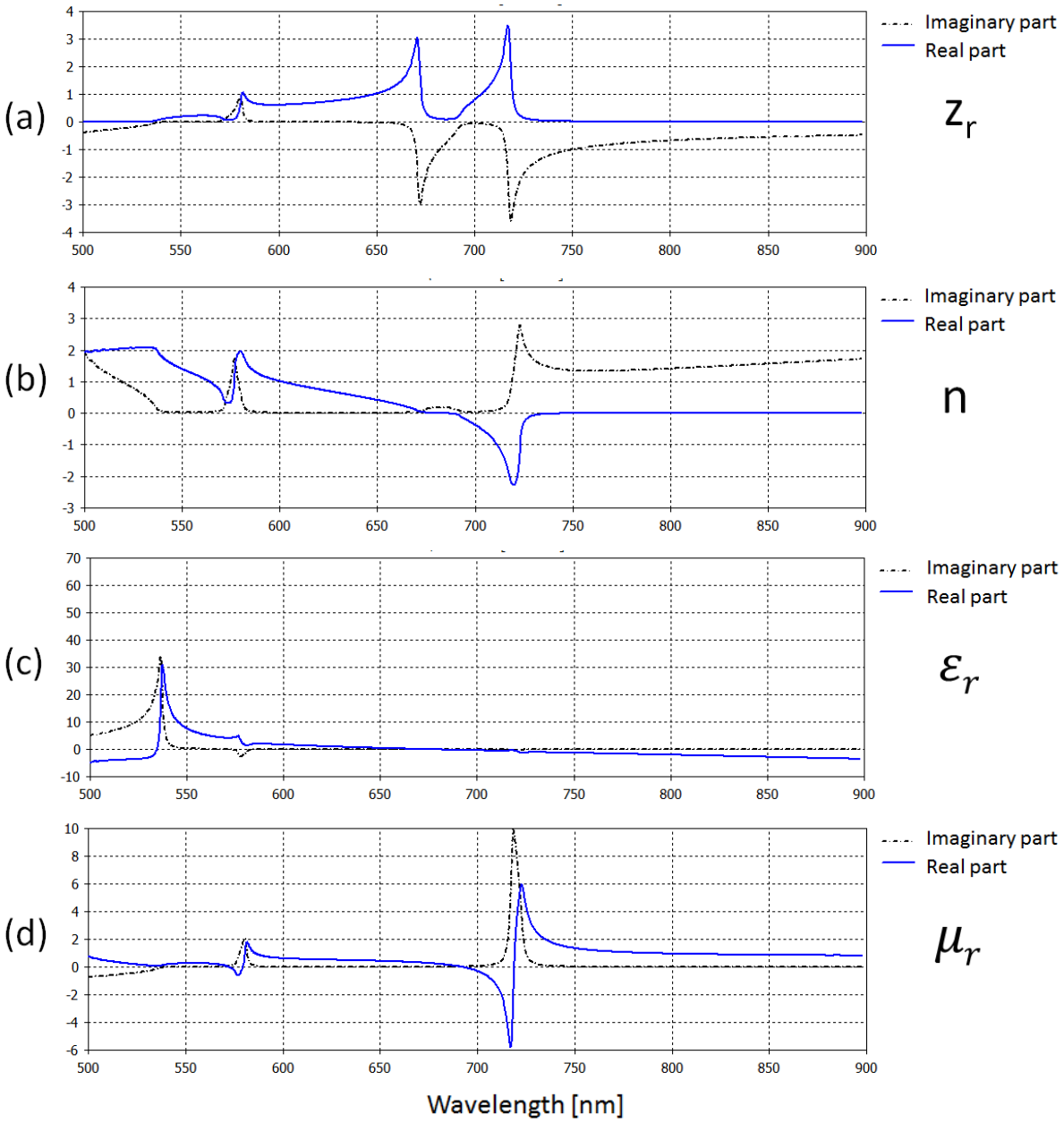

Figure 4.23 Extracted effective parameters of Design A-1-(5) of Table 4.1 on page 31. (a) relative wave impedance, (b) refractive index, (c) relative permittivity, and (d) relative permeability.

Figure 4.23 shows a negative real part of the refractive index (often called just "negative refractive index" or "negative index") over 685 nm ~ 750 nm of wavelength. The metamaterial resonates at wavelengths near 580 nm and 720 nm where the magnetic resonance is dominant near 720 nm.

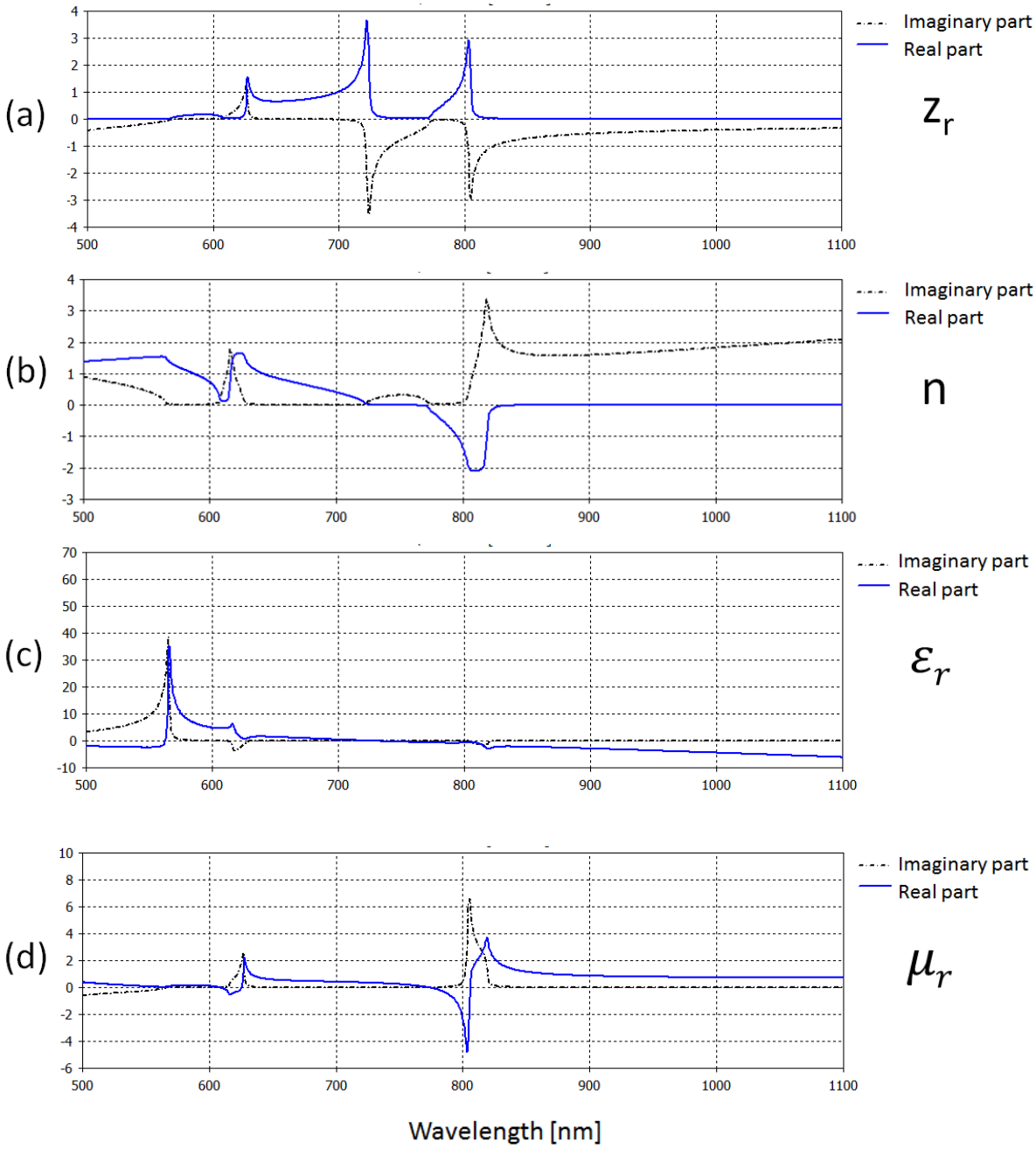

Figure 4.24 Extracted effective parameters of Design A-2-(5) of Table 4.2 on page 34. (a) relative wave impedance, (b) refractive index, (c) relative permittivity, and (d) relative permeability.

Figure 4.24 shows a negative real part of the refractive index over 760 nm ~ 860 nm of wavelenth. The metamaterial resonates at wavelengths near 620 nm and 815 nm where the magnetic resonance is dominant near 815 nm.

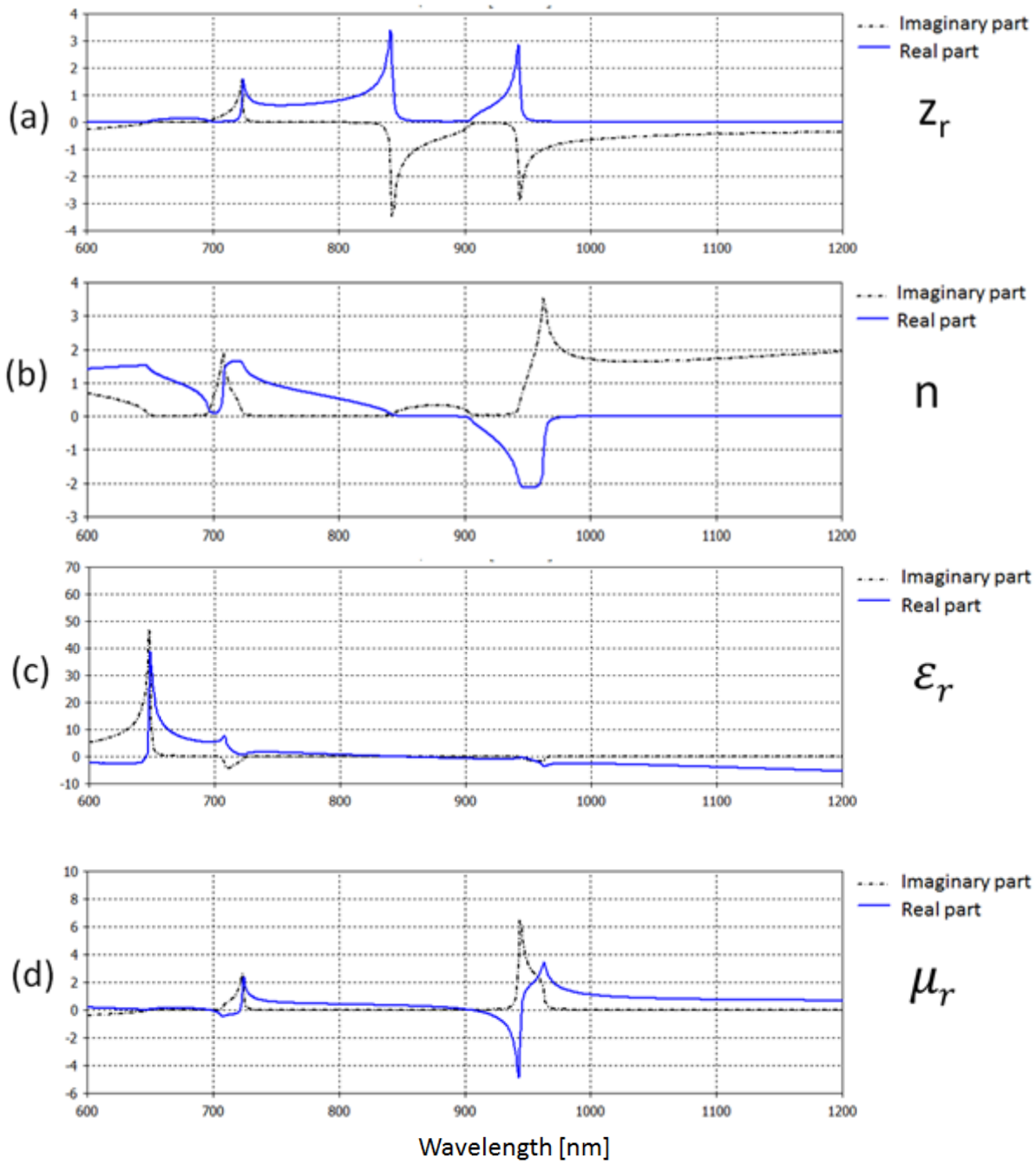

Figure 4.25 Extracted effective parameters of Design A-3-(5) of Table 4.3 on page 37. (a) relative wave impedance, (b) refractive index, (c) relative permittivity, and (d) relative permeability.

Figure 4.25 shows a negative real part of the refractive index over 885 nm ~ 1000 nm of wavelenth. The metamaterial resonates at wavelengths near 710 nm and 960 nm where the magnetic resonance is dominant near 960 nm.

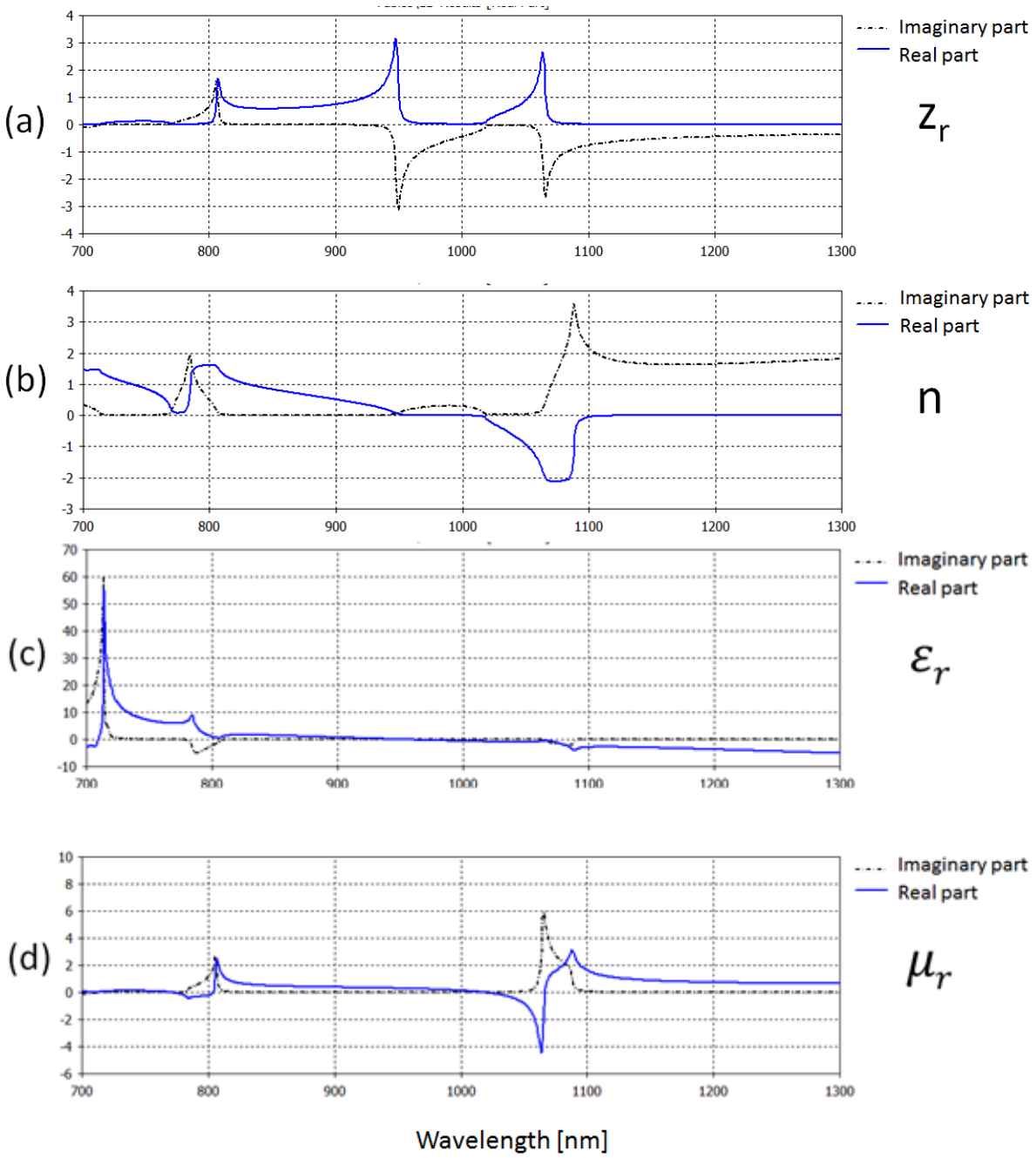

Figure 4.26 Extracted effective parameters of Design A-4-(5) of Table 4.4 on page 40. (a) relative wave impedance, (b) refractive index, (c) relative permittivity, and (d) relative permeability.

Figure 4.26 shows a negative real part of the refractive index over 995 nm ~ 1150 nm of wavelenth. The metamaterial resonates at wavelengths near 780 nm and 1085 nm where the magnetic resonance is dominant near 1085 nm.

5. FABRICATION

5.1 E-beam Evaporator and Profilometer

■ E-beam evaporator

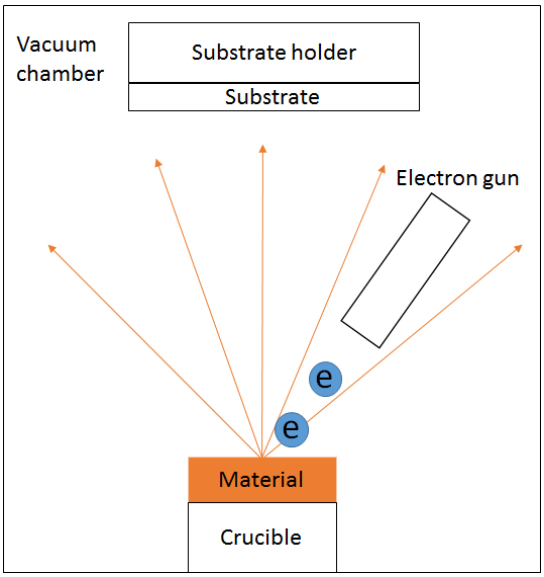

Figure 5.1 Illustration of the e-beam evaporator's operation.

Figure 5.1 depicts how an e-beam evaporator operates. The electron gun shoots electrons that are accelerated to higher kinetic energy levels at the material. These electrons heat the material by colliding with the material's atoms. When the material's atoms evaporate, they fly straightly until they collide with another atom or they settle down on the substrate (the average distance that the atoms travel without a collision is called the 'mean free path'). An e-beam evaporator (PVD 75, Kurt J Lesker) was used to deposit Cu and SiO_2 layers in this work. It was observed that the

layers deposited in lower-quality vacuum (~10^{-5} Torr) tend to be more porous than those deposited in higher-quality vacuum (~10^{-7} Torr).

■ Profilometer

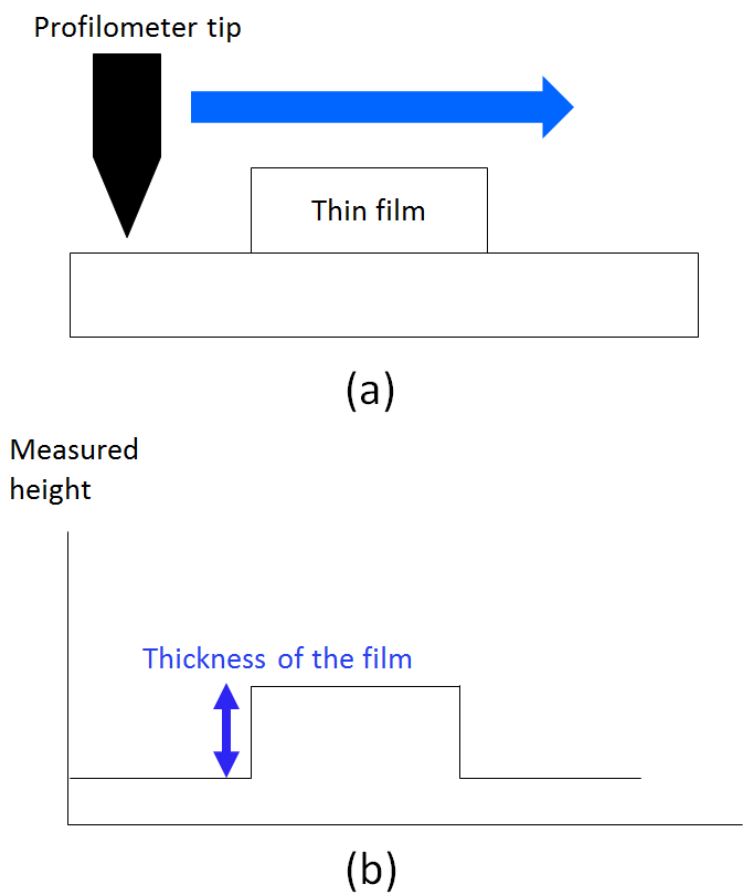

Figure 5.2 Illustration of the profilometer's operation. (a) is a side-view of the profilometer's operation. (b) is the measured profile of the thin film of (a).

Figure 5.2 depicts how a profilometer operates. The profilometer tip scans the specimen surface and reads the relative difference in height. In this work, a profilometer (AlphaStep D-500, KLA Tencor) was used to measure the thicknesses of Cu and SiO_2 layers.

5.2 Design A-1-(5)

Based on simulation, metamaterials of Design A were found to exhibit the most interesting performance (bandpass) among all the six Designs. In addition, the bandpass performance of Design A-1 metamaterials of page 32 is in the visible regime. Therefore, regarding this and the uncertainty of a deposited material's thickness, Design A-1-(5) was selected to be fabricated.

5.2.1 Calibration of E-beam Evaporator

■ Calibration for t_m = 25 nm (Cu)

Deposition conditions of the e-beam evaporator for a Cu layer are as follows. The deposition rate and final thickness were set 8 Å/s and 250 Å respectively. The substrate was rotated in the Forward Direction (rotation directions are defined by default in the machine). The shutter of the substrate was set to open when the deposition rate stabilizes at 8 Å/s.

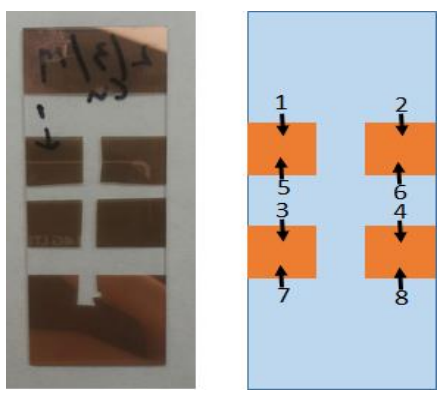

Figure 5.3 A Cu layer deposited on a glass substrate. The left image is the real sample. Numbers and arrows in the right image represent the locations and directions of the profilometer measurements.

After deposition, the thickness of the Cu layer was measured by the profilometer at the eight different locations shown in Figure 5.3. These thickness values are given in Table 5.1.

Table 5.1 Measured thicknesses of the Cu layer at the eight different locations shown in Figure 5.3.

position	measured thickness (nm)
1	25.8
2	20.4
3	29.3
4	26.5
5	12.6
6	32.5
7	19.7
8	22.2
average	23.6
standard deviation	± 5.8

■ Calibration for t_{die} = 75 nm (SiO_2)

Deposition conditions of the e-beam evaporator for a SiO_2 layer are as follows. The deposition rate and final thickness were set 4 Å/s and 600 Å respectively. The glass substrate was rotated in the Forward Direction. The substrate shutter was set to open when the deposition rate stabilizes at 4 Å/s.

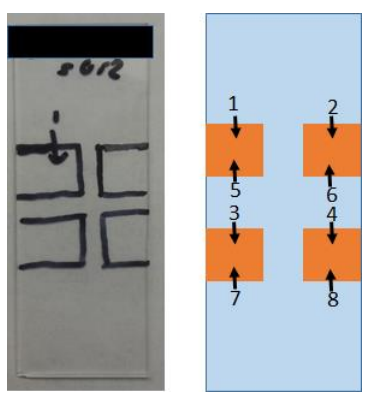

Figure 5.4 A SiO_2 layer deposited on a glass substrate. The left image is the real sample. Numbers and arrows in the right image represent the locations and directions of the profilometer measurements.

After deposition, the thickness of the SiO_2 layer was measured by the profilometer at the eight different locations shown in Figure 5.4. These thickness values are given in Table 5.2.

Table 5.2 Measured thicknesses of the SiO_2 layer at the eight different locations shown in Figure 5.4.

position	measured thickness (nm)
1	76.1
2	76.1
3	69.5
4	71.1
5	77.5
6	79.7
7	92.6
8	82.7
average	78.2
standard deviation	± 6.8

■ Deposition of $Cu/SiO_2/Cu$ layers

Deposition conditions for Cu and SiO_2 layers were same as above.

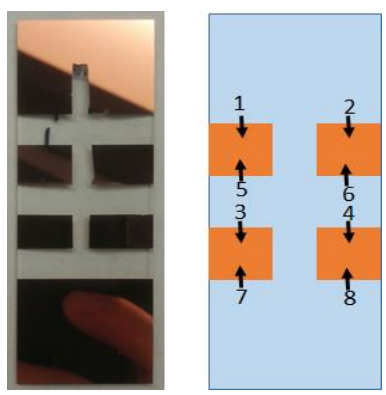

Figure 5.5 $Cu/SiO_2/Cu$ layers deposited on a glass substrate. The left image is the real sample. Numbers and arrows in the right image represent the locations and directions of the profilometer measurements.

After deposition, the thickness of the Cu/SiO_2/Cu layers was measured by the profilometer at the eight different locations shown in Figure 5.5. These thickness values are given in Table 5.3.

Table 5.3 Measured thicknesses of the Cu/SiO_2/Cu layers at the eight different locations shown in Figure 5.5.

position	measured thickness (nm)
1	122.6
2	120.3
3	136.1
4	128.9
5	126.1
6	125.0
7	130.5
8	121.0
average	126.3
standard deviation	± 5.0

5.2.2 Metamaterial Fabrication

An electron-beam resist was patterned on a 500 μm-thick glass wafer by electron-beam lithography (the patterned resist on the wafer looked in color and the color changed depending on the observation angle while the rest part of the wafer was just transparent). Then, Cu/SiO_2/Cu layers were deposited on the wafer, and lift-off was conducted at 40 ~ 60 ℃. This process is described in Figure 5.6.

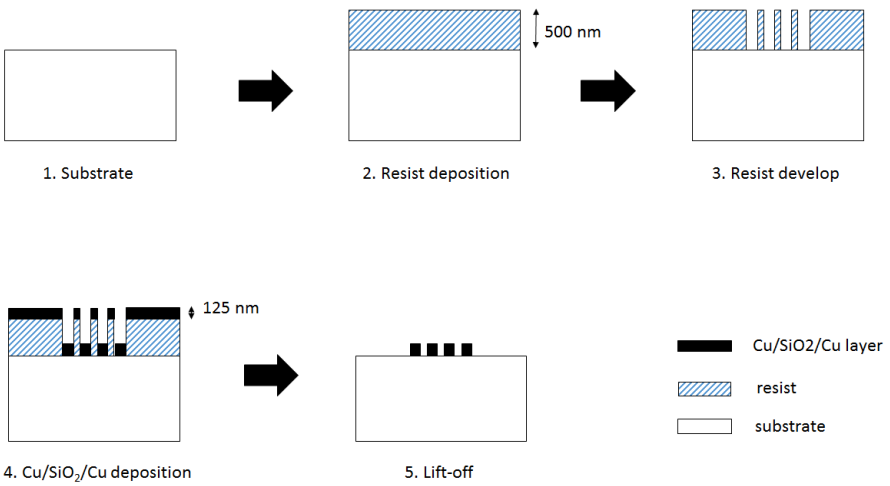

Figure 5.6 Schematic diagrams of the fabrication process.

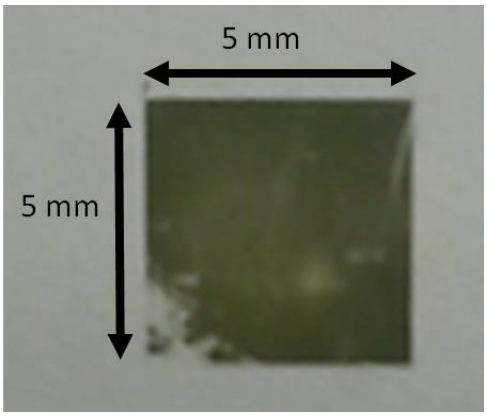

Figure 5.7 The fabricated Design A-1-(5) metamaterial on a glass substrate. The bottom left side of the metamaterial was slightly removed in a sonicator during lift-off.

5.3 Design A-3-(5)

Design A-3 metamaterials of page 38 are the largest structure among the Design A metamaterials which exhibit a bandpass performance at wavelengths shorter than 1100 nm (this wavelength is the longest measurable wavelength of the spectrophotometer used for transmittance measurements in this study). Therefore, Design A-3-(5) was selected to be fabricated regarding fabrication resolution, performance wavelengths, and the uncertainty of a deposited material's thickness.

5.3.1 Calibration of E-beam Evaporator

■ Calibration for t_m = 40 nm (Cu)

The deposition rate and final thickness were set 8 Å/s and 400 Å respectively, and other conditions were the same as in Section 5.1.1. The average value and standard deviation of the measured thicknesses of the Cu layer were 41.8 nm and 1.8 nm respectively (the thicknesses were measured in the same way as in Section 5.1.1).

■ Calibration for t_{die} = 130 nm (Cu)

The deposition rate and final thickness were set 4 Å/s and 1040 Å respectively, and other conditions were the same as in Section 5.1.1. The average value and standard deviation of the measured thicknesses of the SiO_2 layer were 129.4 nm and 2.3 nm respectively (the thicknesses were measured in the same way as in Section 5.1.1).

■ Deposition of $Cu/SiO_2/Cu$ layers

Deposition conditions for each material were the same as above. The average value and standard deviation of the measured thicknesses of the $Cu/SiO_2/Cu$ layers were 226.1 nm and 0.4 nm respectively.

5.3.2 Metamaterial Fabrication

An electron-beam resist was patterned on a 500 μm-thick glass wafer by electron-beam lithography (the patterned resist on the wafer looked in color and the color changed depending on the observation angle while the rest part of the wafer was just transparent). Then, $Cu/SiO_2/Cu$ layers were deposited on the wafer, and lift-off was conducted at 40 ~ 60 ℃. This process is described in Figure 5.6.

6. TEST AND MEASUREMENT

A spectrophotometer (Evolution™ 300 UV-Vis Spectrophotometer, Thermo Fisher Scientific) was used to measure transmittance. The spectrophotometer was calibrated for the aperture size of the fabricated metamaterial.

6.1 Design A-1-(5)

Figure 6.1 shows simulated and measured transmittances of the Design A-1-(5) metamaterial. The two transmittances do not agree and are not even similar. Figure 6.2 shows SEM pictures of the fabricated Design A-1-(5) metamaterial. More quantity of Cu (bright part) is observed than the designed quantity (refer to Figure 3.1 and Table 4.1).

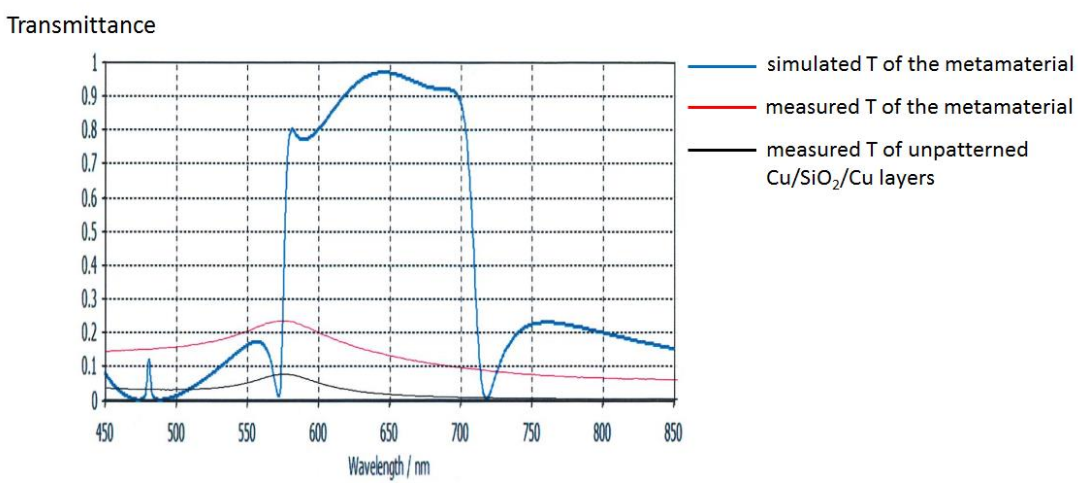

Figure 6.1 Simulated and measured transmittances of the Design A-1-(5) metamaterial. The measured transmittance of the metamaterial is compared with its simulated transmittance and with the measured transmittance of unpatterned Cu/SiO_2/Cu layers. The metamaterial's Cu/SiO_2/Cu layers and unpatterned Cu/SiO_2/Cu layers each have the equal thickness and were deposited on the same glass substrate.

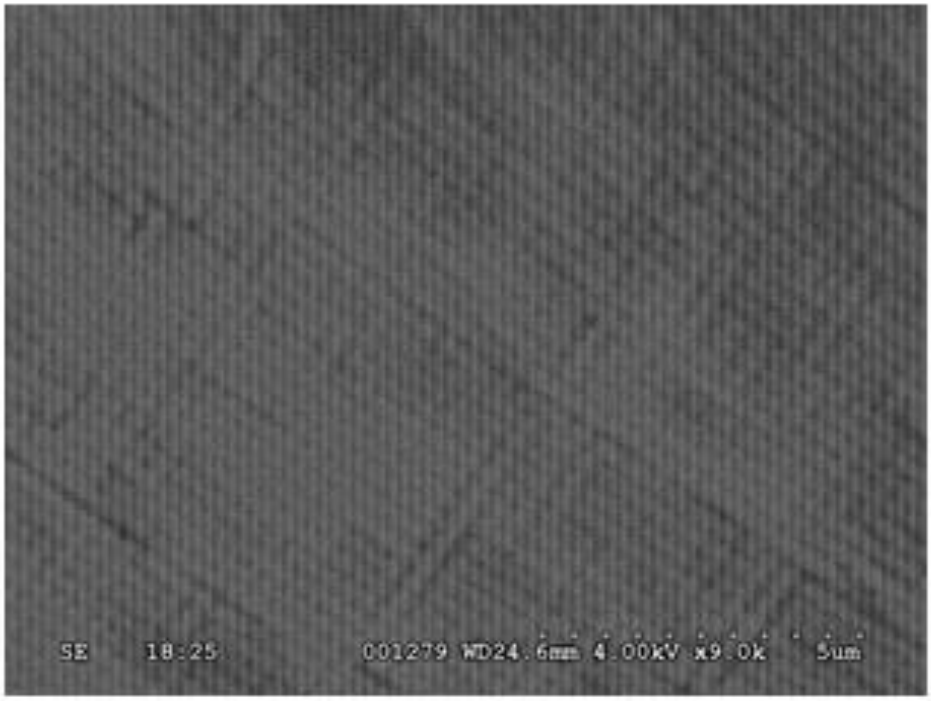

(a)

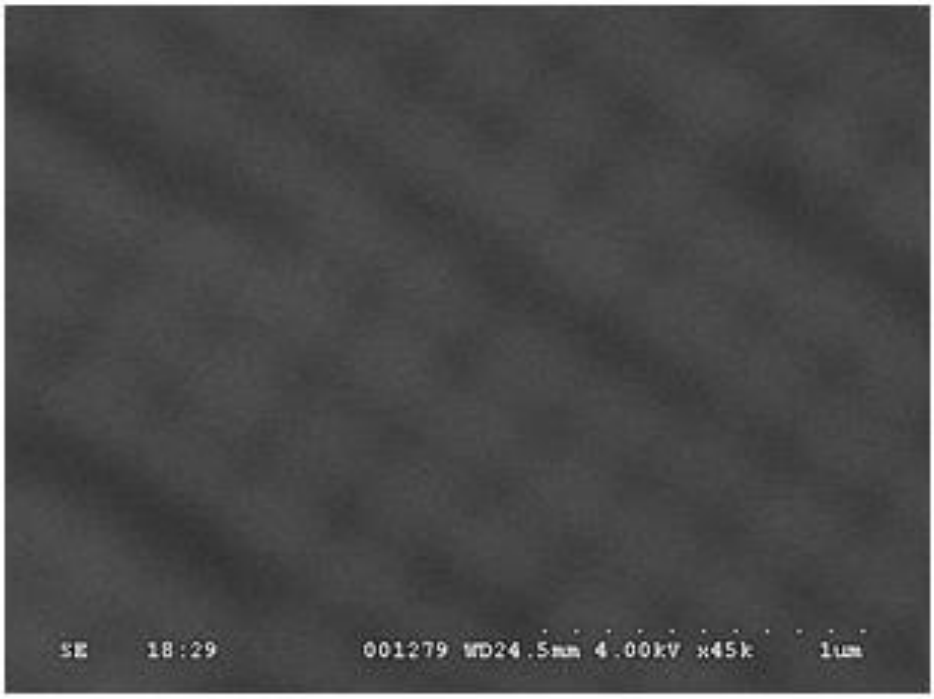

(b)

Figure 6.2 SEM images of the fabricated Design A-1-(5) metamaterial (bright part is Cu).

6.2 Design A-3-(5)

Figure 6.3 shows simulated and measured transmittances of the Design A-3-(5) metamaterial. The simulated transmittance exhibits a bandpass area over 708 nm ~ 960 nm of wavelength while that of the measured transmittance is over 200 nm ~ 764 nm with lower values of transmittance. Figure 6.4 shows SEM pictures of the fabricated Design A-3-(5) metamaterial. Measured parameters of the unit cell (a = 539 nm, d = 191 nm) are different from those of the simulated design (a = 500 nm, d = 250 nm).

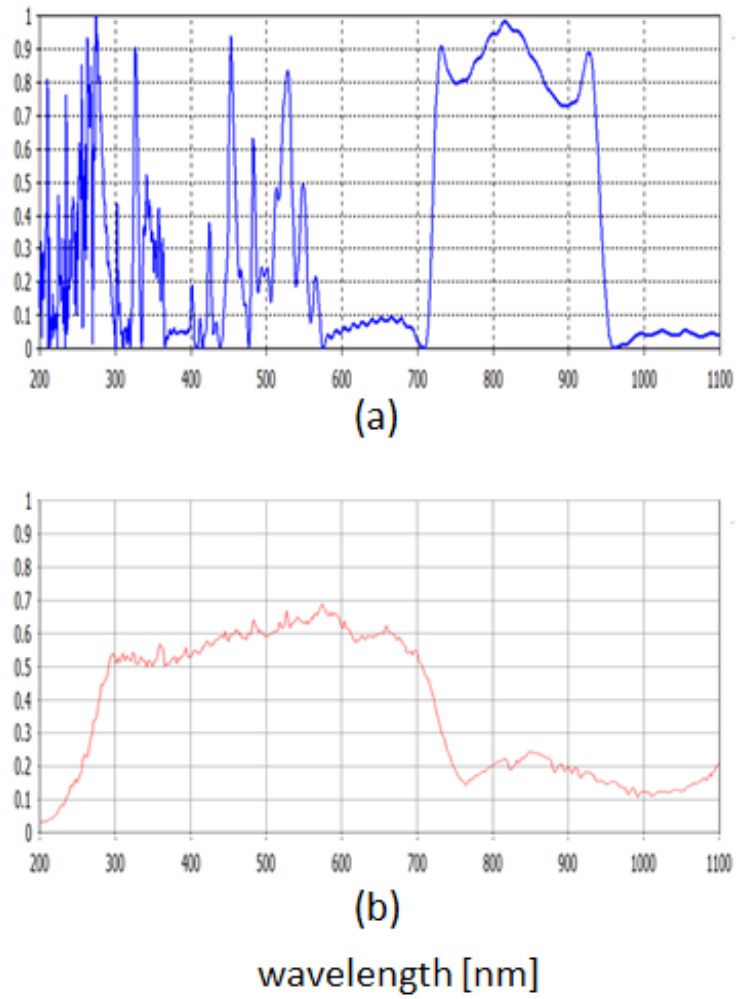

Figure 6.3 simulated (a) and measured (b) transmittances of the Design A-3-(5) metamaterial

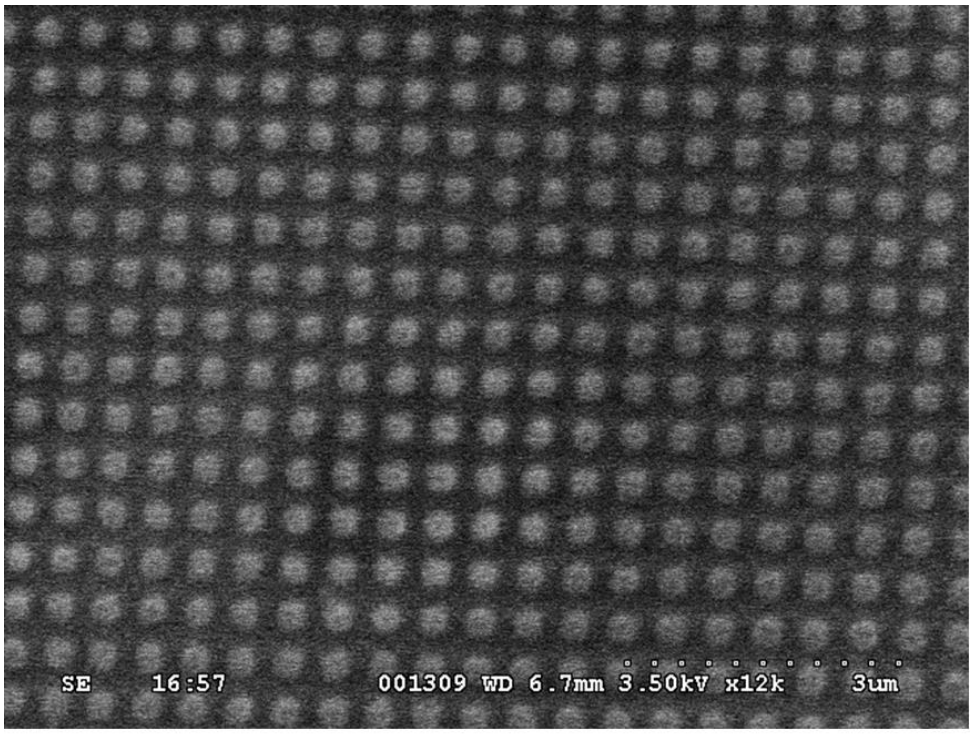

(a)

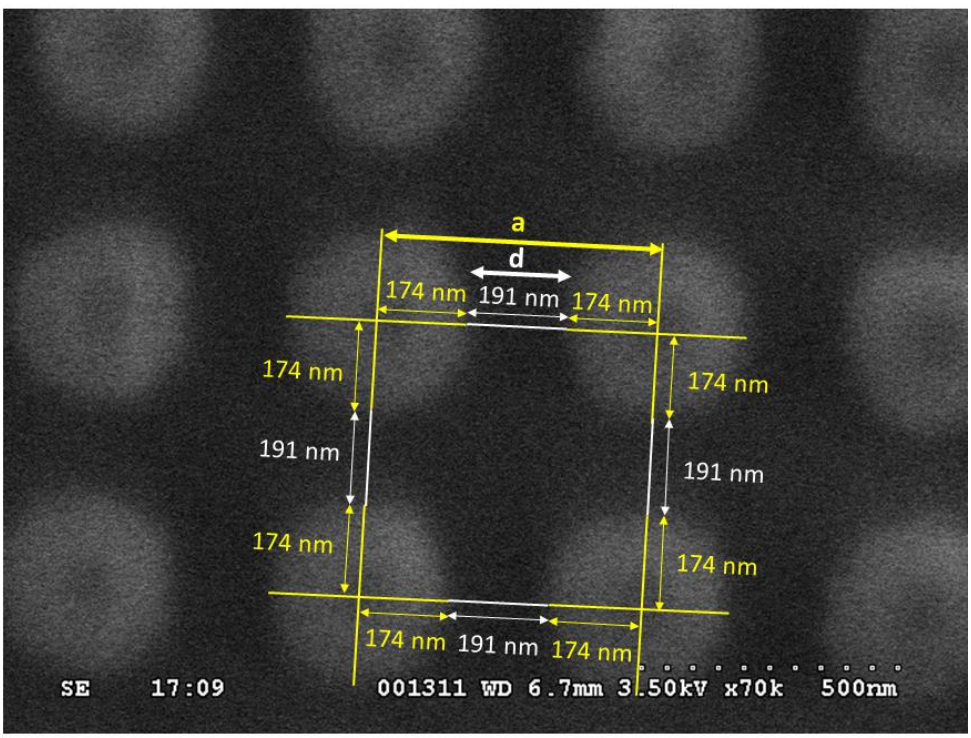

(b)

Figure 6.4 SEM images of the fabricated Design A-3-(5) metamaterial (dark part is Cu). Measured parameters of the unit cell (a = 539 nm, d = 191 nm) are notated in (b).

7. DISCUSSION

7.1 Results of Design A-1-(5) Metamaterial

There is a possibility that the lifted Cu atoms were re-attached to the Cu strips of the metamaterial during the lift-off as there was a large amount of lifted Cu chunks in the lift-off bath [32]. This might have caused the results of Fig 6.1 and Fig 6.2. To verify whether the re-attachment was enough to produce the results of Figure 6.1, simulations were conducted with varying amounts of re-attached Cu. Figure 7.1 shows the conditions and results of the simulation work. Surprisingly, Figure 7.1 (c) and (d) show that re-attached Cu with 42 ~ 44 nm thickness ("t_reatta" in Figure 7.1 (a)) can produce transmittance that is very similar to that of the unpatterned Cu/SiO_2/Cu layers, which is the case of the two measured transmittances of Figure 6.1.

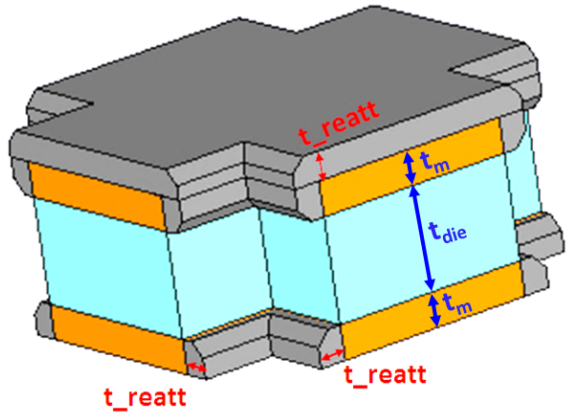

(a)

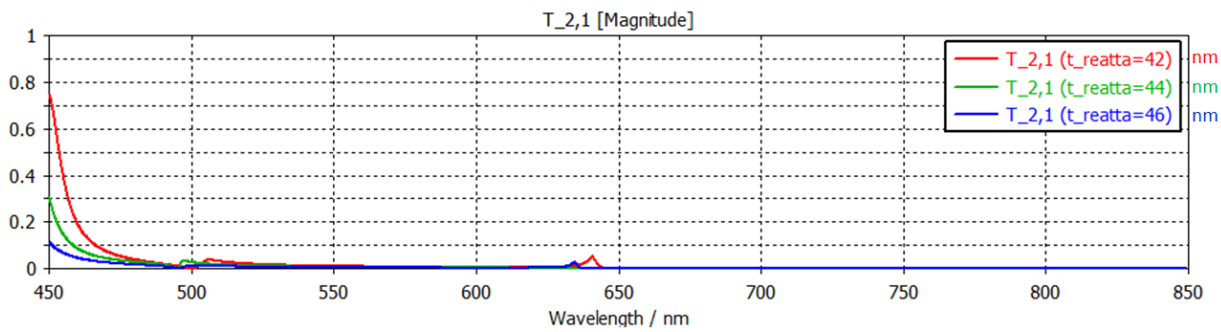

(b)

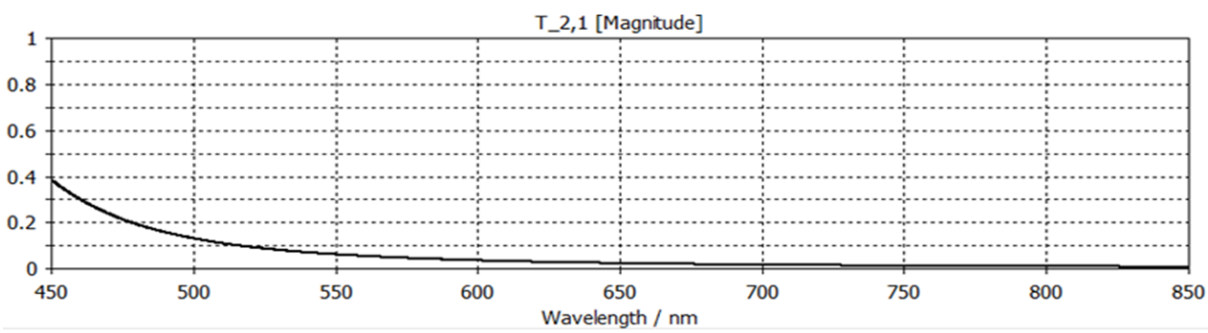

(c)

Figure 7.1 Simulation for Cu re-attachment. (a) is the unit cell (t_m = 25 nm, t_{die} = 75 nm) of the metamaterial with re-attached Cu. The re-attached Cu is colored in grey to distinguish from deposited Cu, and the thickness of re-attached Cu is written as 't_reatt". Here the kinetics of atomic re-attachment is considered, but this effect was found to have a minor effect on simulated results compared to when there is no chamfer. (b) is simulated transmittance of the unit cell (a). (c) is simulated transmittance of unpatterned Cu/SiO_2/Cu layers with the equal thicknesses as those of the metamaterial without re-attached Cu.

7.2 Results of Design A-3-(5) Metamaterial

Based on the results of Figure 6.4, two kinds of unit cell were simulated as shown in Figure 7.2. The shape of Cu strips in Figure 6.4 is not considered in Figure 7.2 (a) and is considered in Figure 7.2 (c). In both cases, simulated transmittance is still somewhat different from the measured transmittance of Figure 6.3 (b). However, the band area of Figure 7.2 (d) is wider than that of Figure 6.3 (a), which is closer to the bandwidth of the measured transmittance.

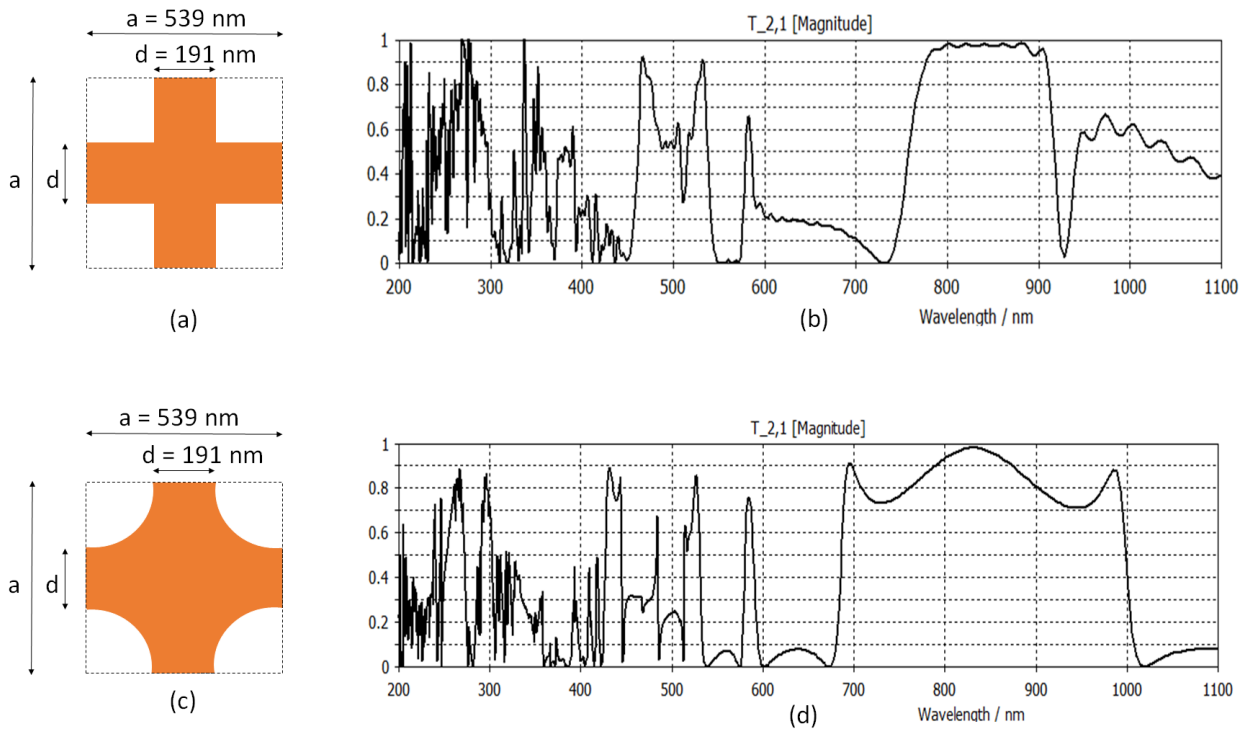

Figure 7.2 Simulation of the Design A-3-(5) metamaterial based on the results of Figure 6.4. (a) is the unit cell in which the shape of Cu strips in Figure 6.4 is not considered. (b) is simulated transmittance of the unit cell (a). (c) is the unit cell in which the shape of Cu strips in Figure 6.4 is considered. (d) is simulated transmittance of the unit cell (c).

8. CONCLUSION

Simulated and measured results of the metamaterials were a bit different as discussed in Chapter 6 and Chapter 7. However, in spite of this, the Design A-3-(5) metamaterial exhibited an unusual transmittance that has a wide bandpass area (Fig 6.3 (b)). This performance is not found in natural materials, nor is it based on interference between light and thin films (the principle traditional optical filters work). Moreover, to the best of knowledge, neither simulation work nor measured result that presents the wide bandpass of a metamaterial at visible frequencies has been reported yet. Therefore, the results of this study provide a foundation in research in using metamaterials as an optical filter instead of traditional filters in the visible spectrum.

9. FUTURE WORK

1) Calibration of e-beam pattern writer (e-beam lithography)

The widths of fishnet arms (‘d’ value in Figure 3.1) of the simulated and fabricated Design A-3-(5) metamaterials are 250 nm and 191 nm respectively. The value 250 nm, which was designed in a mask design software (KLayout), resulted in 191 nm in the fabrication. One of the future works would be calibrating the e-beam pattern writer with varying d values in the mask design software so that the targeted d value can be obtained.

2) Experiments with larger scales of metamaterials

The simulated and measured band regions of the Design A-3-(5) metamaterial are different on the wavelength scale (Figure 6.3); the measured band region is over shorter wavelengths than that of the simulated band region. Design A metamaterials based on the ratio of a : d = 2 : 1 (Figure 3.1) with larger scales could be further studied to see the relation between their simulated and measured band regions.

LIST OF REFERENCES

[1] **The University of Bonn. "Second Harmonic Generation in Metamaterials". Web. <https://www.hikari.uni-bonn.de/research/metamaterials>**

[2] **R.S. Kshetrimayum. "A brief intro to metamaterials". IEEE Potentials, Vol. 23, Issue: 5, (2004). Print.**

[3] **Jason Valentine, Shuang Zhang, Thomas Zentgraf, Erick Ulin-Avila, Dentcho A. Genov, Guy Bartal & Xiang Zhang. "Three-dimensional optical metamaterial with a negative refractive index". Nature, Vol. 455, (2008). Print.**

[4] **Alan Zhan, Shane Colburn, Rahul Trivedi, Taylor K. Fryett, Christopher M. Dodson, and Arka Majumdar. "Low-Contrast Dielectric Metasurface Optics". ACS Photonics, Vol. 3, (2016). Print.**

[5] **Walter S. Wall, Scott M. Rudolph, Sun K. Hong, and Kenneth L. Morgan. "Broadband Switching Nonlinear Metamaterial". IEEE Antennas and Wireless Propagation Letters, Vol. 13, (2014). Print.**

[6] **Varittha Sanphuang, Nima Ghalichechian, Niru K. Nahar, and John L. Volakis. "Reconfigurable THz Filters Using Phase-Change Material and Integrated Heater". IEEE Transactions on Terahertz Science and Technology, Vol. 6, No. 4, (2016). Print.**

[7] **W Stork, N. Streibl, H. Haidner, and P. Kipfer. "Artificial distributed-index media fabricated by zero-order gratings". Optics Letters, Vol. 16, No. 24, (1991). Print.**

[8] **Wikipedia. "Maxwell's equations". Web. <https://en.wikipedia.org/wiki/Maxwell's_equations>**

[9] **Sergio Granieri. "Optical Materials". Rose-Hulman Institute of Technology. Lecture notes.**

[10] **Sergio Granieri. "Electric and Magnetic Fields". Rose-Hulman Institute of Technology. Lecture.**

[11] **Sophocles J. Orfanidis . "Electromagnetic Waves and Antennas". Web. <http://eceweb1.rutgers.edu/~orfanidi/ewa/>, p. 2. Book.**

[12] **David J. Griffiths. "Introduction to electrodynamics". Pearson, ISBN 978-93-325-5044-5, 4th edition, pp. 417-418, (2013). Book.**

[13] **Encyclopædia Britannica. "Dielectric". Web. <https://global.britannica.com/science/dielectric">**

[14] Farhan Rana. "Waves in Isotropic Media: Dielectrics and Conductors". Cornell University. Lecture notes.

[15] John S. Seybold. "Introduction to RF propagation". Wiley, p. 22, (2005). Book.

[16] M. A. Ordal, Robert J. Bell, R. W. Alexander, Jr, L. L. Long, and M. R. Querry. "Optical properties of fourteen metals in the infrared and far infrared: Al, Co, Cu, Au, Fe, Pb, Mo, Ni, Pd, Pt, Ag, Ti, V, and W.". Applied Optics, Vol. 24, No. 24, (1985). Print.

[17] R. M. Morgan, David W. Lynch. "Optical Properties of Dilute Ag-In Alloys". Physical Review, Vol. 172, (1968). Print.

[18] Frank L. Pedrotti, Leno S. Pedrotti. "Introduction to Optics". Prentice-Hall international, Inc, 2nd edition, Ch. 27, (1993). Book.

[19] Robert P. Lucht. "Drude Model for dielectric constant of metals". Purdue University. Lecture notes.

[20] CST. "Material Overview (HF)". CST Help section.

[21] G. Dolling, M. Wegener, S. Linden. "Negative-index metamaterial at 780 nm wavelength". Optics Letters, Vol. 32, No. 1, (2007). Print.

[22] Shuang Zhang, Wenjun Fan, K. J. Malloy and S. R. J. Brueck. "Near-infrared double negative metamaterials". Optics Express, Vol. 13, No. 13, (2005). Print.

[23] CST. "Time Domain Solver Overview". CST Help section.

[24] Refractiveindex.info. "Optical constants of SiO2 (Silicon dioxide, Silica, Quartz) Lemarchand 2013: Thin film; n,k 0.25-2.5 µm". Web. <https://refractiveindex.info/?shelf=main&book=SiO2&page=Lemarchand>

[25] Horiba. "Lorentz Dispersion Model". Web. <http://www.horiba.com/fileadmin/uploads/Scientific/Downloads/OpticalSchool_CN/TN/ellipsometer/Lorentz_Dispersion_Model.pdf >

[26] M. A. Ordal, L. L. Long, R. J. Bell, S. E. Bell, R. R. Bell, R. W. Alexander, Jr., and C. A. Ward. "Optical properties of the metals Al, Co, Cu, Au, Fe, Pb, Ni, Pd, Pt, Ag, Ti, and W in the infrared and far infrared". Applied Optics, Vol. 22, No. 7, (1983). Print.

[27] Xudong Chen, Tomasz M. Grzegorczyk, Bae-Ian Wu, Joe Pacheco, Jr., and Jin Au Kong. "Robust method to retrieve the constitutive effective parameters of metamaterials". Physical Review, E 70, (2004). Print.

[28] D. R. Smith and S. Schultz, P. Markos and C. M. Soukoulis, "Determination of effective permittivity and permeability of metamaterials". Physical Review, B 65, (2002). Print.

[29] CST. "S-Parameters / Extract Material Properties from S-Parameters". CST Help section.

[30] A. M. NICOLSON, G. F. ROSS. "Measurement of the Intrinsic Properties of Materials by Time-Domain Techniques". IEEE Transactions on Instrumentation and Measurement, VOL. IM-19, No. 4, (1970). Print.

[31] V. G. Veselago. "The electrodynamics of substances with simultaneously negative values of ε and μ". Soviet Physics Uspekhi, Vol. 10, No. 4, (1968). Print.

[32] Georgia Tech IEN. "Nanolithography". Web. <http://nanolithography.gatech.edu ></

APPENDIX A: Maple Coding for the Refractive Index and Reflectance of SiO_2

Optical values of silicon dioxide are from [25].

```
> n := sqrt(1 + wp^2 / ((w0^2 - w^2) - i·w·r))
> w0 := 1.823·10^16   # [rad Hz]  SiO2  [Horiba]
> wp := sqrt((w0)^2·(2.12 - 1))   # [rad Hz]  SiO2  [Horiba]
> r := 1.52·10^14   # [rad Hz]  SiO2  [Horiba]
>
> c := 300000000000000 # [um/s]
> w := 2·π·c / λ
> λp := c·2·π / wp   # plasma wavelength [um]
> λ0 := c·2·π / w0   # resonance wavelength [um]
> plot(Re(n), λ = 0.01 .. 2)   # wavelength : 10 nm ~ 2 um
> plot(Im(n), λ = 0.01 .. 2)   # wavelength : 10 nm ~ 2 um
>
> r := (1 - n) / (1 + n)   # reflection coefficient of the metal at normal incidence
> plot(r·conjugate(r), λ = 0.01 .. 2)   # reflectance over wavelengths 10 nm ~ 2 um
```

APPENDIX B: Maple Coding for the Refractive Index and Reflectance of Cu

Optical values of cupper are from [16].

```
> n := sqrt(1 - wp^2/(w^2 + i·w·r))
> wp := 1.12·10^16    # [rad Hz]  Cu  [ordal new]
> r := 1.38·10^13  # [radHz]  Cu   [ordal new]
>
> c := 300000000000000 # [um/s]
> w := 2·π·c/λ
> λp := c·2·π/wp   # plasma wavelength [um]
> plot(Re(n), λ = 0.0001 .. 10)   # wavelength : 0.1 nm ~ 10 um
> plot(Im(n), λ = 0.0001 .. 10)   # wavelength : 0.1 nm ~ 10 um
>
> r := (1 - n)/(1 + n)   # reflection coefficient of the metal at normal incidence
> plot(r·conjugate(r), λ = 0.0001 .. 10)   # reflectance over wavelengths 0.1 nm ~ 10 um
```